2014

Synthesis and characterization of liquid crystalline epoxy resins

Yuzhan Li
Iowa State University

Synthesis and characterization of liquid crystalline epoxy resins

by

Yuzhan Li

A dissertation submitted to the graduate faculty
in partial fulfillment of the requirements for the degree of
DOCTOR OF PHILOSOPHY

Major: Materials Science and Engineering

Program of Study Committee:
Michael R. Kessler, Major Professor
Mufit Akinc
Xiaoli Tan
Jason Chen
Samy Madbouly

Iowa State University
Ames, Iowa
2014

TABLE OF CONTENTS

LIST OF FIGURES

LIST OF TABLES

ACKNOWLEDGEMENTS

I would like to sincerely thank my advisor, Dr. Michael R. Kessler, for providing me the opportunity to join this wonderful research group and for his continuous guidance, support and encouragement throughout my graduate studies. I would also like to express my thanks to Dr. Mufit Akinc, Dr. Xiaoli Tan, Dr. Samy Madbouly, and Dr. Jason Chen for serving on my advisory committee and providing additional technique guidance.

I would like to thank Dr. Prashanth Badrinarayanan for his great help at the beginning of this project. I would like to thank Dr. Shu Xu, Dr. Arkady Ellern, Dr. Mahendra Thunga, Dr. Scott Schlorholtz, Dr. Yaroslav Mudryk, Dr. Elena Moukhina and Dr. Orlando Rios for their valuable technical support and helpful discussion. I would also like to thank members of the polymer composites research group, Dr. Vijay Kumar, Dr. Hongyu Cui, Dr. Peter Hondred, Dr. Eliseo De León, Dr. Tom Garrison, Danny Vennerberg, Mitch Rock, Chaoqun Zhang, Ruqi Chen, Rui Ding, and Hongchao Wu, for creating an enjoyable working environment.

Finally, I would like to thank my mother, Baorong Zhao, my father, Shishui Li, and my girlfriend, Jingyi Zhang. I couldn’t have done this without your continuous support and encouragement.

ABSTRACT

Fiber reinforced polymer matrix composites (FRPs) have been developed for many decades and used in a wide variety of applications. However, the residual stresses caused by the mismatch in the coefficient of thermal expansion (CTE) between the polymer matrices and the fiber reinforcements during the processing of FRPs is a crucial factor affecting the performance of the composites, which can lead to a reduction of mechanical properties and loss of dimensional stability, thereby limiting the use of FRPs in high performance applications. Additionally, the relatively poor matrix properties is another factor affecting overall performance of the composites, including chemical resistance, moisture absorption, and long term durability of FRPs. A potential strategy to solve the problems mentioned above involves the development of novel polymer matrices with improved physical, thermal, and mechanical properties with low thermal expansion to ensure minimal mismatch in CTE with the fiber reinforcements, which can reduce the magnitude of residual stresses, facilitating the development of FRPs for advanced applications.

Liquid crystalline epoxy resins (LCERs) are a unique class of thermosetting materials formed upon curing of low molecular weight, rigid rod epoxy monomers, resulting in the retention of a liquid crystalline (LC) phase by the three dimensional networks. LCERs exhibit a polydomain structure, thereby combining the outstanding properties of liquid crystals and thermosets. The rigid and ordered structure of LC domains is expected to reduce the CTE of the resins as well as improve the thermal and mechanical properties of the resins. In addition, liquid crystals possess properties that can be controlled by external fields, greatly improving the design flexibility. These attractive features make LCERs good

candidates for polymer matrices in high performance composites.

The goal of this research is to synthesize a LCER based on biphenyl mesogen, characterize the thermal, physical, and mechanical properties of the resin, and evaluate the potential use of LCERs as polymer matrices in high performance composites.

CHAPTER 1. GENERAL INTRODUCTION

1.1 Introduction

Composites are materials that consist of two or more chemically and physically different phases separated by a distinct interface. The different phases (matrix phase and reinforcing phase) are combined to produce a system with more useful structural or functional properties not attainable by any of the constituent alone. In composite materials, the matrix phase acts as a load transfer medium and supports the reinforcement materials by maintaining their relative positions. The reinforcing phase usually has superior physical and mechanical properties, greatly enhancing the matrix properties [1, 2].

In recent years, fiber reinforced polymer matrix composites (FRPs) have become one of the most important classes of composites with a wide variety of applications ranging from electronic devices to aerospace structures. Because of their high strength to weight ratios, FRPs are playing a crucial role in facilitating the development of lighter and more energy efficient systems. However, there are still several critical issues limiting the use of FRPs in high performance applications, including the relatively poor out-of-plane properties and the residual stresses induced dimensional instability. For example, after processing and subsequent cooling of composite laminates from high temperature to the service temperature, residual stresses build up due to the mismatch in coefficient of thermal expansion (CTE) between the fibers and the polymer matrix, leading to the formation of stress-induced voids, cracks, and delamination, which greatly reduce the mechanical performance of the composites [3-7]. Additionally, the presence of residual stresses affects the dimensional stability of the composites by inducing fiber misalignment and warpage of laminates, severely limiting the use of FRPs in dimensionally critical applications such as

satellites antennas and space exploration vehicles [8].

A potential strategy to improve the performance of FRPs involves the development of novel polymer matrices with improved mechanical properties and low thermal expansion to reduce the magnitude of residual stresses.

The objective of this work is to investigate a unique class of thermosetting materials known as liquid crystalline epoxy resins (LCERs) and evaluate the potential use of these materials as polymer matrices in carbon fiber reinforced composites. LCERs have a polydomain structure with individual liquid crystalline (LC) domains distributed in the crosslinking networks, thereby combining the outstanding properties of liquid crystals and thermosets. The presence of the rigid LC domains is expected to improve thermal and mechanical properties of the resins. In addition, liquid crystals possess properties that can be controlled by external fields, greatly improving the design flexibility. These attractive features make LCERs good candidates for polymer matrices in high performance composites.

1.2 Dissertation organization

This work is organized into main chapters, which are manuscripts that have been published in scholarly journals.

Chapter 1 gives a general introduction that outlines the background and motivation for the development of novel polymer matrices for FRPs. Specific focus is placed on the critical issues that limit the use of FPRs in high performance applications, such as the residual stresses developed during the processing step. This chapter also serves as a review chapter, summarizing recent advances in the field of LCERs.

Chapter 2 involves studies on synthesis and characterization of a biphenyl-based LCER. The thermal properties, LC morphologies, and cure behavior of the epoxy monomer was investigated through various experimental techniques. The effects of curing condition on LC phase formation, glass transition temperature (T_g), CTE, and dynamic mechanical properties of fully cured resins were also studied.

Chapter 3 discusses the cure kinetics of the LCER. Specific focus was placed on the effects of LC phase formation on reaction kinetics. Both a model-free isoconversional method and a model-fitting method were used to understand the unusual cure behavior of the LCER. A tentative multi-step kinetic model was developed to describe the curing reaction.

Chapter 4 outlines efforts to investigate viscoelastic properties of the LCER. The creep behavior of the resin cured in LC phase and non-LC phase was compared and evaluated using a viscoelastic model to understand the reinforcing effect of the LC phase. The long-term performance of the resin was predicted using the time-temperature superposition principle.

Chapter 5 introduces molecular orientation of the LCER. Macroscopically oriented resins were prepared by curing in a high strength magnetic field. The orientation was quantified by an orientation parameter determined with two-dimensional X-ray diffraction. The effects of orientation on T_g, CTE, and dynamic mechanical properties of the LCER were investigated.

Chapter 6 gives a series of general conclusions drawn from this thesis and provides suggestions for future work.

1.3 Background

1.3.1 Carbon fiber reinforced polymer matrix composites (CFRPs)

FRPs have been developed and manufactured for decades. Because of their high strength to weight ratios, FRPs have a wide variety of applications, including aerospace, automobiles, sporting goods, and infrastructure [9, 10]. However, the increasing demand for advanced FRPs has pushed scientists and engineers to explore new systems to meet the requirements for high performance applications. For example, the dimensional stability of FRPs is a crucial factor in material selection when they are used in aerospace applications such as satellites antennas or space exploration vehicles. They must be dimensionally stable over a wide range of temperatures, and must be able to withstand the microcracking that results from temperature cycling and outgassing [8].

Advanced FRPs are characterized by the use of high strength fiber reinforcements and high performance resin systems. Carbon fibers were developed to fill this need, which combine a high modulus and strength with low density. They have become one of the most important reinforcing materials for advanced FRPs in recent years [11-14]. Carbon fibers can be made from precursor fibers such as polyacrylonitrile (PAN), pitch, or rayon. Typically, the PAN-based carbon fibers have higher tensile strength and resistance to compressive failure, which makes them the ideal choice for applications requiring significant fiber strength. Although fibers are the major structural constituent in composites, the polymer matrix also plays an important role by holding the fibers in their proper positions, protecting the fibers from environmental attack, and transferring loads between fibers [15]. The polymer matrix can be either thermosets or thermoplastics depending on the application of the composites. A proper combination of polymer matrix and fiber

reinforcements can produce FRPs with many advantages, such as light weight, high specific strength and stiffness, tailorable properties, and increased design flexibility.

1.3.2 Liquid crystalline thermosets (LCTs)

The first investigation of LCTs can be traced back to a paper by de Gennes in 1969, in which the potential for the development of LC networks in polymers through crosslinking of reactive end groups was suggested [16]. LCTs may generally be defined as low molar mass, multifunctional monomers, which can be cured thermally, chemically, or photochemically in the melt state, leading to a highly crosslinked, high glass transition temperature material which exhibits LC order [17-19]. Liquid crystals are a special class of substance that exists as an intermediate state between the three-dimensionally ordered crystals and completely disordered, isotropic liquids. The LC phase observed in LCTs often falls in to the category of thermotropic liquid crystals, which may possess several different mesophases that depends on temperature, including nematic, smectic, and cholesteric. Figure 1.1 shows three types of mesophases often found in LCTs.

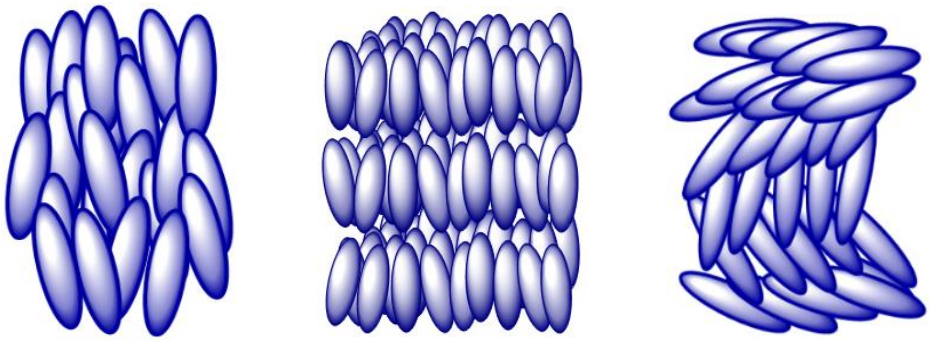

Figure 1.1 Typical LC phases observed in LCTs. From left to right: nematic phase, smectic phase, and cholesteric phase.

The nematic phase is characterized by long range orientational order but lack of positional order, while the smectic phase possesses orientational order as well as layered ordering. The cholesteric phase is featured by a nematic ordering of molecules within layers that are arranged in a helical manner.

A large number of LCT monomers with different reactive end groups have been synthesized, including epoxy [20-23], acrylate [24-27], maleimide [28, 29], and cyanate ester [30-33]. These LCT monomers follow the general rules for LC behavior that have been found for nonreactive low molar mass liquid crystals. Upon reacting with appropriate curing agents, the LC order can be retained, resulting in a material exhibiting a polydomain structure, thereby combining the useful benefits of both crosslinking thermosets and liquid crystals. The advantages of LCTs include good mechanical properties and chemical resistance, low shrinkage upon curing, higher fracture toughness, and the ability to be oriented mechanically or under the influence of an electric or magnetic field.

1.4 Literature review

1.4.1 Residual stresses in FRPs

During the processing of composite laminates, considerable residual stresses can build up because of the higher dimensional change of the polymer matrix compared to the fiber reinforcements, which results in a loss of mechanical properties as well as dimensional stability [34, 35]. Generally, the processing cycle for FRPs includes three steps. First, the laminated composites are heated from room temperature to the first dwell temperature and held for a period of time to allow entrapped air, water, or volatiles to escape the polymer matrix, improving compaction of the part. Afterwards, the temperature

is increased to the second dwell temperature to facilitate the curing reaction of the polymer matrix. Finally, the composites are cooled down to room temperature at a constant rate [36, 37].

Residual stresses in the FRPs are present immediately after processing and can be realized at different mechanical levels, leading to various forms of defects. On the micromechanical level, the mismatch in CTE between the fibers and the matrix is the driving force for the formation of residual stresses [38]. Thermosetting polymers are usually characterized by high CTE values. Fibers, on the other hand, have lower, anisotropic CTEs. Carbon fibers, for example, have a slightly negative CTE in the longitudinal direction and a near-zero positive CTE in the transverse direction. Consequently, when composite laminates are cooled down from processing temperature, the polymer matrix contracts significantly more than the carbon fibers, leading to a compressive residual stress on the fibers and a tensile stress on the surrounding matrix. The presence of these residual stresses can affect the properties of the composites in many ways [39]. In some cases the residual stresses can be strong enough to result in fiber fragmentation, significantly reducing the tensile, flexural, and compression mechanical properties of the composites. At the interfacial region, fiber-matrix debonding may occur, which greatly limits the load transfer efficiency. Furthermore, different debonding regions may join together to form microcracks, which can lead to transverse ply cracks and subsequent delamination or failure of the composites. Additionally, the residual stresses can affect matrix-dominated properties, such as mechanical properties, creep resistance, fracture toughness, moisture absorption, and temperature resistance. On the macromechanical level, residual stresses result from the mismatch of CTE between

composites plies. When cross-ply laminates are prepared, different plies impose constraints to each other due to the lamina anisotropy, creating considerable amount of residual stresses in the interlaminar region. These residual stresses can lead to premature delamination with significant loss of strength and stiffness of the composites. Interlaminar residual stresses also affects dimensional stability by inducing warpage of the composite and can pose constraints on fabrication parts with precise dimension. Several approaches have been made to mitigate the residual stresses in FRPs, including optimizing curing cycles [40-43] and incorporating negative or near zero thermal expansion materials. Wang et al. incorporated functionalized single-walled carbon nanotubes (SWNTs) into an epoxy to reduce the CTE of the resin and a reduction of up to 52% was observed [44]. Badrinarayanan et al. synthesized zirconium tungstate nanoparticles with negative CTE and incorporated them into a carbon fiber reinforced bisphenol E cyanate ester resin [45]. The results showed that the residual stress induced laminate warpage can be significantly reduced due to the introduction of zirconium tungstate. Shokrieh et al. incorporated carbon nanofibers (CNFs) into a carbon fiber reinforced epoxy and measured the residual stresses using a slitting method. It was found that the addition of 0.1%, 0.5%, and 1 wt.% CNFs led to 4.4%, 18.8%, and 25.1% reductions in residual stress, respectively [46].

Since the mismatch in the CTE between the polymer matrix and fiber reinforcements is the primary reason for the formation of residual stresses, investigation of polymer matrices with low CTEs becomes a promising solution, and is expected to effectively reduce residual stresses and improve the dimensional stability of PMCs, facilitating the development of high performance composites.

1.4.2 Liquid crystalline epoxy resin (LCER)

LCERs are the most extensively investigated among LCTs due to their excellent thermomechanical properties, especially their good mechanical strength, low dielectric constant, low shrinkage upon curing, and ease of processing. The unique properties of LCERs make them attractive candidates in a wide variety of applications, e.g. microelectronics, optical wave guides, adhesives, color filters, and structural materials. LCERs can be produced by the curing reaction between low molecular weight, rigid epoxy monomers with amine or anhydride. A typical structure of LCER monomers is shown in Figure 1.2, which contains a rigid core and functional end epoxy groups, bridged through alkyl flexible spacers.

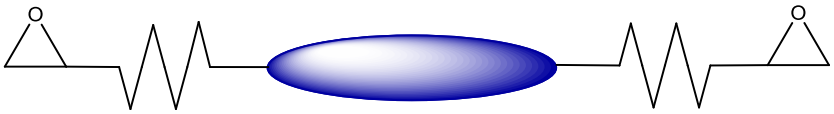

Figure 1.2 Typical chemical structure of LCER monomers.

Early investigation of LCERs involves synthesis and characterization of LC epoxy monomers with various mesogens [47-56], flexible spacers [22, 57-59], and substituent groups [60, 61]. Table 1.1 shows a list of epoxy monomers with various chemical structures. Giamberini *et al.* investigated epoxy monomers based on different mesogenic groups, including biphenyl, methylstilbene, azomethine, and naphthyl [21]. They found that the LC phases and morphologies are closely related with the aspect ratio of the mesogens. Lee *et al.* synthesized aromatic ester based LC epoxy monomers with different substituents on the mesogenic central group and found that introducing chlorine or methyl group on the mesogen can decrease the melting point and clearing point of the monomers, thereby

improving the processability of the LCERs [60].

Table 1.1 Typical chemical structure of mesogens.

Mesogenic groups	Chemical structure
biphenyl	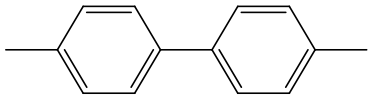
methylstilbene	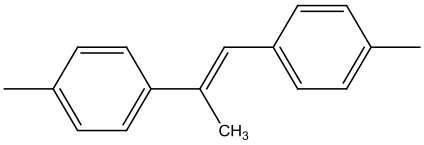
azomethine	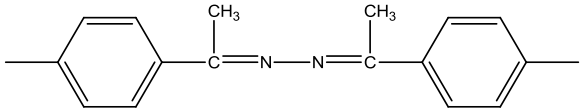
naphthyl	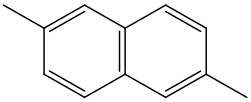
	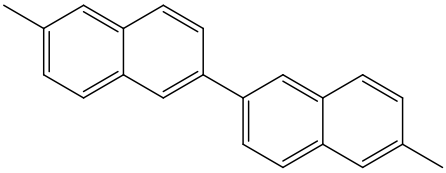
phenyl benzoate	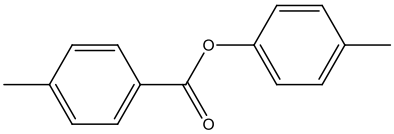
	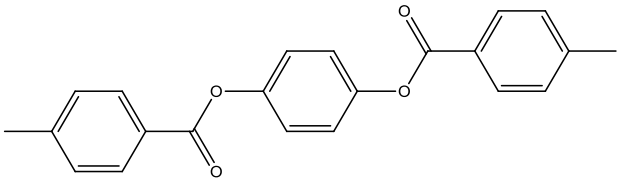

A large amount work has been performed to investigate the curing behavior [62-66], network formation [67, 68], and phase evolution [69, 70] of the LCERs. It was found that the epoxy monomers may not be liquid crystalline themselves. The LC phase will form

during curing and can be locked by the crosslinking networks. Lin *et al.* studied the curing reaction between 4,4'-dihydroxy-a-methylstilbene (DOMS) and sulfanilamide (SAA) using differential scanning calorimetry (DSC), polarized optical microscopy, and x-ray scattering [71]. They found that the LC phase formed during the curing reaction exhibits a layered structure at nanometer scale with mesogenic units aligned perpendicular to the layer surfaces. Cho *et al.* studied the same system using parallel plate rheology and constructed a liquid crystalline phase time-temperature transformation diagram for the DOMS/SAA system [72, 73].

Since the curing reaction is accompanied by the formation of an LC phase, studies have been carried out to investigate the cure kinetics of LCERs [74-84]. The presence of the LC phase has a dramatic effect on polymerization rates. Liu *et al.* investigated the cure kinetics of DOMS/SAA system using DSC under isothermal conditions [85]. A significant deviation from the autocatalytic model was observed when the LC phase transfers from nematic to smectic. An increase in reaction rate was also observed. Vyazovkin *et al.* applied an isoconversional method to study the cure kinetics of a system containing 4,4'-diglycidyloxybiphenyl (BP) and 2,6-diaminopyridine (DAP) [86]. It was found that the curing process is accompanied by the formation of a smectic phase, which results in a decrease in the effective activation energy of the reacting system.

Due to the presence of the rigid and ordered LC domains, the thermal and mechanical properties of fully cured resins are strongly affected, which have been reported by a number of researchers [87-94]. It was found that the fracture toughness of the resins cured in LC phase exhibit significant improvement. Ortiz *et al.* prepared a LCER system with a smectic phase based on DOMS and 4,4'-methylenedianiline (MDA) [95]. A conventional, non-

LCER was also prepared by curing diglycidyl ether bisphenol A (DGEBA) with MDA. Fracture toughness tests were performed using fully cured samples with a chevron notch. The load-displacement curves and fracture morphologies of two systems were compared. It was found that the fracture surface of DGEBA/MDA system appears smooth and featureless under scanning electron microscopy (SEM), while that of the DOMS/MDA system with smectic LC phase exhibits an extremely rough and highly deformed fracture surface, suggesting significant bulk plastic deformation. The author proposed that when a crack tip approaches a single LC domain, neighboring domains can deform and undergo significant plastic deformation, leading to slow, stable crack propagation and an increased fracture toughness for the LCER system. Harada *et al.* investigated the fracture behavior of a LCER system based on diglycidyl ether of terephthalylidene-bis-(4-amino-3-methlphenol) (DGETAM) and m-phenylenediamine (MDA) using polarized infrared spectrum [96]. They found that the system cured in smectic phase shows improved fracture toughness, which is attributed to the extension of crack propagation and reorientation of the network chains near the propagated crack.

Another interesting and important feature of LCERs is their ability to be oriented under mechanical [87, 97-99], electric [100, 101], or magnetic fields [102-107]. The alignment results in a material with anisotropic physical and mechanical properties, offering opportunities to create materials with improved tailorability. Shiota *et al.* synthesized a LCER based on phenyl benzoate mesogens and cured it with SAA under an applied ac electric fields. It was found that the LC molecules align parallel to the electric field below 10 kHz, while the molecules align normal to the electric field above 20 kHz. Similar results were also observed by Korner *et al.* for a liquid crystalline dicyanate system

[108]. They found that the dielectric anisotropy of an aligned LC and its interaction with an ac field depends on both frequency and temperature. The dielectric permittivity parallel to the molecular long axis changes with frequency, whereas the perpendicular dielectric permittivity is almost constant, leading to a frequency threshold at which the LC molecules changes their orientation. Liquid crystals also can be aligned under magnetic fields. Benicewicz *et al.* examined the effect of magnetic field strength on the orientation of a LCER formed from the reaction between DOMS and SAA [109]. They found that the oriented LCER exhibits a smectic LC phase with the layer normal parallel to the field direction and shows a maximum degree of orientation approximately 0.8 at a field strength of 12 Tesla. Due to the anisotropy of diamagnetic susceptibility and cooperative motion of LC molecules, they tend to aligned themselves along the magnetic field direction. The use of magnetic field to orient LCERs has several advantages over force field and electric field. For example, the effect field strength remains relatively constant when bulk samples are cured.

Other properties of LCERs, such as dielectric properties [110, 111], thermal stability [112], and moisture resistance [113] have also been investigated by a number of researchers. The unique structure and excellent properties of LCERs make them attractive candidates for matrices in FRPs for high performance applications.

1.5 References

[1] High-Performance Structural Fibers for Advanced Polymer Matrix Composites: The National Academies Press, 2005.

[2] Jose JP and Joseph K. Advances in Polymer Composites: Macro- and Microcomposites – State of the Art, New Challenges, and Opportunities. Polymer Composites: Wiley-VCH Verlag GmbH & Co. KGaA, 2012. pp. 1-16.

[3] Nairn JA and Zoller P. Journal of Materials Science 1985;20(1):355-367.

[4] Gascoigne HE. Experimental Mechanics 1994;34(1):27-36.

[5] DiLandro L and Pegoraro M. Composites Part A-Applied Science and Manufacturing 1996;27(9):847-853.

[6] Cowley KD and Beaumont PWR. Composites Science and Technology 1997;57(11):1445-1455.

[7] Hancox NL. Materials & Design 1998;19(3):85-91.

[8] Going to Extremes: Meeting the Emerging Demand for Durable Polymer Matrix Composites: The National Academies Press, 2005.

[9] Chung DDL. Carbon Fiber Composites: Butterworth-Heinemann, 1994.

[10] Composites CHPSFAPM, Board NMA, Sciences DEP, and Council NR. High-Performance Structural Fibers for Advanced Polymer Matrix Composites: National Academies Press, 2005.

[11] Dorey G. Journal of Physics D-Applied Physics 1987;20(3):245-256.

[12] Ruland W. Advanced Materials 1990;2(11):528-536.

[13] Chand S. Journal of Materials Science 2000;35(6):1303-1313.

[14] Frank E, Hermanutz F, and Buchmeiser MR. Macromolecular Materials and Engineering 2012;297(6):493-501.

[15] D'Amore A and Zarrelli M. Composite Materials. Encyclopedia of Polymer Science and Technology: John Wiley & Sons, Inc., 2002.

[16] Gennes PGd and Prost J. The Physics of Liquid Crystals: Clarendon Press, 1995.

[17] Douglas EP. Liquid Crystalline Thermosets. Encyclopedia of Polymer Science and Technology: John Wiley & Sons, Inc., 2002.

[18] Barclay GG and Ober CK. Progress in Polymer Science 1993;18(5):899-945.

[19] Shiota A and Ober CK. Progress in Polymer Science 1997;22(5):975-1000.

[20] Carfagna C, Amendola E, and Giamberini M. Progress in Polymer Science 1997;22(8):1607-1647.

[21] Giamberini M, Amendola E, and Carfagna C. Molecular Crystals and Liquid Crystals Science and Technology Section A-Molecular Crystals and Liquid Crystals 1995;266:9-22.

[22] Mallon JJ and Adams PM. Journal of Polymer Science Part A-Polymer Chemistry 1993;31(9):2249-2260.

[23] Jahromi S, Lub J, and Mol GN. Polymer 1994;35(3):622-629.

[24] Hikmet RAM and Broer DJ. Polymer 1991;32(9):1627-1632.

[25] Hikmet RAM, Lub J, and Vanderbrink PM. Macromolecules 1992;25(16):4194-4199.

[26] Litt MH, Whang WT, Yen KT, and Qian XJ. Journal of Polymer Science Part A-Polymer Chemistry 1993;31(1):183-191.

[27] Holter D, Frey H, Mulhaupt R, and Klee JE. Macromolecules 1996;29(22):7003-7011.

[28] Hoyt AE and Benicewicz BC. Journal of Polymer Science Part A-Polymer Chemistry 1990;28(12):3403-3415.

[29] Hoyt AE and Benicewicz BC. Journal of Polymer Science Part A-Polymer Chemistry 1990;28(12):3417-3427.

[30] Barclay GG, Ober CK, Papathomas KI, and Wang DW. Macromolecules 1992;25(11):2947-2954.

[31] Mormann W and Zimmermann J. Liquid Crystals 1995;19(2):227-233.

[32] Mormann W and Zimmermann JG. Macromolecules 1996;29(4):1105-1109.

[33] Mormann W and Kuckertz C. Macromolecular Chemistry and Physics 1998;199(5):845-851.

[34] Hahn HT. Journal of Composite Materials 1976;10(OCT):266-278.

[35] Kim KS and Hahn HT. Composites Science and Technology 1989;36(2):121-132.

[36] White SR and Hahn HT. Journal of Composite Materials 1992;26(16):2402-2422.

[37] White SR and Hahn HT. Journal of Composite Materials 1992;26(16):2423-2453.

[38] Parlevliet PP, Bersee HEN, and Beukers A. Composites Part A-Applied Science and Manufacturing 2006;37(11):1847-1857.

[39] Parlevliet PP, Bersee HEN, and Beukers A. Composites Part A-Applied Science and Manufacturing 2007;38(6):1581-1596.

[40] White SR and Hahn HT. Journal of Composite Materials 1993;27(14):1352-1378.

[41] Kim SS, Murayama H, Kageyama K, Uzawa K, and Kanai M. Composites Part a-Applied Science and Manufacturing 2012;43(8):1197-1202.

[42] Tavakol B, Roozbehjavan P, Ahmed A, Das R, Joven R, Koushyar H, Rodriguez A, and Minaie B. Journal of Applied Polymer Science 2013;128(2):941-950.

[43] Gopal AK, Adali S, and Verijenko VE. Composite Structures 2000;48(1-3):99-106.

[44] Wang S, Liang Z, Gonnet P, Liao YH, Wang B, and Zhang C. Advanced Functional Materials 2007;17(1):87-92.

[45] Badrinarayanan P, Rogalski MK, and Kessler MR. Acs Applied Materials & Interfaces 2012;4(2):510-517.

[46] Shokrieh MM, Daneshvar A, Akbari S, and Chitsazzadeh M. Carbon 2013;59:255-263.

[47] Choi EJ, Ahn HK, Lee JK, and Jin JI. Polymer 2000;41(21):7617-7625.

[48] Lee JY and Jang JS. Journal of Polymer Science Part A-Polymer Chemistry 1999;37(4):419-425.

[49] Mihara T, Nishimiya Y, and Koide N. Journal of Applied Polymer Science 1998;68(12):1979-1990.

[50] Lee JY and Jang JS. Polymer 2006;47(9):3036-3042.

[51] Mormann W, Broche M, and Schwarz P. Macromolecular Chemistry and Physics 1997;198(11):3615-3626.

[52] Mormann W and Brocher M. Macromolecular Chemistry and Physics 1996;197(6):1841-1851.

[53] Lee JY, Jang JS, Hwang SS, Hong SM, and Kim KU. Polymer 1998;39(24):6121-6126.

[54] Broer DJ, Lub J, and Mol GN. Macromolecules 1993;26(6):1244-1247.

[55] Su WFA, Chen KC, and Tseng SY. Journal of Applied Polymer Science 2000;78(2):446-451.

[56] Carfagna C, Amendola E, and Giamberini M. Macromolecular Chemistry and Physics 1994;195(7):2307-2315.

[57] Lee JY, Jang JS, Hong SM, Hwang SS, and Kim KU. Polymer 1999;40(11):3197-3202.

[58] Barclay GG, Ober CK, Papathomas KI, and Wang DW. Journal of Polymer Science Part a-Polymer Chemistry 1992;30(9):1831-1843.

[59] Shiota A and Ober CK. Journal of Polymer Science Part A-Polymer Chemistry 1996;34(7):1291-1303.

[60] Lee JY and Jang JS. Journal of Polymer Science Part A-Polymer Chemistry 1998;36(6):911-917.

[61] Lee JY. Polymer Bulletin 2006;57(6):983-988.

[62] Lee JY, Shim MJ, and Kim SW. Journal of Applied Polymer Science 2002;83(11):2419-2425.

[63] Ochi M, Shimizu Y, Nakanishi Y, and Murata Y. Journal of Polymer Science Part B-Polymer Physics 1997;35(2):397-405.

[64] Carfagna C, Amendola E, and Giamberini M. Composite Structures 1994;27(1-2):37-43.

[65] Carfagna C, Amendola E, Giamberini M, Filippov AG, and Bauer RS. Liquid Crystals 1993;13(4):571-584.

[66] Liu GD, Gao JG, Song LL, Hou WJ, and Zhang LC. Macromolecular Chemistry and Physics 2006;207(23):2222-2231.

[67] Shiota A and Ober CK. Polymer 1997;38(23):5857-5867.

[68] Harada M, Ando J, Hattori S, Sakurai S, Sakamoto N, Yamasaki T, Masunaga H, and Ochi M. Polymer Journal 2013;45(1):43-49.

[69] Lin QH, Yee AF, Earls JD, Hefner RE, and Sue HJ. Polymer 1994;35(12):2679-2682.

[70] Lu MG, Shim MJ, and Kim SW. Macromolecular Chemistry and Physics 2001;202(2):223-230.

[71] Lin QH, Yee AF, Sue HJ, Earls JD, and Hefner RE. Journal of Polymer Science Part B-Polymer Physics 1997;35(14):2363-2378.

[72] Cho SH and Douglas EP. Macromolecules 2002;35(11):4550-4552.

[73] Cho S, Douglas EP, and Lee JY. Polymer Engineering and Science 2006;46(5):623-629.

[74] Amendola E, Carfagna C, Giamberini M, and Pisaniello G. Macromolecular Chemistry and Physics 1995;196(5):1577-1591.

[75] Micco G, Giamberini M, Amendola E, Carfagna C, and Astarita G. Industrial & Engineering Chemistry Research 1997;36(8):2976-2983.

[76] Liu GD, Zhou B, Zhao DM, Li Q, and Gao JG. Macromolecular Chemistry and Physics 2008;209(11):1160-1169.

[77] Lee JY, Song YW, and Shim MJ. Journal of Industrial and Engineering Chemistry 2004;10(4):601-607.

[78] Cai ZQ, Sun JZ, Wang DD, and Zhou QY. Journal of Polymer Science Part A-Polymer Chemistry 2007;45(17):3922-3928.

[79] Liu YL, Cai ZQ, Wen XF, Pi PH, Zheng DF, Cheng JA, and Yang ZR. Thermochimica Acta 2011;513(1-2):88-93.

[80] Lee JY, Shim MJ, Lee HK, and Kim SW. Journal of Applied Polymer Science 2001;82(10):2372-2380.

[81] Zhang YX and Vyazovkin S. Polymer 2006;47(19):6659-6663.

[82] Mititelu A, Hamaide T, Novat C, Dupuy J, Cascaval CN, Simionescu BC, and Navard P. Macromolecular Chemistry and Physics 2000;201(12):1209-1213.

[83] Rosu D, Mititelu A, and Cascaval CN. Polymer Testing 2004;23(2):209-215.

[84] Punchaipetch P, Ambrogi V, Giamberini M, Brostow W, Carfagna C, and D'Souza NA. Polymer 2001;42(5):2067-2075.

[85] Liu JP, Wang CC, Campbell GA, Earls JD, and Priester RD. Journal of Polymer Science Part A-Polymer Chemistry 1997;35(6):1105-1124.

[86] Vyazovkin S, Mititelu A, and Sbirrazzuoli N. Macromolecular Rapid Communications 2003;24(18):1060-1065.

[87] Shiota A and Ober CK. Journal of Polymer Science Part B-Polymer Physics 1998;36(1):31-38.

[88] Robinson EJ, Douglas EP, and Mecholsky JJ. Polymer Engineering and Science 2002;42(2):269-279.

[89] Harada M, Watanabe Y, Tanaka Y, and Ochi M. Journal of Polymer Science Part B-Polymer Physics 2006;44(17):2486-2494.

[90] Harada M, Sumitomo K, Nishimoto Y, and Ochi M. Journal of Polymer Science Part B-Polymer Physics 2009;47(2):156-165.

[91] Liu YL, Cai ZQ, Wang WC, Wen XF, Pi PH, Zheng DF, Cheng JA, and Yang ZR. Macromolecular Materials and Engineering 2011;296(1):83-91.

[92] Harada M, Aoyama K, and Ochi M. Journal of Polymer Science Part B-Polymer Physics 2004;42(22):4044-4052.

[93] Douglas EP. Polymer Reviews 2006;46(2):127-141.

[94] Punchaipetch P, Ambrogi V, Giamberini M, Brostow W, Carfagna C, and D'Souza A. Polymer 2002;43(3):839-848.

[95] Ortiz C, Kim R, Rodighiero E, Ober CK, and Kramer EJ. Macromolecules 1998;31(13):4074-4088.

[96] Harada M, Okamoto N, and Ochi M. Journal of Polymer Science Part B-Polymer Physics 2010;48(22):2337-2345.

[97] Barclay GG, McNamee SG, Ober CK, Papathomas KI, and Wang DW. Journal of Polymer Science Part A-Polymer Chemistry 1992;30(9):1845-1853.

[98] Lee JY. Journal of Applied Polymer Science 2006;102(1):684-689.

[99] Lee JY and Jang J. Polymer Bulletin 2007;59(2):261-267.

[100] Shiota A and Ober CK. Macromolecules 1997;30(15):4278-4287.

[101] Koerner H, Ober CK, and Ku H. Polymer 2011;52(10):2206-2213.

[102] Tan CB, Sun H, Fung BM, and Grady BP. Macromolecules 2000;33(17):6249-6254.

[103] Lincoln DM and Douglas EP. Polymer Engineering and Science 1999;39(10):1903-1912.

[104] Harada M, Ochi M, Tobita M, Kimura T, Ishigaki T, Shimoyama N, and Aoki H. Journal of Polymer Science Part B-Polymer Physics 2004;42(5):758-765.

[105] Jahromi S, Kuipers WAG, Norder B, and Mijs WJ. Macromolecules 1995;28(7):2201-2211.

[106] Jahromi S. Macromolecules 1994;27(10):2804-2813.

[107] Pottie L, Costa-Torro F, Tessier M, Davidson P, and Fradet A. Liquid Crystals 2008;35(8):913-924.

[108] Korner H, Shiota A, Bunning TJ, and Ober CK. Science 1996;272(5259):252-255.

[109] Benicewicz BC, Smith ME, Earls JD, Priester RD, Setz SM, Duran RS, and Douglas EP. Macromolecules 1998;31(15):4730-4738.

[110] Lee JY, Song YW, Kim SW, and Lee HK. Materials Chemistry and Physics 2003;77(2):455-460.

[111] Lu MG, Shim MJ, and Kim SW. Journal of Applied Polymer Science 2000;77(7):1568-1573.

[112] Vincent L, Mija A, and Sbiffazzuoli N. Polymer Degradation and Stability 2007;92(11):2051-2057.

[113] Nie L, Burgess A, and Ryan A. Macromolecular Chemistry and Physics 2013;214(2):225-235.

CHAPTER 2. LIQUID CRYSTALLINE EPOXY RESIN BASED ON BIPHENYL MESOGEN: THERMAL CHARACTERIZATION

A paper published in *Polymer*[1]

Yuzhan Li[2], Prashanth Badrinarayanan[3], Michael R. Kessler[4,5]

2.1 Abstract

An epoxy monomer of 4,4'-diglycidyloxybiphenyl (BP) was synthesized and cured with a tetra-functional amine, sulfanilamide (SAA), to produce novel liquid crystalline epoxy resins (LCERs). The thermal properties, liquid crystalline morphologies, and cure behavior of the monomer were studied using differential scanning calorimetry, wide angle X-ray diffraction, and polarized optical microscopy. The effects of curing condition on the glass transition temperature, coefficient of thermal expansion, and dynamic mechanical properties of the resins were determined through thermomechanical analysis and dynamic mechanical analysis, respectively. The effects of cure condition on the formation of the liquid crystalline phase were also examined. The results show that BP is not a liquid crystalline epoxy monomer and an irreversible crystal transition exists in the temperature range of 120 ºC -140 ºC. The use of SAA results in the formation of a smectic liquid crystalline phase. Compared to the resins cured into an amorphous network, the LCERs

---

[1] Reprinted with permission of *Polymer*, 2013, 54(12), 3017-3025.
[2] Graduate student, Department of Materials Science and Engineering, Iowa State University
[3] Research scientist, DuPont
[4] Professor and Director, School of Mechanical and Materials Engineering, Washington State University
[5] Author for correspondence

exhibited a polydomain structure with individual liquid crystalline domain distributed in the resin matrix, which results in better thermomechanical properties.

2.2 Introduction

Liquid crystalline thermosets (LCTs) are a unique class of thermosetting materials formed upon curing of low molecular weight, rigid rod, multifunctional monomers resulting in the retention of a liquid crystalline phase by the three dimensional crosslinking networks. A great number of LCTs based on different functional end groups have been synthesized and studied [1-3], including epoxy [4-9], acrylate [10-12], maleimide [13, 14], and cyanate ester [15, 16]. Liquid crystalline epoxy resins (LCERs) are of great interest to scientists and engineers and have been investigated because of their unique properties, e.g. low shrinkage upon curing, good thermal stability, and excellent thermomechanical properties [17-20]. Furthermore, one of the drawbacks of traditional epoxy resins, their brittleness, which severely limits their applications, can be improved by introducing liquid crystalline (LC) domains into the amorphous matrix [21-25]. Unlike other toughening methods such as incorporating rubber particles, the presence of LC domains will not lead to a decrease in the glass transition temperature (T_g) or moduli of the material. These desirable properties make LCERs good candidates for a wide range of potential applications, such as optical switches, electronic packaging, and matrices for high performance composites.

Su and coworkers synthesized a main-chain LCER using biphenyl mesogen and studied the effects of chemical structure changes on the thermal and mechanical properties of the resin [26, 27]. Robinson and coworkers reported a methylstilbene based LCER which

exhibited better fracture toughness compared to the same resin cured in amorphous phase [28]. A liquid crystalline phase time-temperature-transformation diagram was also constructed by studying the gelation and vitrification point using oscillatory parallel plate rheology [29, 30]. Barclay and coworkers investigated the alignment of a methylstilbene based LCER by applying high strength magnetic field upon curing [31, 32]. The resulting resin showed a substantial reduction in the coefficient of thermal expansion (CTE) in the direction of orientation compared to the unaligned samples. While the thermal and mechanical properties of various LCERs have been reported, several fundamental aspects including the nature of LC formation and the thermomechanical properties of fully cured LCERs are still not fully understood.

In this paper, the LC properties and curing behavior of an epoxy resin are examined extensively. The influence of curing condition on the formation of LC phase is investigated. In addition, the LC phase of fully cured resins is characterized using various experimental techniques. The glass transition temperature, dynamic mechanical properties, and thermal expansivity of the resins cured in LC and non-LC state are examined systematically.

2.3 Experimental

2.3.1 Materials

4,4’-dihydroxybiphenyl with 97% purity, benzyltrimethylammonium bromide, and sulfanilamide (SAA) were purchased from Sigma-Aldrich (Milwaukee, WI). Epichlorohydrin with 99% purity was obtained from Acros Organics (Belgium). Sodium hydroxide, isopropyl alcohol, chloroform, methanol, hydrochloric acid, and acetone were supplied by Fisher Scientific (Fair Lawn, NJ). All chemicals were used as received without

further purification.

2.3.2 Synthesis of 4,4’-diglycidyloxybiphenyl (BP)

The epoxy monomer was synthesized according to a procedure reported in an earlier work by Su and coworkers [27]. A mixture of 4,4’-dihydroxybiphenyl (57.26g), benzyltrimethylammonium bromide (2.09g) and epichlorohydrin (481ml) was placed in a three-neck flask and refluxed for 40 min. NaOH (24.6g) was dissolved in 139ml of water to prepare 15% NaOH aqueous solution. Then the solution was added into the flask dropwise over a period of 3 hours under reflux. The reaction was carried out for an additional hour at room temperature. The excess epichlorohydrin was removed by vacuum distillation and the final product was washed with water and methanol. A white powder was obtained by recrystallization from isopropyl alcohol and chloroform.

2.3.3 Sample preparation and curing process

Uncured resin samples were prepared by dissolving BP and SAA in tetrahydrofuran (THF) in a stoichiometric ratio. Then the solvent was removed at room temperature and the mixture was dried under vacuum for 24 hours to prevent further reaction. To study the curing behavior, the mixture was loaded into aluminum differential scanning calorimeter (DSC) pans and hermetically sealed. A small hole was made in the center of the lids to prevent pressure buildup. To study the thermomechanical properties of fully cured resins, the samples were cured in a convection oven at 170 ºC, 180 ºC, 190 ºC, and 200 ºC for 12 hours and post-cured at 230 ºC for 2 hour.

2.3.4 Characterization of BP and fully cured resins

The chemical structure of BP was characterized using fourier transform infrared spectroscopy (FTIR) and nuclear magnetic resonance (NMR). The FTIR spectrum was recorded on a Bruker's IFS66V FTIR with a resolution of 2 cm^{-1} from 400 to 4000 cm^{-1} at room temperature. The characteristic peaks at 2927 cm^{-1}, 1606 cm^{-1}, 1500 cm^{-1}, 1244 cm^{-1}, 1037 cm^{-1} and 910 cm^{-1} can be assigned to the stretching of (CH_2), stretching of (C=C), bending of (C=C), stretching of (C-O) on aromatic rings, stretching of (C-O) on aliphatic chain, and epoxy group, respectively. The ^1H NMR spectrum was obtained by means of a Varian VXR-300 NMR instrument at room temperature, in the presence of $CDCl_3$ as the solvent. ^1H NMR (CDCl3): δ2.78(2H, dd, CH_2 of epoxy), δ2.93(2H, dd, CH_2 of epoxy), δ3.38(2H, m, CH of epoxy), δ4.01(2H, CH_2 dd, of glycidyl), δ4.25(2H, dd, CH_2 of glycidyl), δ6.96(4H, d, biphenyl), δ7.45(4H, d, biphenyl).

The epoxy equivalent weight (EEW) of BP was determined by titration using the hydrohalogenation method. Concentrated hydrochloric acid was added into dimethylformamide to produce hydrochlorination reagent. Cresol red solution was used as acid-base indicator and was prepared by dissolving cresol red in a mixture of acetone and distilled water. A small amount of BP was dissolved in the hydrochlorination reagent. Then the excess acid was titrated with a 0.1N sodium hydroxide solution. The EEW was found to be 170.6, which is consistent with the value previously reported by Su [27]. The chemical structures of the epoxy monomer and the curing agent are illustrated in Figure 2.1.

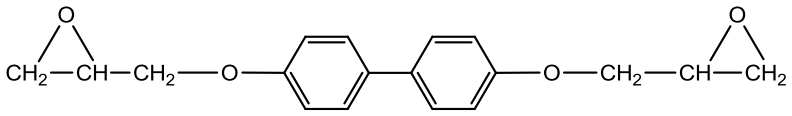

4,4’-diglycidyloxybiphenyl (BP)

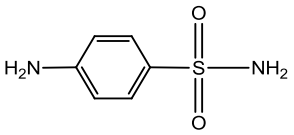

Sulfanilamide (SAA)

Figure 2.1 Chemical structures of the epoxy monomer and the curing agent.

The thermal properties of BP and the fully cured resins were studied using a Q2000 DSC (TA Instruments, Inc.). The DSC cell was purged with helium gas at a flow rate of 25 mL/min. The epoxy monomer was tested at a heating and cooling rate of 10 ºC /min. For the fully cured resins, the first heating scan was used to erase the thermal history. While the second heating scan was recorded to evaluate T_g.

To study the curing behavior, the mixture of BP and SAA was loaded into a hermetic aluminum DSC pan then sealed with a lid. A series of isothermal cure studies were carried out using a Q20 DSC (TA Instruments, Inc.). The DSC cell was purged with nitrogen gas at a flow rate of 50 mL/min. The samples were cured at 150 ºC, 160 ºC, 170 ºC, 180 ºC, 190 ºC, 200 ºC, and 210 ºC for 180 minutes respectively.

Morphologies of BP were investigated using a polarized optical microscope (POM) from Olympus (model BX51-TRF equipped with a Linkam LTS-350 hot stage and TMS-94 temperature controller). Small amounts of BP (2~3mg) was pre-melted on a microscope slide then covered with a piece of cover glass to form a uniform thin film. The samples

were heated and cooled repeatedly from room temperature to 170 ºC at a rate of 1ºC/min to investigate the change of birefringence. The isothermal cure of BP with SAA was also monitored using POM. The formation and development of the LC phase were examined under polarized light.

Wide angle X-ray diffraction (WAXD) was used to explore the crystal structure of BP and the fully cured LCERs. For the epoxy monomer, a high temperature XRD experiment was carried out using Rigaku Rint 2000 diffractometer equipped with a high temperature furnace. The diffraction patterns were collected at 30 ºC, 100 ºC, 140 ºC on heating process and 100 ºC, 30 ºC on cooling process respectively with a Zr-filtered MoKα radiation. In the experiment, a platinum plate was used as a sample holder, and the scan rate was 0.15º/min over a scan angle from 0º to 40º. For the fully cured resins, the diffraction patterns were collected using Scintag XDS2000 powder diffractometer with Kevex Peltier cooled silicon detector and Ni-filtered CuKα radiation. The scan rate was 2º/min over a scan angle from 0º to 40º.

Dynamic mechanical properties of the fully cured resins were studied using a model Q800 dynamic mechanical analyzer (DMA, TA Instruments, Inc.). All the samples were heated from room temperature to 280 ºC at 3 ºC/min, at 1Hz frequency and 25μm amplitude in three-point bending mode.

The coefficient of thermal expansion (CTE) of the fully cured resins was measured with a model Q400 thermomechanical analyzer (TMA, TA Instruments, Inc.) in expansion mode with a heat-cool-heat cycle at a rate of 5 ºC/min-3 ºC/min-3 ºC/min. The second heating scan was recorded to calculate the value of CTE.

Thermal stability of the fully cured LCERs was investigated using thermogravimetric

analyzer (TGA) on a model Q50 TGA (TA Instruments, Inc.). About 10 mg of resins was placed in an alumina pan and heated from room temperature to 800 ºC at a rate of 20 ºC/min under an air purge of 60 mL/min.

2.4 Results and discussion

2.4.1 Thermal behavior and morphologies of BP

The DSC thermogram of the epoxy monomer is shown in Figure 2.2. Two endothermic peaks were observed in the first heating scan, while in the second heating scan, the first peak was absent. The second peak and the shoulder attached are the melting of BP and its low molecular weight fraction, which was confirmed by Gel permeation chromatography studies.

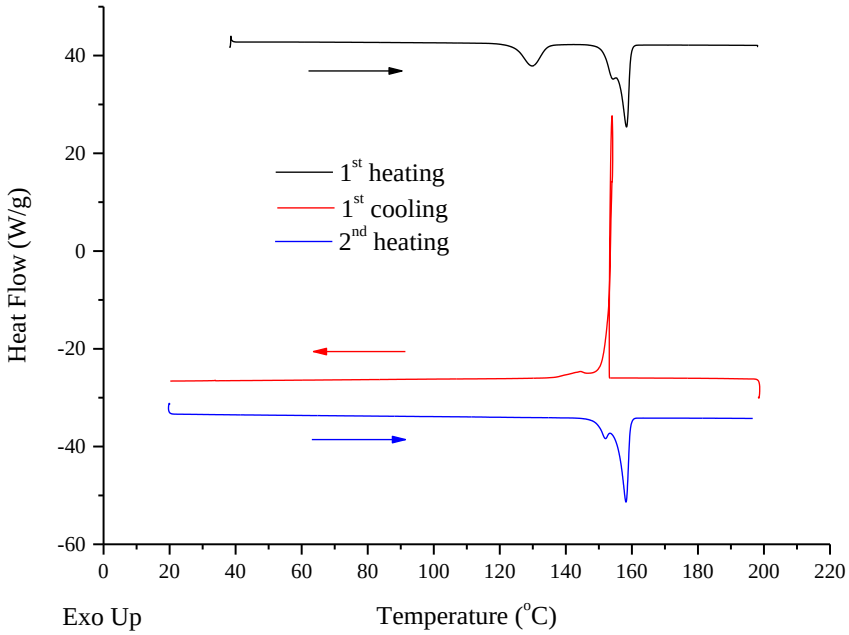

Figure 2.2 DSC thermograms of BP.

The monomer was further studied using NMR and high temperature XRD to explore the different thermal behavior in the first and second heating DSC scans. In order to study the effect of the small endothermic peak in the first heating DSC scan on the chemical structure of BP, room temperature NMR spectra of the monomer dried at 100 ºC and 140 ºC were collected and compared. As shown in Figure 2.3, the two NMR spectra have identical peak position and area, indicating that the small endothermic peak in the DSC curve does not have any influence on the chemical structure of the monomer. A change of crystal structure could be a possible explanation for the different thermal behavior observed in the DSC scans.

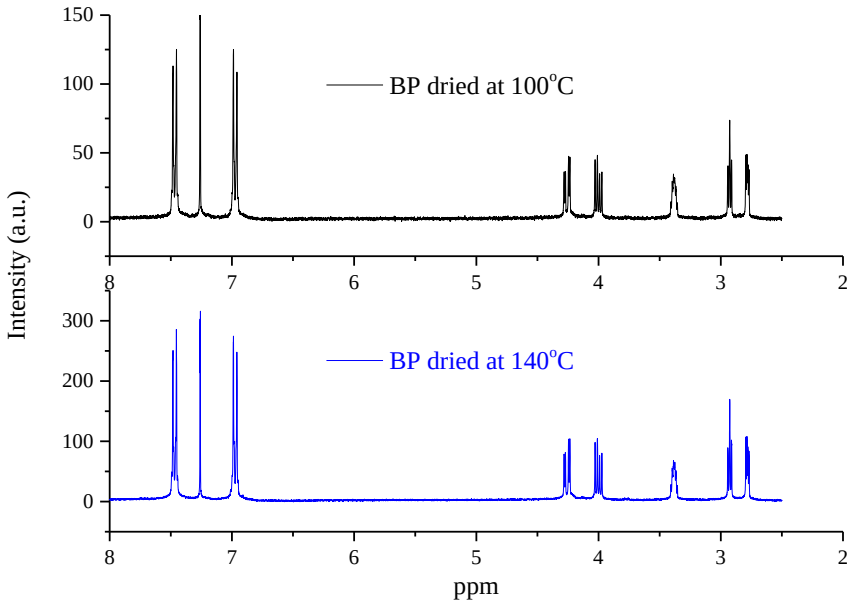

Figure 2.3 NMR spectra of BP after drying at 100ºC and 140ºC respectively.

A high temperature XRD experiment was carried to explore the possibility of a structural change. The full diffraction patterns are shown in Figure 2.4. The peaks at around

18º, 21º, 29º, 35º, and 36º are the diffraction from platinum sample holder. The shape and position of these peaks remains essentially identical. The slight shift is due to the change of lattice parameter of platinum at different temperatures. However, for the peaks in the region highlighted with dotted line, a distinct change of peak shape and position can be seen, which indicates that the crystal structure of BP at 100 ºC and 140 ºC are different. Furthermore, this crystal structure transition is irreversible, which is in agreement with the DSC data. Nevertheless, we were unable to identify the exact crystal structure of BP since it is not a pure compound. Based on the DSC and XRD data, we could conclude that the small endothermic peak in the first heating DSC scan is related to the change of crystal structure of BP and the transition process is irreversible.

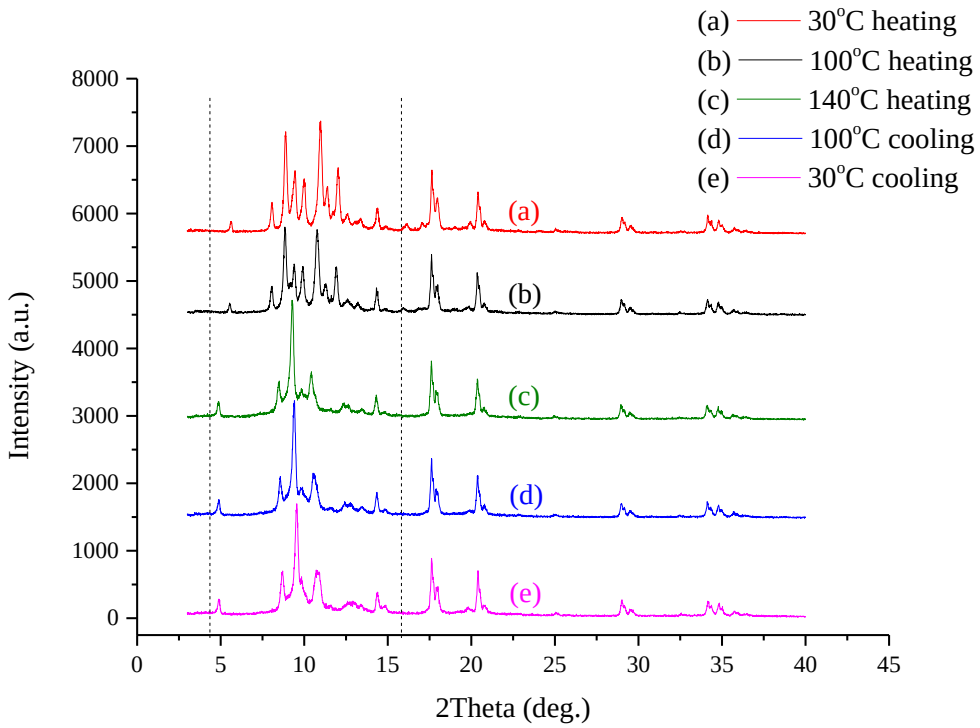

Figure 2.4 XRD spectra of BP upon heating and cooling. (a) 30ºC on heating; (b) 100ºC on heating; (c) 140ºC on heating; (d) 100ºC on cooling; (e) 30ºC on cooling.

The thermal behavior of BP is not well understood and there are differing reports in the literature regarding the LC behavior of this monomer. For example, Su and coworkers reported a smectic LC phase in the temperature range of 128-153 ºC when the monomer was heated, while Lee and coworkers were not able to detect any LC phase upon heating but observed a smectic LC phase on cooling of the monomer from the isotropic state [27, 33].

In order to clarify the LC properties of BP, we examined the morphologies at different temperatures under polarized light since it is well known that POM is a powerful tool for characterization of LC phases. POM results shown in Figure 2.5 indicate that the monomer starts to melt at 158 ºC, in a good agreement with the DSC data. At 164 ºC, all the crystallites are melted and the POM image is completely dark. In the cooling process, small crystallites start to grow at about 162 ºC and morphologies of the crystallites do not change much after 154 ºC. Nematic LC phase usually displays schlieren texture while smectic LC phase usually shows a fan-shaped focal-conic texture. In our studies, no LC birefringence can be observed under polarized light in both heating and cooling processes, indicating that BP is not a LC epoxy monomer.

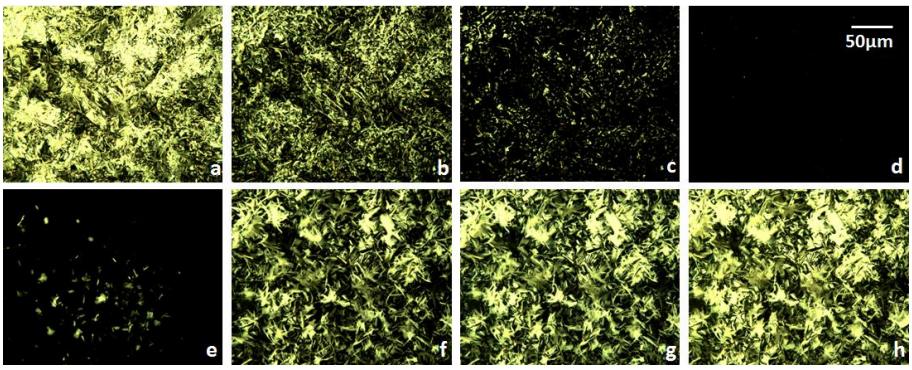

Figure 2.5 POM images of BP upon heating and cooling.
Heating process: (a) 25 ºC, (b) 158 ºC, (c) 162 ºC, (d) 164 ºC.
Cooling process: (e) 162 ºC, (f) 158 ºC, (g) 154 ºC, (h) 25 ºC.

2.4.2 Curing behavior and LC properties of the resins

A dynamic DSC scan was performed to study the reaction heat, onset temperature, and peak temperature of the curing reaction, which is important for determining the isothermal curing conditions. As shown in the DSC dynamic scan in Figure 2.6, the exothermic curing reaction of BP and SAA starts immediately after the endothermic melting of the two components. The curing reaction has a wide temperature range from 150 ºC to 260 ºC. When the temperature exceeds 260 ºC, the resin starts to decompose, which is indicated by the onset of an exothermic peak shown in the DSC thermogram.

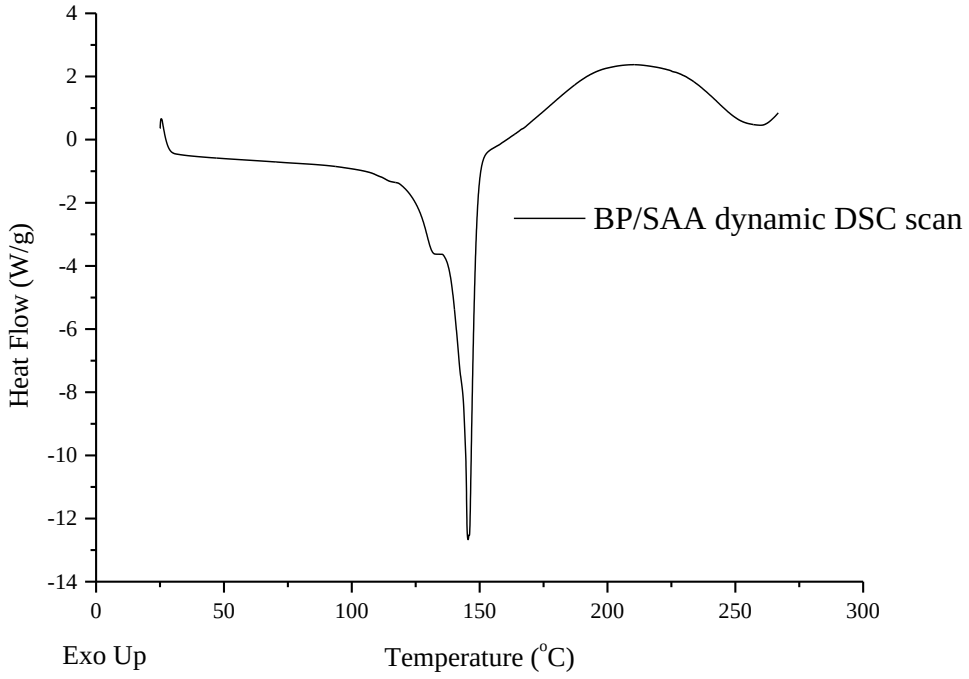

Figure 2.6 Dynamic DSC curing study of BP with SAA.

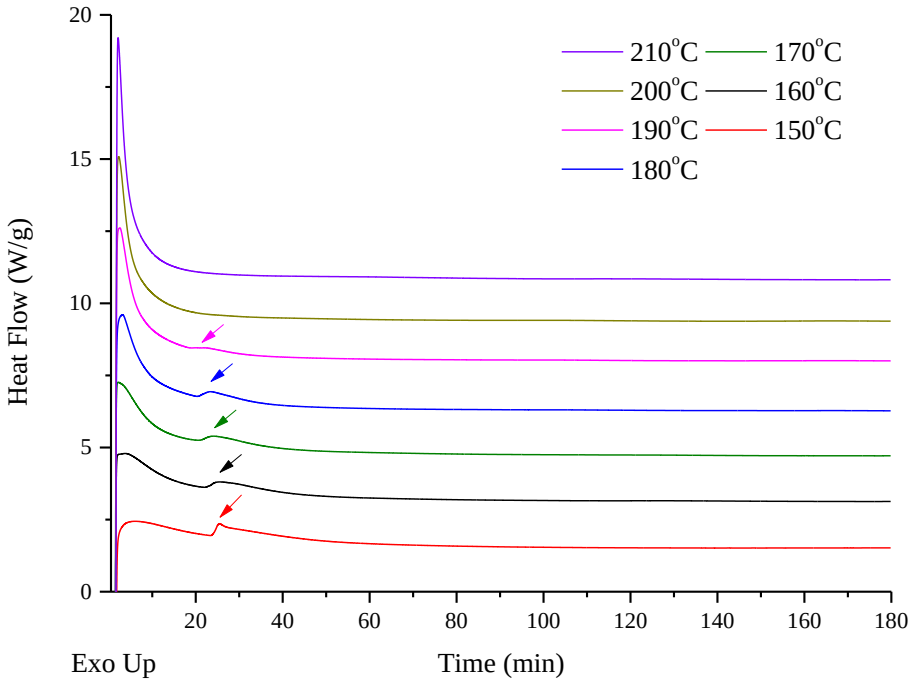

Figure 2.7 Isothermal DSC curing study of BP with SAA at different temperatures.

Figure 2.7 shows a series of isothermal DSC curing studies of uncured resins. An additional exothermic peak indicated by arrows in the figure was observed for cure temperatures from 150 ºC to 190 ºC. For cure temperatures of 200 ºC and higher, this peak was absent. Similar results have been reported by Carfagna and coworkers for 4,4'-dihydroxy-α-methylstilbene (DOMS) and 2,4-Diaminotoluene (DAT) system [34]. The first exothermic peak represents the reaction between the first epoxy group of the monomer and the aromatic amine group of the curing agent. SAA is a tetra-functional curing agent and the two amine groups have different reactivity. The aromatic amine tends to react first due to the electron donating effect of the benzene ring, which results in an extension of the pre-polymer chain. If the cure temperatures can be properly chosen, the chain will keep

growing without extensive branching. According to Flory's lattice theory of liquid crystalline polymers, when the aspect ratio of the polymer chain is greater than 6.4, the LC phase will be relatively stable and can be detected by POM or other experimental techniques [35]. In our case, for cure temperatures from 150 ºC to 190 ºC, the curing reaction does not proceed fast; therefore the pre-polymer chain has enough time to extend. After a certain period of time, LC phase becomes more stable with respect to the isotropic phase. At this time, the resins change from transparent to opaque, indicating the existence of the LC phase.

Table 2.1 Effect of cure temperatures on the formation of LC phase.

Curing Temperature(ºC)	Time second peak appears(min)	Remarks
210 ºC	N/A	Non-LC
200 ºC	N/A	Non-LC
190 ºC	18.26	LC
180 ºC	20.29	LC
170 ºC	20.80	LC
160 ºC	22.17	LC
150 ºC	23.37	LC

The second exothermic peak in the isothermal DSC scans is a result of the rate acceleration of the cure reaction when the system undergoes a phase transition from amorphous phase to LC phase. Carfagna and coworkers reported a decrease of viscosity for DOMS/DAT system when the reacting medium was in the nematic LC phase [34]. Shiota and coworkers studied the smectic structure formation of a liquid crystalline epoxy

resin. The rate acceleration was also observed in isothermal DSC measurement and was attributed to a transition when the reacting medium changes from heterogeneous to homogeneous [36]. In the BP and SAA system examined in this work, the rate acceleration was observed for cure temperatures from 150 ºC to 190 ºC. At this stage of cure, the residual amine reacts with the epoxy group, leading to the formation of a crosslinked network. The LC phase formed previously is still present in the system so that it can be locked by the crosslinking process. At higher cure temperatures, reaction proceeds fast and the pre-polymer chain does not have time to extend. The crosslinking process happens before the aspect ratio of the polymer chain reaches the above mentioned critical value. The formation of the LC phase will be interrupted and the resins will be cured in the amorphous phase. This could explain the absence of the additional exothermic peak for cure temperatures higher than 200ºC.

The curing behavior and the LC properties of the resins were also studied using POM. Based on the DSC data, the isothermal temperature was fixed at 170 ºC and the whole curing process was recorded in the microscope to examine the formation of the LC phase. Figure 2.8 shows several POM images taken at different reaction times. All the pictures were taken from the same area of the same sample. The LC birefringence starts to appear after 19 minutes of the cure reaction, which is close to the time when the second exothermic peak starts to form in the DSC scan. The isothermal curing studies were also carried out for cure temperatures at 180 ºC, 190 ºC, and 200 ºC under POM. The sample was continuously heated at different temperatures for 2 hours to complete the cure reaction, and then morphologies of the fully cured resins were analyzed. The POM images are shown in Figure 2.9. The fan-shaped focal-conic texture for the cure temperatures from 170 ºC to

190 ºC in the figure is a characteristic of the smectic LC phase. The results prove that the LC phase formed in the early stage of the cure reaction has been successfully retained by the crosslinking networks. The results also show that as the cure temperature increases, the smectic LC phase gradually loses its fan-shaped focal-conic texture. For the cure temperature of 200 ºC, the POM image is completely dark, indicating the amorphous structure of the resin. The POM study also revealed that the resins cured in LC phase exhibit a polydomain structure with individual LC domain distributed in an amorphous resin matrix.

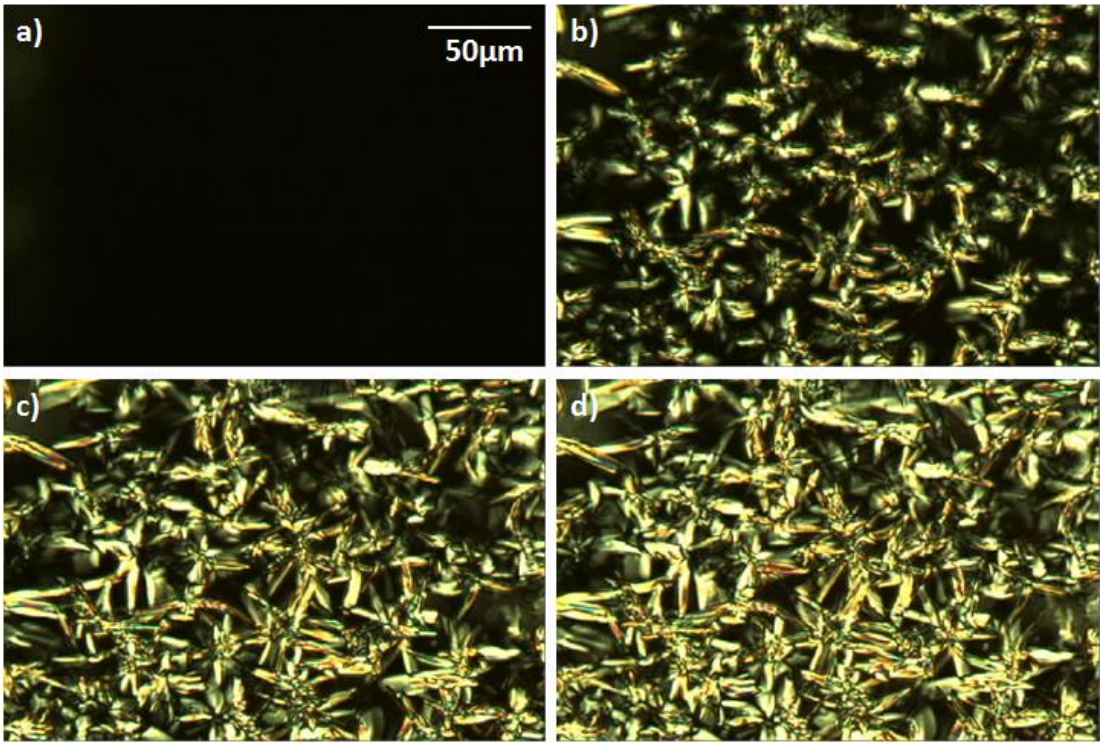

Figure 2.8 POM images of isothermal curing study of BP with SAA at 170 ºC.
(a) 18min; (b) 20min; (c) 22min; (d) 24min

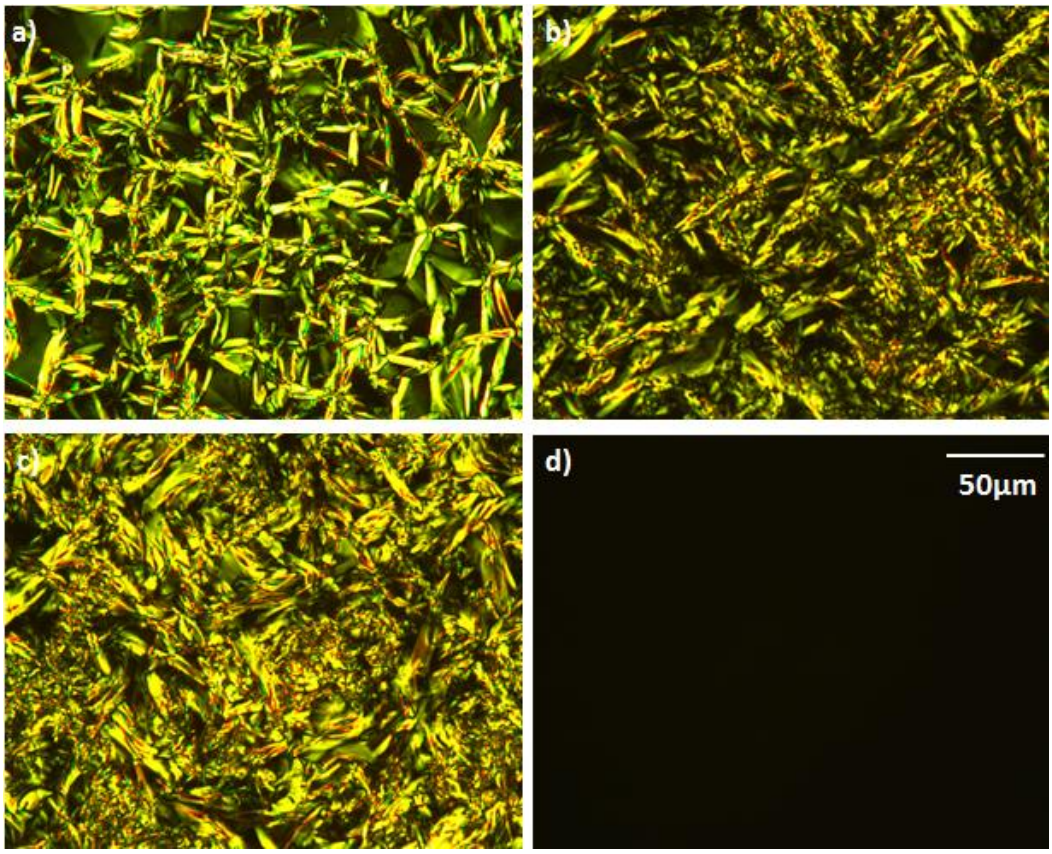

Figure 2.9 POM images after 2h of isothermal cure of BP with SAA at different temperatures. (a) 170 ºC; (b) 180 ºC; (c) 190 ºC; (d) 200 ºC

2.4.3 Thermal and mechanical properties of LCERs

Bulk samples were cured in a convection oven at 170 ºC, 180 ºC, and 190 ºC for 12 hours to produce LCERs with different LC content. Non-LCERs were also prepared by curing the resin at 200 ºC for 12 hours. After the initial cure, all the samples were post-cured at 230 ºC for 2 hours to complete the cure reaction as well as to relax any internal residual stress. A visual comparison between the resins cured at different temperatures is provided in Figure 2.10.

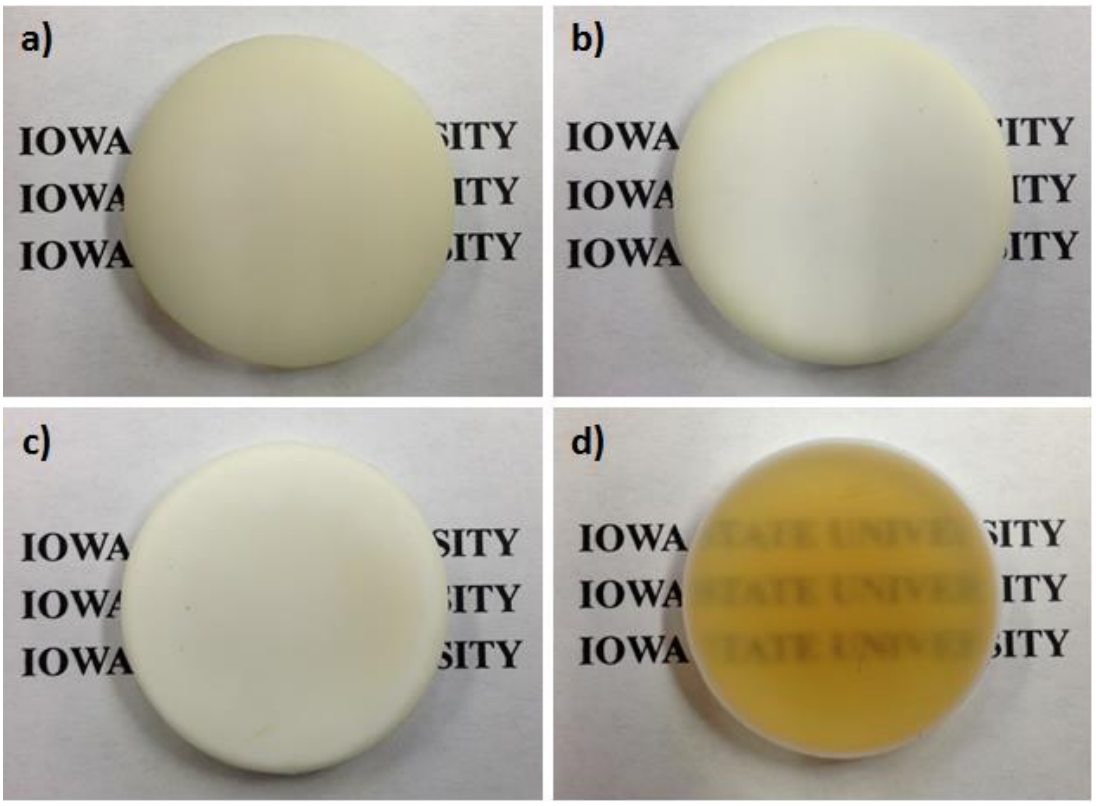

Figure 2.10 Photos of the resins cured at different temperatures showing different optical properties. (a) 170 ºC; (b) 180 ºC; (c) 190 ºC; (d) 200 ºC

The resins with LC domains are opaque due to the light scattering at the boundaries of the liquid crystalline and amorphous regions whereas non-LCERs, which were completely amorphous, are transparent, as shown in the same figure. XRD was also used to confirm the existence of LC phases. The XRD spectra of the LCERs and non-LCERs are compared in Figure 2.11. A small peak at 4.365° having d-spacing of 20.225Å was observed for LCERs while this peak is absent in the case of non-LCERs. The smectic LC phase is characterized by its layered structure. The d-spacing calculated from the XRD spectra indicates that the LCERs have layer spacing about 20Å and have a smectic LC structure. The chemical structure of the mesogen in LCERs was simulated using ChemBio3D software as shown in Figure 2.12. The mesogenic length was found to be

20.4Å which was measured by calculating the bond length after minimizing the energies of the molecules. The distance between two sulfur atoms was used as the mesogenic length. Good agreement between the experimental data and the simulation was obtained, adding further evidence to the presence of a smectic phase in the LCERs.

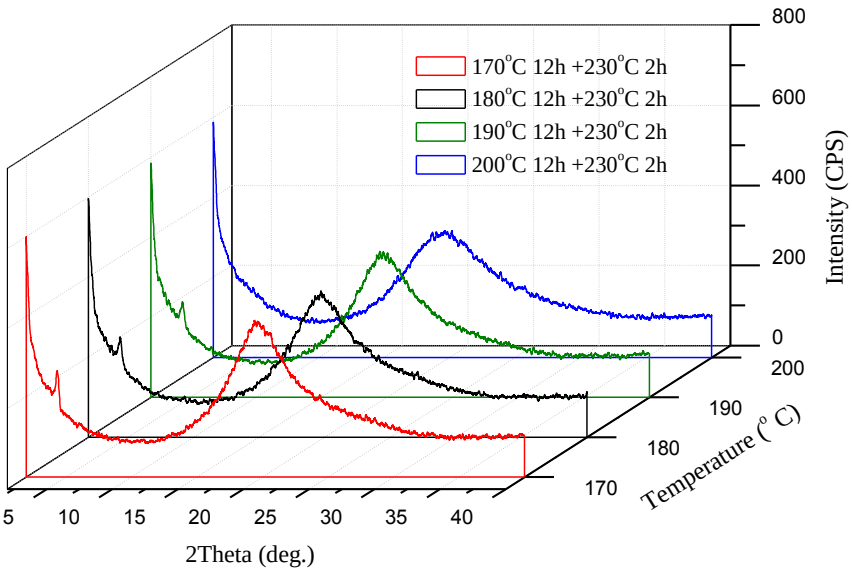

Figure 2.11 XRD spectra of the resins cured at different temperatures.

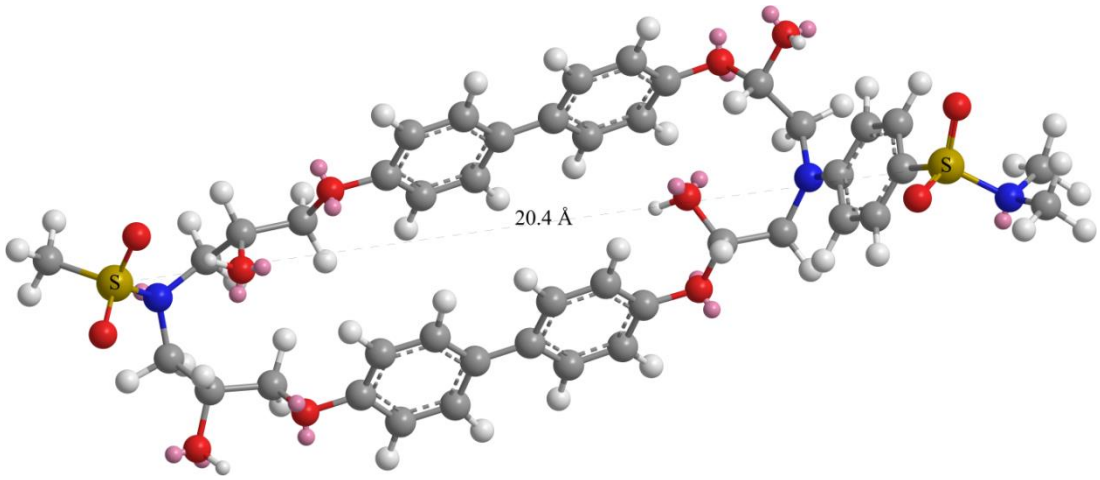

Figure 2.12 Chemical structure simulation of the mesogen of LCERs.

The dynamic mechanical properties, as well as the glass transition temperature of the resins were investigated using dynamic mechanical analysis (DMA). The storage modulus (E') and loss modulus (E'') were determined from the in-phase and out-of-phase response of the resins to an applied strain, representing the elastic and viscous portions respectively. Moreover, the T_g was measured from the peak of the mechanical damping curve (tanδ) which was the ratio of E'' to E'. The DMA curves of the resins cured at different temperatures are shown in Figure 2.13 and the DMA data is summarized in Table 2.2. For semicrystalline polymers, crystallites have a great influence on the elastic modulus of the materials. As shown in Table 2.2, LCERs have higher storage moduli in the glassy region (35 ºC) compared to non-LCERs, which is due to the presence of LC domains. The rigid and ordered structure of the LC domains has higher moduli compared to the amorphous parts, so they behave as rigid fillers in the resin matrix.

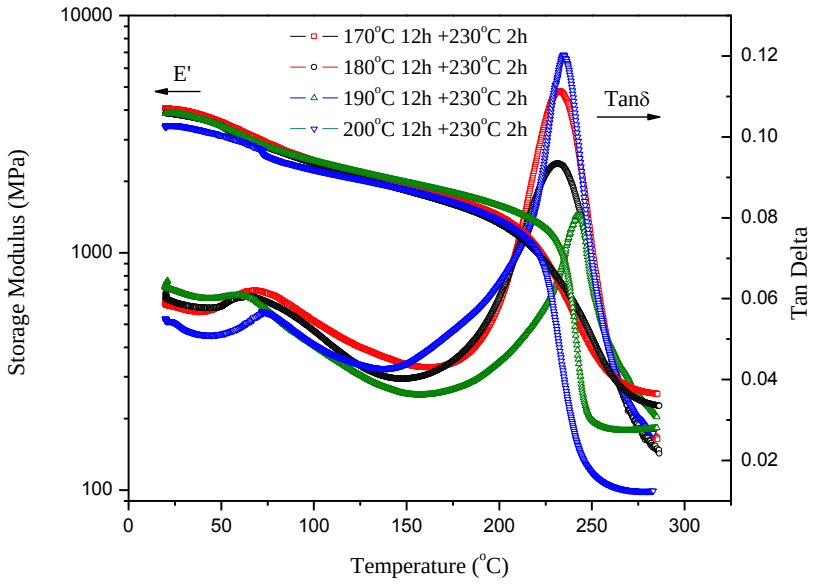

Figure 2.13 Temperature dependence of dynamic mechanical properties of the resins cured at different temperatures.

Table 2.2 Thermomechanical data obtained from DMA, DSC and TMA.

Cure schedule	E' at 35 °C (MPa)	E' at 270 °C (MPa)	T_g[a] (°C)	T_g[b] (°C)	T_g[c] (°C)	CTE[d] (°C)	T_d[e] (°C)	Remarks
170 °C 12h plus 230 °C 2h	3975±55	270±8	232.6	206.2	190.8	63.7	306.3	LCER
180 °C 12h plus 230 °C 2h	3940±14	244±2	231.5	205.2	191.4	69.6	307.0	LCER
190 °C 12h plus 230 °C 2h	4159±34	196±2	241.2	209.2	191.6	64.9	307.7	LCER
200 °C 12h plus 230 °C 2h	3422±20	99±0.3	233.3	196.9	183.3	61.1	309.5	Non-LCER

[a] Taken from the peak of tanδ (DMA).

[b] Taken from the intercept of the slopes of glassy region and rubber region (TMA).

[c] Taken from dynamic scans at 20 °C /min (DSC).

[d] Measured in the temperature range from 50 °C to 70 °C via TMA.

[e] At 5% weight loss (TGA)

LCERs also show higher storage moduli in the rubbery plateau region, which can be attributed to two reasons. First, in addition to the filler effect mentioned earlier, the LC domains also act as crosslinks, tying segments of the polymer chain together [37]. They do not relax or become soft at temperatures higher than T_g, and therefore the movements of the polymer chains are restricted by these rigid LC domains. Second, the higher rubbery moduli of LCERs could be a result of the reduced viscosity and the accelerated reaction rate when the curing process proceeds in the LC phase, as mentioned previously, which leads to a higher crosslink density for LCERs.

The T_g measured from the peak of the tanδ curve also shows that LCERs have higher T_g compared to non-LCERs. Both of the rigid filler effect and the crosslink effect are

responsible for the high T_g observed in LCERs. The free volume of the LCERs is significantly reduced due to the presence of LC domains, thereby decreasing the mobility of the segments in response to an applied thermal energy. The T_g of the resins were also measured using DSC and TMA which is in agreement with the DMA results. In DSC, the T_g is characterized by a step change in the heat capacity of the material, while in TMA the T_g is determined in terms of the change in CTE when the material undergoes a change from glass to rubber. Although measured through three different experimental techniques, LCERs always show higher T_g than non-LCERs. It is noted that the absolute values of T_g measured in each technique is different, which is not unexpected since the underlying property being monitored is not the same. For example, the T_g measurement in DSC involves monitoring a thermodynamic property (heat capacity) whereas the T_g in DMA is obtained from a viscoelastic property (tan δ).

Thermal expansivity of the LCERs and non-LCERs were evaluated using thermomechanical analysis. Results are summarized in Table 2.2. Since thermal history has a great effect on the thermomechnical properties of polymers, all the samples were heated to 250^{o}C to erase the thermal history and release any internal residual stress. Second heating scans were recoded to examine the CTE of the resins. As shown in Table 2.2, the CTE of the resins cured in LC and non-LC state are quite close, which can be attributed to the random distribution of the LC domains in the amorphous matrix.

Thermal stability of the LCERs and non-LCERs was also investigated. Figure 2.15 shows the TGA curves for all the samples. The thermal decomposition temperature (T_d) was defined as the temperature when the samples lost 5% of its initial weight, and the results are summarized in Table 2.2. TGA data shows that the presence of LC domains does

not have a significant influence on the thermal stability of the resins, which indicates that the most important factor that affects the thermal decomposition of a polymeric material is the chemical bonding rather than morphology. In this work, the dynamic mechanical properties and T_g were significantly better for epoxy resins comprising a LC phase. Prior work in the literature has shown that alignment of LC domains may be possible by applying an external field [32, 38-40]. The effect of aligning the LC phase in BP/SAA systems using an external electrical or magnetic field and the effect on ensuing anisotropic thermomechanical and dynamic mechanical properties will be examined in future work.

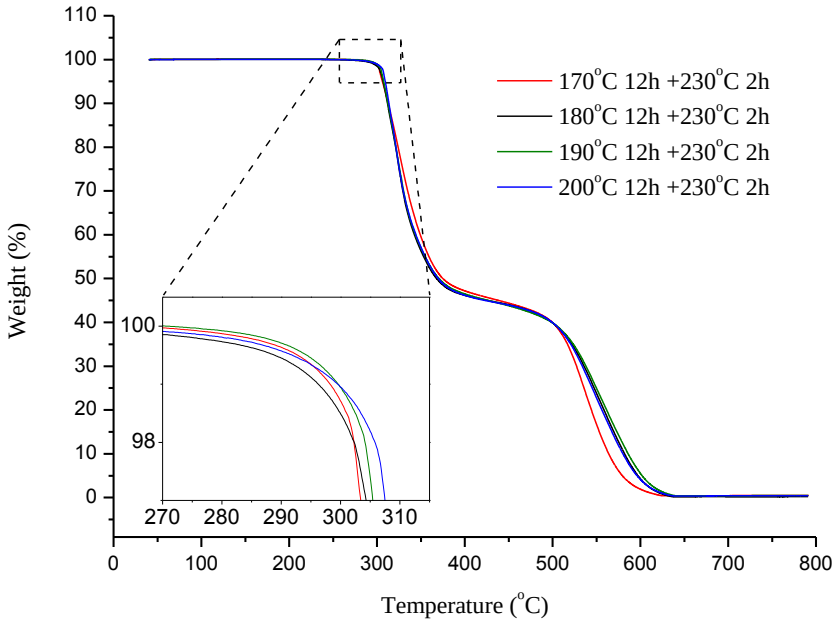

Figure 2.14 Thermogravimetric analysis of resins cured at different temperatures.

2.5 Conclusions

The epoxy monomer BP was successfully synthesized and characterized using various experimental techniques. Results show that BP is not a liquid crystalline epoxy monomer

itself and an irreversible crystal transition exists in the temperature range of 120 ºC -140 ºC. However, upon reacting with SAA, a smectic LC phase starts forming after 20 minutes of the curing reaction. Cure temperature has a great influence on the formation and development of LC phase and an isotropic network is obtained for cure temperatures greater than 200ºC. A rate acceleration of the curing reaction was observed for the resins cured in the LC phase. The effects of the presence of LC phase on the thermal and mechanical properties of the resins were also investigated. LCERs showed higher values of storage modulus in both glassy region and rubbery plateau region compared to non-LCERs, which is due to the rigid structure of the LC domains and reduced viscosity of the system. The glass transition temperature of the resins cured in LC and non-LC state was studied using DMA, DSC, and TMA respectively. All the results show that LCERs have higher T_g because of the rigid filler and crosslink effects of the LC domains, which results in lower mobility of the polymer chain. The presence of LC phase does not have a significant influence on the coefficient of thermal expansion and thermal stability of the resins, possibly due to the random distribution and orientation of the LC domains.

2.6 Acknowledgements

Support under Air Force Office of Scientific Research (AFOSR) Award No. FA9550-12-1-0108 is gratefully acknowledged.

2.7 References

[1] Barclay GG and Ober CK. Progress in Polymer Science 1993;18(5):899-945.

[2] Shiota A and Ober CK. Progress in Polymer Science 1997;22(5):975-1000.

[3] Douglas EP. Liquid Crystalline Thermosets. Encyclopedia of Polymer Science and Technology: John Wiley & Sons, Inc., 2002.

[4] Carfagna C, Amendola E, and Giamberini M. Macromolecular Chemistry and Physics 1994;195(7):2307-2315.

[5] Amendola E, Carfagna C, Giamberini M, and Pisaniello G. Macromolecular Chemistry and Physics 1995;196(5):1577-1591.

[6] Mormann W and Brocher M. Macromolecular Chemistry and Physics 1996;197(6):1841-1851.

[7] Mormann W, Broche M, and Schwarz P. Macromolecular Chemistry and Physics 1997;198(11):3615-3626.

[8] Lin QH, Yee AF, Sue HJ, Earls JD, and Hefner RE. Journal of Polymer Science Part B-Polymer Physics 1997;35(14):2363-2378.

[9] Rosu D, Mititelu A, and Cascaval CN. Polymer Testing 2004;23(2):209-215.

[10] Hikmet RAM, Lub J, and Vanderbrink PM. Macromolecules 1992;25(16):4194-4199.

[11] Litt MH, Whang W-T, Yen K-T, and Qian X-J. Journal of Polymer Science Part A: Polymer Chemistry 1993;31(1):183-191.

[12] Holter D, Frey H, Mulhaupt R, and Klee JE. Macromolecules 1996;29(22):7003-7011.

[13] Hoyt AE and Benicewicz BC. Journal of Polymer Science Part A-Polymer Chemistry 1990;28(12):3403-3415.

[14] Hoyt AE and Benicewicz BC. Journal of Polymer Science Part A-Polymer Chemistry 1990;28(12):3417-3427.

[15] Barclay GG, Ober CK, Papathomas KI, and Wang DW. Macromolecules 1992;25(11):2947-2954.

[16] Mormann W and Zimmermann J. Liquid Crystals 1995;19(2):227-233.

[17] Carfagna C, Amendola E, and Giamberini M. Composite Structures 1994;27(1-2):37-43.

[18] Carfagna C, Amendola E, and Giamberini M. Progress in Polymer Science 1997;22(8):1607-1647.

[19] Kannan P and Sudhakara P. Liquid Crystalline Thermoset Epoxy Resins. High Performance Polymers and Engineering Plastics: John Wiley & Sons, Inc., 2011. pp. 387-422.

[20] Giamberini M, Amendola E, and Carfagna C. Molecular Crystals and Liquid Crystals Science and Technology Section a-Molecular Crystals and Liquid Crystals 1995;266:9-22.

[21] Sue HJ, Earls JD, and Hefner RE. Journal of Materials Science 1997;32(15):4031-4037.

[22] Ortiz C, Kim R, Rodighiero E, Ober CK, and Kramer EJ. Macromolecules 1998;31(13):4074-4088.

[23] Ortiz C, Belenky L, Ober CK, and Kramer EJ. Journal of Materials Science 2000;35(8):2079-2086.

[24] Harada M, Aoyama K, and Ochi M. Journal of Polymer Science Part B-Polymer Physics 2004;42(22):4044-4052.

[25] Harada M, Okamoto N, and Ochi M. Journal of Polymer Science Part B-Polymer Physics 2010;48(22):2337-2345.

[26] Su WFA. Journal of Polymer Science Part A-Polymer Chemistry 1993;31(13):3251-3256.

[27] Su WFA, Chen KC, and Tseng SY. Journal of Applied Polymer Science 2000;78(2):446-451.

[28] Robinson EJ, Douglas EP, and Mecholsky JJ. Polymer Engineering and Science 2002;42(2):269-279.

[29] Cho SH and Douglas EP. Macromolecules 2002;35(11):4550-4552.

[30] Cho S, Douglas EP, and Lee JY. Polymer Engineering and Science 2006;46(5):623-629.

[31] Barclay GG, Ober CK, Papathomas KI, and Wang DW. Journal of Polymer Science Part a-Polymer Chemistry 1992;30(9):1831-1843.

[32] Barclay GG, McNamee SG, Ober CK, Papathomas KI, and Wang DW. Journal of Polymer Science Part a-Polymer Chemistry 1992;30(9):1845-1853.

[33] Lee JY, Jang JS, Hwang SS, Hong SM, and Kim KU. Polymer 1998;39(24):6121-6126.

[34] Carfagna C, Amendola E, Giamberini M, Filippov AG, and Bauer RS. Liquid Crystals 1993;13(4):571-584.

[35] Flory PJ and Ronca G. Molecular Crystals and Liquid Crystals 1979;54(3-4):311-330.

[36] Shiota A and Ober CK. Polymer 1997;38(23):5857-5867.

[37] Nielsen LE and Stockton FD. Journal of Polymer Science Part A: General Papers 1963;1(6):1995-2002.

[38] Benicewicz BC, Smith ME, Earls JD, Priester RD, Setz SM, Duran RS, and Douglas EP. Macromolecules 1998;31(15):4730-4738.

[39] Jahromi S, Kuipers WAG, Norder B, and Mijs WJ. Macromolecules 1995;28(7):2201-2211.

[40] Tan CB, Sun H, Fung BM, and Grady BP. Macromolecules 2000;33(17):6249-6254.

CHAPTER 3. CURE KINETICS OF LIQUID CRYSTALLINE EPOXY RESINS BASED ON BIPHENYL MESOGEN

A paper published in *Journal of Thermal Analysis and Calorimetry*[1]

Yuzhan Li[2], Michael R. Kessler[3,4]

3.1 Abstract

The cure kinetics of a biphenyl based liquid crystalline epoxy resin (LCER) was studied using differential scanning calorimetry (DSC) and polarized optical microscopy. The effects of liquid crystalline (LC) phase formation on the cure kinetics were investigated. Both a model-free isoconversional method and a model-fitting method were used to analyze the DSC data. Results from the isoconversional analysis were applied to develop tentative multi-step kinetic models describing the curing reaction. Kinetic analysis showed that compared to the resins cured in amorphous phase, LCERs exhibited higher values of reaction enthalpy and a complex dependence of activation energy on the degree of cure. The formation of the LC phase resulted in a decrease in activation energy, leading to higher degree of reaction.

3.2 Introduction

Liquid crystalline epoxy resins (LCERs) are a unique class of thermosetting materials

---

[1] Reprinted with permission of *Journal of Thermal Analysis and Calorimetry*, 2014.
[2] Graduate student, Department of Materials Science and Engineering, Iowa State University
[3] Professor and Director, School of Mechanical and Materials Engineering, Washington State University
[4] Author for correspondence

formed by curing of low molecular weight, rigid rod epoxy monomers resulting in the retention of a liquid crystalline (LC) phase by the three dimensional crosslinking networks. The advantages of conventional epoxy resins, e.g. their outstanding chemical resistance, excellent mechanical strength, and good thermal properties, can be retained or further improved [1-3]. Most importantly, one of the drawbacks of traditional epoxy resins, their brittleness, which severely limits their applications, can be overcome by the introduction of the LC phase [4-8]. In addition, the rigid and ordered LC domains can be oriented under external fields, greatly enhancing the processability of the resins [9-12].

While the thermal and mechanical properties of various LCERs have been studied, several fundamental aspects, including the effect of LC formation on the cure kinetics, are still not fully understood. Several researchers studied the kinetics of epoxy-amine curing with a formation of a LC phase: Liu and coworkers investigated the kinetics of the curing reaction between 4,4’-diglycidyloxy-α-methylstilbene (DOMS) and sulfanilamide (SAA) under isothermal conditions [13]. They found that the formation of an LC phase had a significant influence on polymerization rates and led to a noticeable deviation from the autocatalytic model. Amendola and coworkers examined the reaction of DOMS with 2,4-diaminotoluene (DAT) and found that the secondary amine was more reactive than the primary amine [14]. Similar results were also reported by Mititelu and coworkers for the cure reaction between 4,4’-diglycidyloxybiphenyl (BP) and 4,4'-diaminodiphenylsulfone (DDS) [15]. However, currently there is no comprehensive explanation for this behavior.

In our group, we investigated a LCER system formed upon the curing reaction between BP and SAA [16, 17]. It was found that BP is not a liquid crystalline epoxy monomer; however, the use of SAA resulted in the formation of a smectic LC phase. A

reduction of viscosity was observed during the curing reaction, which is considered to be closely related to the LC phase formation. Therefore, a detailed cure kinetics study is necessary to fully understand the curing process of this system.

The reaction mechanisms of epoxy resins are complicated and the formation of an LC phase introduces further complexity into the overall cure kinetics. Differential scanning calorimetry (DSC) is commonly used to investigate the curing process of thermosets [18, 19]. In recent years, temperature modulated DSC (TMDSC) was recognized as a useful technique for characterizing the curing reaction, that can separate reversible and non-reversible heat flow signals, allowing the investigation of processes with complex kinetic mechanism. The DSC data can be analyzed using both model-free isoconversional methods and model-fitting methods. The isoconversional kinetics analysis methods (ICM) describe the kinetics of a reaction process by using multiple single-step kinetics equations [20-23]. If changes in the mechanism are associated with changes in the activation energy, they can be detected. Therefore, the ICM is capable of detecting multi-step reactions and can provide reasonable estimations of the kinetic parameters of each step. Such kinetic information can then be used as initial parameters in the model-fitting process.

In this study, the reaction kinetics of LCERs and non-LCERs prepared from the same epoxy monomer were studied using both conventional and modulated DSC experiments. Both model-free ICM and model-fitting methods were utilized to analyze the cure kinetics. The effects of the formation of an LC phase on the overall reaction kinetics were examined using different techniques. Detailed discussion on the cure kinetics of this system is provided.

3.3 Experimental

3.3.1 Materials

4,4’-dihydroxybiphenyl with 97% purity, benzyltrimethylammonium bromide, and sulfanilamide (SAA) were purchased from Sigma-Aldrich (Milwaukee, WI). Epichlorohydrin with 99% purity was obtained from Acros Organics (Belgium). Sodium hydroxide, isopropanol, chloroform, methanol, hydrochloric acid, and acetone were supplied by Fisher Scientific (Fair Lawn, NJ). All chemicals were used as received without further purification.

3.3.2 Synthesis and characterization of 4,4’-diglycidyloxybiphenyl (BP)

The epoxy monomer was synthesized according to a procedure reported in an earlier work by Su and coworkers [24]. A mixture of 4,4’-dihydroxybiphenyl (57.26 g), benzyltrimethylammonium bromide (2.09 g) and epichlorohydrin (481 ml) was placed in a three-neck flask and refluxed for 40 min. NaOH (24.6 g) was dissolved in 139ml of water to prepare 15% NaOH aqueous solution. Then the solution was added into the flask dropwise over a period of 3 hours under reflux. The reaction was carried out for an additional hour at room temperature. The excess epichlorohydrin was removed by vacuum distillation and the final product was washed with water and methanol. A white powder was obtained by recrystallization from isopropanol/chloroform (2:1).

The chemical structure of BP was characterized using Fourier transform infrared spectroscopy (FTIR) and nuclear magnetic resonance (NMR). The FTIR spectrum was recorded on a Bruker IFS66V FTIR with a resolution of 2 cm^{-1} from 400 to 4000 cm^{-1} at room temperature. IR (THF solution, cm^{-1}): 2927 (stretching of CH_2), 1606 (stretching of

C=C), 1500 (bending of C=C), 1244 (stretching of C-O on aromatic rings), 1037 (stretching of C-O on aliphatic chain) and 910 (epoxy group). The ^{1}H NMR spectrum was obtained by means of a Varian VXR-300 NMR instrument at room temperature, in the presence of $CDCl_3$ as the solvent. ^{1}H NMR (300 MHz, CDCl3, δ, ppm): 2.78 (d, 2H, CH_2 of epoxy), 2.93 (d, 2H, CH_2 of epoxy), 3.38 (m, 2H, CH of epoxy), 4.01 (d, 2H, CH_2 of glycidyl), 4.25 (d, 2H, CH_2 of glycidyl), 6.96 (d, 4H, biphenyl), 7.45 (d, 4H, biphenyl). The chemical structures of the epoxy monomer and the curing agent are illustrated in Figure 3.1.

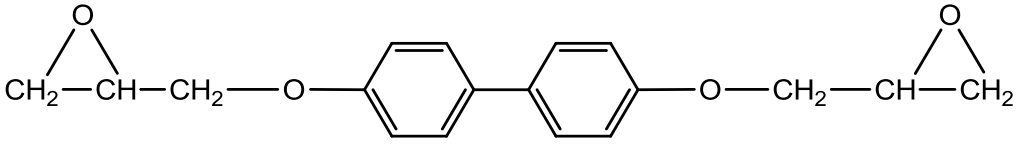

4,4’-diglycidyloxybiphenyl (BP)

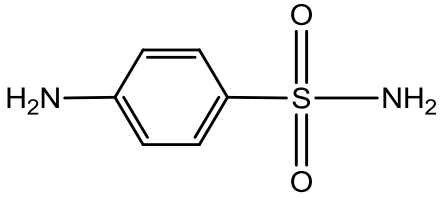

Sulfanilamide (SAA)

Figure 3.1 Chemical structure of the epoxy monomer and the curing agent.

3.3.3 Sample preparation and kinetic analysis

Uncured resin samples were prepared by dissolving BP and SAA in tetrahydrofuran (THF) in a stoichiometric ratio. Then the solvent was removed at room temperature and the mixture was ground into fine powder and dried under vacuum for 24 hours to prevent further reaction.

Reaction kinetics of BP with SAA was investigated using a TA Instruments Q2000 differential scanning calorimeter (DSC) with a liquid nitrogen cooling system. The temperature and heat capacity calibration of the DSC were carried out using indium and sapphire standards respectively. A dry helium flow of 25 mL/min was used as the purge gas for all DSC experiments. The powder mixture was loaded into aluminum DSC pans and hermetically sealed. A small hole was made in the center of the lids to prevent pressure buildup. The sample mass was controlled between 7-9 mg. Tests were performed in a dynamic mode at various heating rates: 1, 2, 3, 4, 10, 15, 20, 25 ºC min^{-1}. TMDSC experiments were carried out at 2 ºC min^{-1} under a modulation amplitude of ±0.5 ºC and a period of 60 s using the same instrument. The kinetic analysis was performed utilizing the Netzsch Thermokinetics program.

The dynamic curing experiments of BP with SAA were also performed using a polarized optical microscope (POM) from Olympus (model BX51-TRF equipped with a Linkam LTS-350 hot stage and TMS-94 temperature controller). The morphologies of the resins with different LC content were examined under polarized light.

3.4 Results and discussion

3.4.1 Curing behavior

The original DSC scans at different heating rates are shown in Figure 3.2 (low heating rates) and Figure 3.3 (high heating rates), indicating a complex dependence of curing behavior on heating rates. In both cases, multiple endothermic peaks were observed. Of particular note is that the temperatures of these peaks were considerably lower than the melting temperature of either pure BP (156 ºC) or pure SAA (165 ºC). Therefore, it is

thought that the sample mixing step may result in the formation of a eutectic system, leading to the complex melting behavior of the mixture. The curing reaction starts immediately after the melting of the mixture and is characterized by the broad exothermic peak. For the resins cured at 1, 2, 3, and 4 ºC min^{-1}, two exothermic peaks were observed, while for the resins cured at 10, 15, 20, and 25 ºC min^{-1}, only one was observed, suggesting that the curing condition has a dramatic influence on the reaction kinetics.

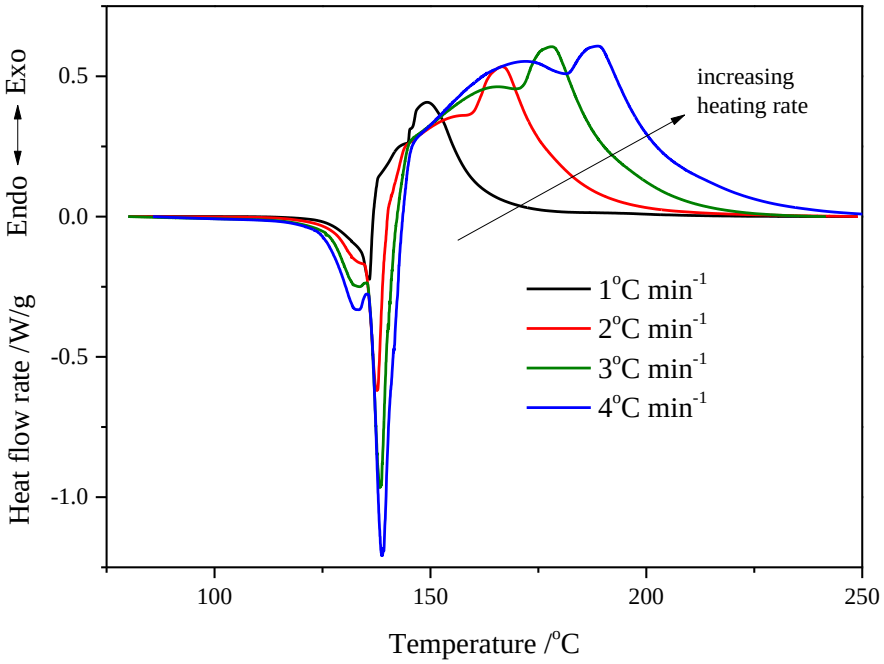

Figure 3.2 Dynamic DSC curing curves at heating rates of 1, 2, 3, and 4 ºC min^{-1}, respectively.

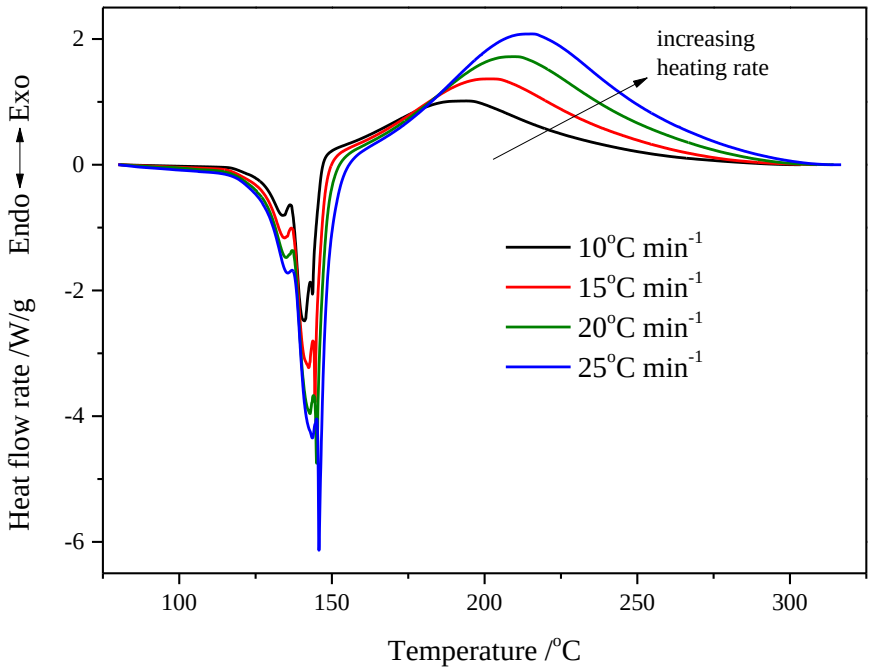

Figure 3.3 Dynamic DSC curing curves at heating rates of 10, 15, 20, and 25 ºC min^{-1}, respectively.

Subsequently, dynamic curing experiments under the same conditions were carried out using POM to monitor the formation of the LC phase. The POM images of the resins cured at 1, 4, and 10 ºC min^{-1} are shown in Figure 3.4. At low heating rates, bright birefringence was observed, indicating the polycrystalline structure of the resins. The dark spots in Figure 3.4a and Figure 3.4b are air bubbles trapped during the curing reaction. Our previous study showed that these domains exhibited a smectic LC phase which is characterized by a layered structure [16]. However, for the resins cured at high heating rates, 15, 20, and 25 ºC min^{-1}, the POM image is completely dark, indicating the absence of an LC phase. The initial and final sample sizes and the total enthalpy of the curing reaction measured for each sample are summarized in Table 3.1. The resins exhibiting a

LC phase after curing show significantly higher values of reaction enthalpy, which may be attributable to the higher degree of reaction as a result of the LC formation. It has been known from our earlier study that the formation of the LC phase can result in a decrease in viscosity [17], which favors the reaction between the epoxy monomers and the curing agents, and thus leads to the higher degree of reaction observed in LCER system.

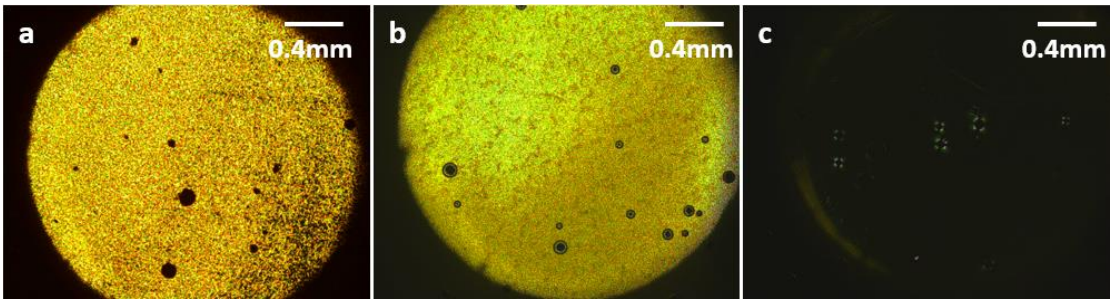

Figure 3.4 POM images of resins cured at 1, 4, and 10 ºC min^{-1}, respectively at the magnification of 50x.

Table 3.1 Sample size and total enthalpy of reaction.

Heating Rate / ℃ min^{-1}	Sample Size Initial /mg	Final /mg	Total Enthalpy of Reaction /J g^{-1}	Remarks
1	8.07	8.11	352	LCERs
2	7.79	7.81	358	LCERs
3	7.57	7.61	356	LCERs
4	8.36	8.39	325	LCERs
10	7.42	7.49	212	Non-LCERs
15	7.60	7.66	219	Non-LCERs
20	7.75	7.84	226	Non-LCERs
25	7.02	7.07	237	Non-LCERs

In order to investigate the effect of LC formation on the cure kinetics, TMDSC was utilized to separate the reversible and non-reversible heat flow of the curing reaction. The TMDSC curve of the resin cured at 2 ºC min^{-1} with temperature modulation of ±0.5 ºC is shown in Figure 3.5. In the reversible heat flow curve, two endothermic peaks were observed with peak temperatures of 142 ºC and 163 ºC, respectively, as indicated by the arrows in Figure 3.5. The first peak represented the melting process of the initial reactant, while the second peak was related to the formation of the LC phase. Of particular note is that the LC phase transition is an endothermic process, which might be a result of the negative entropy change caused by the formation of an ordered LC phase from an isotropic phase. In the non-reversible heat flow curve, two endothermic peaks were observed, which was unexpected and could be related to the irreversible melting of the eutectic system. Two exothermic peaks were also present in the non-reversible heat flow curve, which can be attributed to a ring-opening reaction of epoxy group and the rate acceleration of the curing reaction caused by the LC formation, respectively.

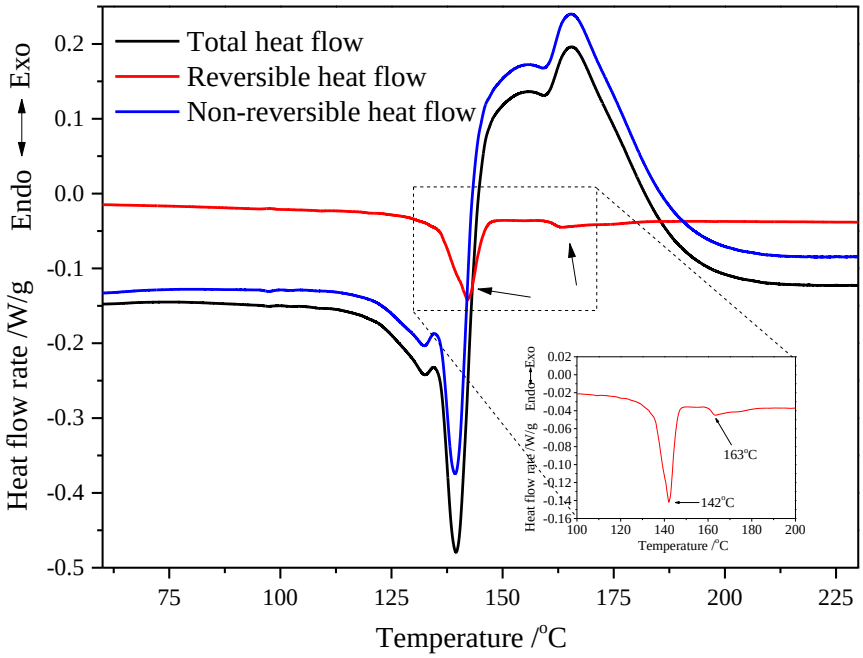

Figure 3.5 Total heat flow, reversible and non-reversible heat flow of the curing reaction measured by TMDSC at a heating rate of 2 ºC min^{-1}.

3.4.2 Model-free isoconversional kinetic analysis

In kinetic analysis, the rate of reaction can be described by Equation 1

$$\frac{\mathrm{d}\alpha}{\mathrm{d}t} = k(T)\, f(\alpha) = A\exp\left(-\frac{E}{RT}\right) f(\alpha) \qquad (1)$$

where $k(T)$ is the temperature-dependent rate constant, and $f(\alpha)$ is the reaction model, $k(T)$ is commonly described by the Arrhenius equation in which R is the universal gas constant, E is the activation energy, and A is the pre-exponential factor. The heat flow rate dH/dt measured by DSC is directly related to the reaction rate by the following equation and ΔH can be determined from integration of the DSC peak [25].

$$\frac{d\alpha}{dt} = \frac{dH/dt}{\Delta H} \tag{2}$$

In this study, the Friedman differential ICM was used to analyze the DSC data [26], which can be derived by taking the logarithm of Equation 1.

$$\ln\left(\frac{d\alpha}{dt}\right)_{\alpha,i} = \ln\left(A_\alpha f(\alpha)\right) - \frac{E_\alpha}{RT_{\alpha,i}} \tag{3}$$

For a specific α at each heating rate β_i, the value of $(d\alpha/dt)_{\alpha,i}$ and $T_{\alpha,i}$ are determined from the DSC curves. The activation energy is then calculated from the plots of $\ln(d\alpha/dt)_{\alpha,i}$ vs $1/T_{\alpha,i}$. The advantage of the Friedman method is that the DSC data can be readily used in the calculation. The Friedman plots determined from Equation 3 for both LCERs and non-LCERs are shown in Figure 3.6 and Figure 3.7, respectively. The straight lines correspond to the linear fits for α values ranging from 0.02 to 0.98.

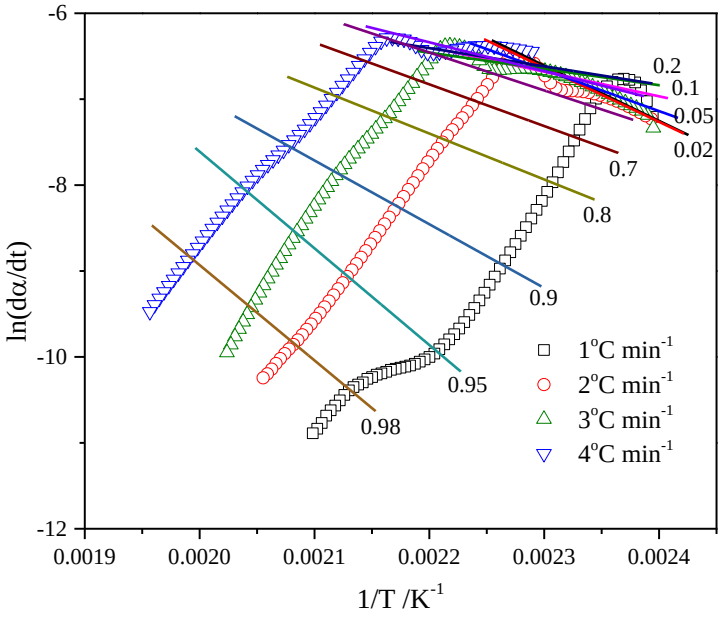

Figure 3.6 Friedman plot for LCERs.

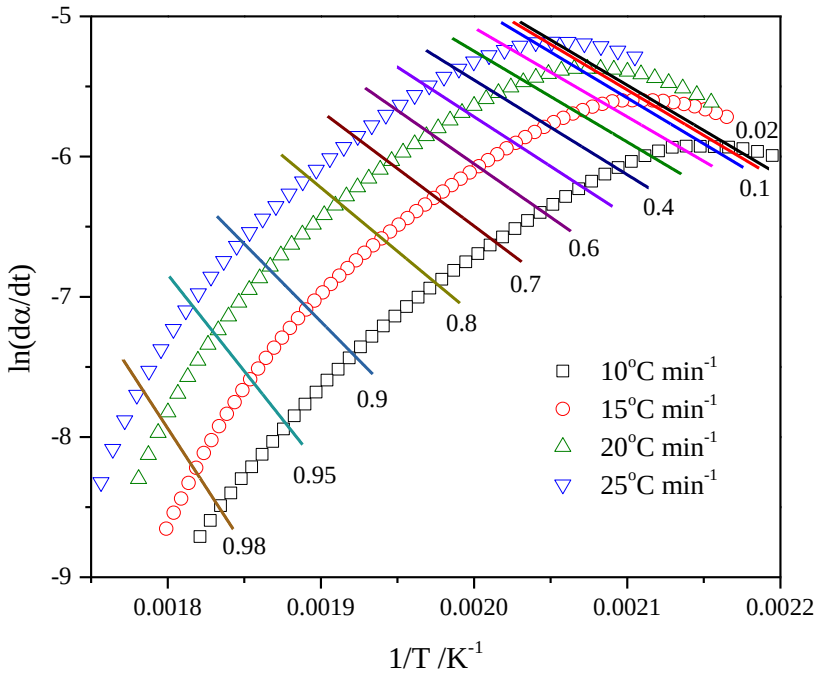

Figure 3.7 Friedman plot for non-LCERs.

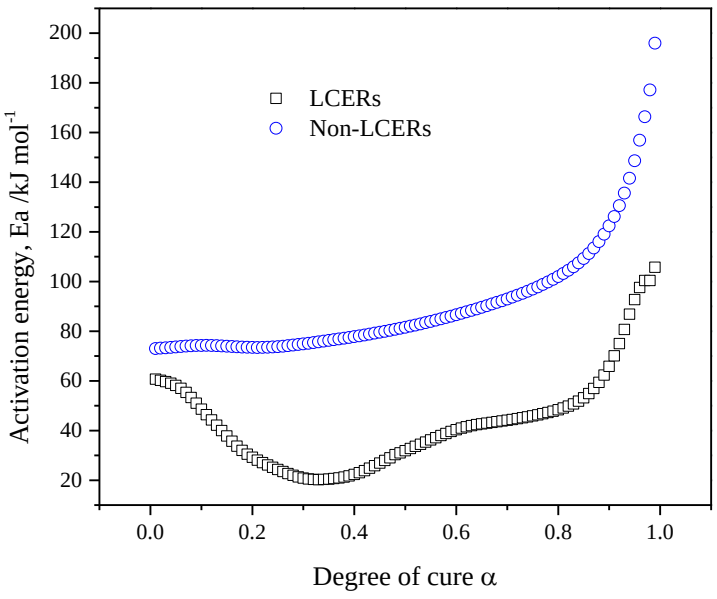

Figure 3.8 Activation energy dependence of degree of cure for LCERs and non-LCERs.

The variation in activation energy with degree of cure for both LCERs and non-LCERs determined from the Friedman plots are shown in Figure 3.8. For both systems, a dramatic increase in activation energy was observed in the later stage of curing ($\alpha > 0.8$), which indicated the presence of diffusion-controlled cure when the system approached the vitrification point caused by the increase in the glass transition temperature as a result of the curing reaction. Similar results were reported by several researchers for the curing reaction between rigid rod epoxy monomers with aromatic amines [27, 28]. However, it can be seen that the two systems show completely different extents of change in activation energy before the degree of cure reaches 0.8. For non-LCERs, a gradual increase of activation energy from 72 to 90 kJ mol^{-1} was observed. While for LCERs, the activation energy exhibited a complex dependence on the degree of cure. The activation energy showed a significant decrease in the conversion range from 0 to 0.3. As mentioned previously, the formation of the LC phase at an early stage of curing led to a decrease in viscosity of the system, which facilitated the reaction between epoxy and amine, thereby lowering the activation energy. Another possible explanation is that when the LC phase transforms from an isotropic phase to a more ordered smectic LC phase, the alignment of the LC mesogens created an advantageous situation for their crosslinking, resulting in an acceleration of the overall reaction rate. As the curing reaction proceeded, the activation energy showed a gradual increase, which can be attributed to the increase in viscosity of the reacting system.

3.4.3 Model-fitting kinetic analysis

The kinetic parameters obtained from Friedman isoconversional analysis were then used to develop a multi-step reaction model. Based on the results of the original DSC scans and the activation energy plots, a five-step reaction model was designed to model the curing of LCERs, as shown in Table 3.2. Here, the LC formation (A→B) step was regarded as an independent reaction step and was modelled using a function based on n-dimensional nucleation growth according to the Avrami-Erofeev equation. The two endothermic melting processes and the two exothermic curing processes were modelled using a function based on n^{th}-order reaction with autocatalysis. The curing of non-LCERs was also modelled using a five-step model, with the difference that the LC phase formation step was removed and the whole curing process was considered to be the combination of three melting processes and two curing processes in a consecutive manner.

Table 3.2 Multi-step models used to model the curing reaction.

LCERs		Non-LCERs	
Model	$A \xrightarrow{A_n} B$ $C \xrightarrow{C_n} D \xrightarrow{C_n} E \xrightarrow{C_n} F \xrightarrow{C_n} G$	Model	$A \xrightarrow{C_n} B \xrightarrow{C_n} C \xrightarrow{C_n} D \xrightarrow{C_n} E \xrightarrow{C_n} F$
$A \xrightarrow{A_n} B$	LC formation	$A \xrightarrow{C_n} B \xrightarrow{C_n} C \xrightarrow{C_n} D$	Melting processes
$C \xrightarrow{C_n} D \xrightarrow{C_n} E$	Melting processes	$D \xrightarrow{C_n} E \xrightarrow{C_n} F$	Curing processes
$E \xrightarrow{C_n} F \xrightarrow{C_n} G$	Curing processes		
A_n	n-dimensional nucleation based on Avrami-Erofeev equation, where $f(\alpha) = n\alpha(-\ln\alpha)^{(n-1)/n}$		
C_n	n^{th} order reaction with autocatalysis, where $f(\alpha) = (1-\alpha)^n(1+K_{cat}\alpha)$		

In kinetic modeling, for the experiments carried out at a constant heating rate, Equation 1 can be rearranged so that

$$\frac{\mathrm{d}\alpha}{\mathrm{d}T} = \frac{A}{\beta}\exp\left(-\frac{E}{RT}\right) f(\alpha) \tag{4}$$

where $\beta = \mathrm{d}T/\mathrm{d}t$ is the heating rate. In the model-fitting method, a multivariate version of the Borchardt and Daniels method was used for the evaluation of dynamic DSC data [25, 29]. The kinetics parameters were obtained by a linearizing transformation of Equation 4 so that

$$\ln\frac{\mathrm{d}\alpha/\mathrm{d}T}{f(\alpha)} = \ln\left(\frac{A}{\beta}\right) - \frac{E}{RT} \tag{5}$$

This linear equation can be used to determine the optimal fit of the kinetic parameters by multiple linear regression.

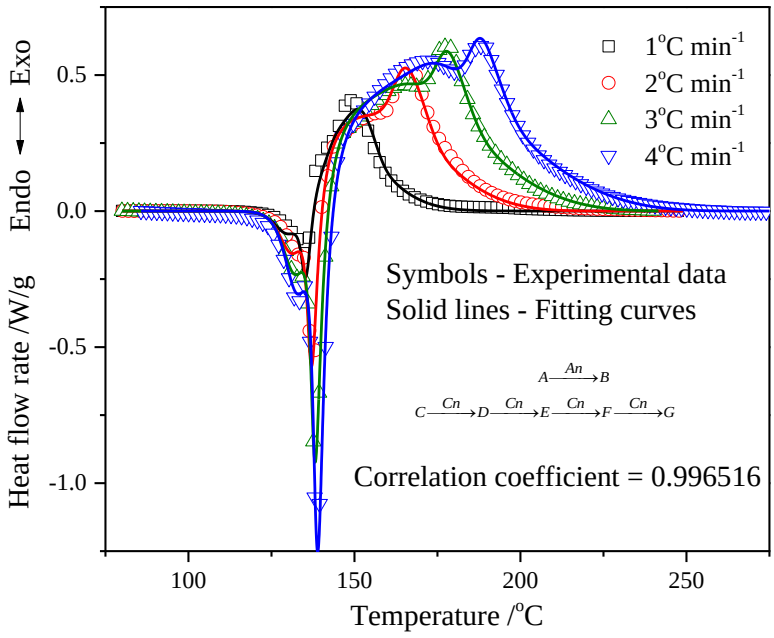

Figure 3.9 Fitting results for LCERs.

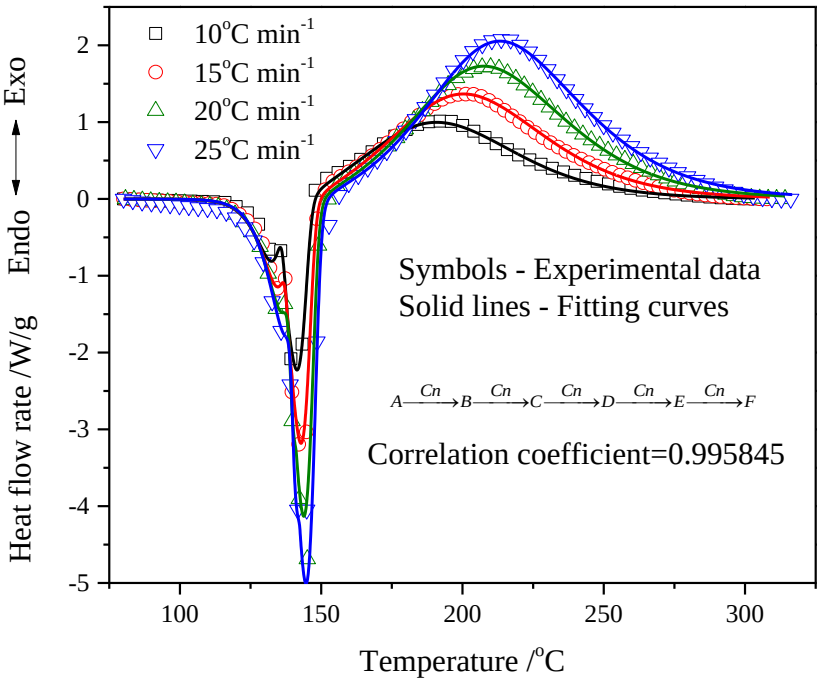

Figure 3.10 Fitting results for non-LCERs.

The fitting results are shown in Figure 3.9 and Figure 3.10 and the kinetic parameters extracted from the modelling were listed in Table 3.3 and Table 3.4 for LCERs and non-LCERs, respectively. In both cases, the experimental data are well fitted, suggesting that the multi-step model provides a good description of the curing process of BP with SAA. It should be noted that the models cannot completely simulate the complex melting behavior of the system; however, as far as the curing reactions are concerned, the models are capable of simulating the curing reaction of the system and providing information of the effects of the LC phase formation on the overall cure kinetics.

Table 3.3 Kinetic parameters for LCERs.

Reaction steps	Model	Log[A] /s^{-1}	E /kJ mol^{-1}	n	Log[K_{cat}]	Contribution
1	An	1.82±2.38E-2	41.93±0.15	14.11±1.58	N/A	-0.11±4.89E-3
2	Cn	67.99±0.18	540.72±1.62	1.61±0.31	-3.99±2.72	-0.10±8.15E-3
3	Cn	66.30±8.2E-2	540.50±0.56	3.54±0.23	1.37±9.77E-2	-0.29±1.15E-2
4	Cn	-0.16±0.13	21.38±1.17	0.87±1.95E-2	-3.98±10.2	0.79±2.28E-2
5	Cn	0.36±7.16E-2	28.84±0.83	0.70±7.28E-2	0.91±5.76E-2	0.71±1.19E-2

Table 3.4 Kinetic parameters for non-LCERs.

Reaction steps	Model	Log[A] /s^{-1}	E /kJ mol^{-1}	n	Log[K_{cat}]	Contribution
1	Cn	31.22±4.3E-2	254.04±0.36	0.61±1.5E-2	-3.91±0.30	-0.23±6.27E-3
2	Cn	50.72±0.73	413.04±5.88	0.95±8.7E-2	-3.90±3.39	-2.87E-5±3.9E-2
3	Cn	89.20±1.67	693.38±12.06	3.55±0.56	-3.92±9.19E-4	-0.43±3.32E-2
4	Cn	6.31±0.30	75.58±2.38	1.69±5.9E-2	-3.90±4.32	2.66E-6±0.32
5	Cn	3.57±0.43	45.65±3.96	0.77±0.12	-0.18±0.26	1.66±5.28E-3

3.5 Conclusions

In this work, the curing reaction of BP with SAA was investigated. The DSC studies showed that the curing condition had a significant influence on the structure of the epoxy resins. At low heating rates (1 - 4 ºC min^{-1}), the formation of a LC phase was observed upon curing. While at heating rates of 10 ºC min^{-1} and higher, the LC phase was absent and resins had an amorphous structure. Friedman's isoconversional method was used to analyze the dynamic DSC data. Based on the ICM results, multi-step reaction models were developed to model the curing reaction for both LCERs and non-LCERs. It was found that the formation of a LC phase led to a decrease in activation energy, facilitating the curing reaction and resulting in higher degree of reaction.

3.6 Acknowledgements

The authors would like to thank Dr. Elena Moukhina for her technical support and helpful discussion. Support under Air Force Office of Scientific Research (AFOSR) Award No. FA9550-12-1-0108 is gratefully acknowledged.

3.7 References

[1] Barclay GG and Ober CK. Progress in Polymer Science 1993;18(5):899-945.

[2] Carfagna C, Amendola E, and Giamberini M. Progress in Polymer Science 1997;22(8):1607-1647.

[3] Shiota A and Ober CK. Progress in Polymer Science 1997;22(5):975-1000.

[4] Ortiz C, Belenky L, Ober CK, and Kramer EJ. Journal of Materials Science 2000;35(8):2079-2086.

[5] Ortiz C, Kim R, Rodighiero E, Ober CK, and Kramer EJ. Macromolecules 1998;31(13):4074-4088.

[6] Harada M, Aoyama K, and Ochi M. Journal of Polymer Science Part B-Polymer Physics 2004;42(22):4044-4052.

[7] Harada M, Okamoto N, and Ochi M. Journal of Polymer Science Part B-Polymer Physics 2010;48(22):2337-2345.

[8] Harada M, Sumitomo K, Nishimoto Y, and Ochi M. Journal of Polymer Science Part B-Polymer Physics 2009;47(2):156-165.

[9] Barclay GG, McNamee SG, Ober CK, Papathomas KI, and Wang DW. Journal of Polymer Science Part A-Polymer Chemistry 1992;30(9):1845-1853.

[10] Benicewicz BC, Smith ME, Earls JD, Priester RD, Setz SM, Duran RS, and Douglas EP. Macromolecules 1998;31(15):4730-4738.

[11] Tan CB, Sun H, Fung BM, and Grady BP. Macromolecules 2000;33(17):6249-6254.

[12] Jahromi S, Kuipers WAG, Norder B, and Mijs WJ. Macromolecules 1995;28(7):2201-2211.

[13] Liu JP, Wang CC, Campbell GA, Earls JD, and Priester RD. Journal of Polymer Science Part a-Polymer Chemistry 1997;35(6):1105-1124.

[14] Amendola E, Carfagna C, Giamberini M, and Pisaniello G. Macromolecular Chemistry and Physics 1995;196(5):1577-1591.

[15] Mititelu A, Hamaide T, Novat C, Dupuy J, Cascaval CN, Simionescu BC, and Navard P. Macromolecular Chemistry and Physics 2000;201(12):1209-1213.

[16] Li Y, Badrinarayanan P, and Kessler MR. Polymer 2013;54(12):3017-3025.

[17] Li Y and Kessler MR. Polymer 2013;54(21):5741-5746.

[18] Wang H-M, Zhang Y-C, Zhu L-R, Zhang B-L, and Zhang Y-Y. Journal of Thermal Analysis and Calorimetry 2012;107(3):1205-1211.

[19] Liu Z, Xiao J, Bai S, and Zhang W. Journal of Thermal Analysis and Calorimetry 2012;109(3):1555-1561.

[20] Sbirrazzuoli N, Vyazovkin S, Mititelu A, Sladic C, and Vincent L. Macromolecular Chemistry and Physics 2003;204(15):1815-1821.

[21] Vyazovkin S, Mititelu A, and Sbirrazzuoli N. Macromolecular Rapid Communications 2003;24(18):1060-1065.

[22] Vyazovkin S and Sbirrazzuoli N. Macromolecular Rapid Communications 2006;27(18):1515-1532.

[23] Vyazovkin S and Sbirrazzuoli N. Macromolecules 1996;29(6):1867-1873.

[24] Su WFA, Chen KC, and Tseng SY. Journal of Applied Polymer Science 2000;78(2):446-451.

[25] Kessler MR and White SR. Journal of Polymer Science Part a-Polymer Chemistry 2002;40(14):2373-2383.

[26] Friedman HL. Journal of Polymer Science Part C-Polymer Symposium 1964(6PC):183-&.

[27] Zhang Y and Vyazovkin S. Polymer 2006;47(19):6659-6663.

[28] Cai Z-Q, Sun J, Wang D, and Zhou Q. Journal of Polymer Science Part A-Polymer Chemistry 2007;45(17):3922-3928.

[29] Borchardt HJ and Daniels F. Journal of the American Chemical Society 1957;79(1):41-46.

CHAPTER 4. CREEP-RESISTANT BEHAVIOR OF SELF-REINFORCING LIQUID CRYSTALLINE EPOXY RESINS

A paper published in *Polymer*[1]

Yuzhan Li[2], Michael R. Kessler[3,4]

4.1 Abstract

The creep behavior of a liquid crystalline epoxy resin (LCER) was investigated and compared with that of a non-LCER prepared from the same epoxy monomer. The experimental data was evaluated using Burgers' model to explain the reinforcing effect of the liquid crystalline (LC) phase. The long-term performance of the material was predicted using the time-temperature superposition principle. The results revealed that the introduction of an LC phase into the resin network can reduce creep strain and creep strain rate of the material, especially at elevated temperatures. Parameters extracted from the simulation indicated that instantaneous elasticity, retardant elasticity, and permanent flow resistance of the resins were enhanced by the presence of the LC phase. A rigid filler effect and a crosslinking effect are proposed to explain the reinforcing mechanisms.

4.2 Introduction

Epoxy resins are one of the most important thermosets; they are used as engineering

[1] Reprinted with permission of *Polymer*, 2014, 8(10), 2021-2027.
[2] Graduate student, Department of Materials Science and Engineering, Iowa State University
[3] Professor and Director, School of Mechanical and Materials Engineering, Washington State University
[4] Author for correspondence

materials for a wide variety of applications ranging from microelectronics to aerospace structures because of their excellent chemical, thermal, and mechanical properties. However, like all polymers they are characterized by their viscoelastic behavior, such as stress relaxation and tensile creep as functions of time. Although they are defined by their highly crosslinked networks, epoxy resins are subject to changing mechanical properties over time, especially at elevated temperatures, a crucial factor that could affect the long-term performance and durability of these materials. One approach to mitigate this unfavorable time-dependent behavior is the addition of nanoparticles. For example, Yang and coworkers investigated the creep behavior of a TiO_2 reinforced polyamide and reported that the creep resistance of the reinforced nanocomposites was significantly enhanced [1, 2]. More recently, Dai and coworkers prepared carbon nanotube reinforced polycarbonate nanocomposites and reported a significant decrease in creep strain for the systems containing 2% multi-walled carbon nanotubes [3]. However, one of the key issues for the successful preparation of nanocomposites is the dispersion of the nanoparticles, which often requires complicated processing steps, *e.g.*, functionalization of the nanoparticles, greatly increasing the cost of the composites. More importantly, poor dispersion can counteract the useful benefits of the nanoparticles, even result in a decrease in mechanical properties.

Liquid crystalline epoxy resins (LCERs) are a unique class of epoxy resins that are formed upon curing of low molecular weight, rigid rod epoxy monomers with aromatic amine curing agents, resulting in the retention of a liquid crystalline (LC) phase in the 3-dimensional crosslinking networks [4]. Compared with conventional amorphous epoxy resins, LCERs exhibit improved thermal and mechanical properties because of the presence

of a rigid and ordered LC phase [5-8]; therefore, they are regarded as self-reinforcing materials and have shown great potential in applications as polymer matrices in high performance composites [9-12]. Several research groups have investigated the properties of LCERs prepared from different epoxy monomers, including thermal properties [13-15], dynamic mechanical properties [16-18], fracture toughness [5, 7], moisture resistance [19], and response to external fields [20-24]. In a previous work, we prepared a biphenyl-based LCER from the curing reaction between 4,4'-diglycidyloxybiphenyl (BP) and sulfanilamide (SAA) [25]. Although the epoxy monomer was not liquid crystalline, the use of SAA can lead to the formation of a smectic LC phase during cure. The curing temperatures had significant influence on the LC phase formation. The resins cured in the LC phase exhibited a polydomain structure and better thermomechanical properties. However, the effects of the LC phase on viscoelastic properties of the material have not yet been studied. Therefore, in order to fully understand the reinforcing mechanism of the LC phase, the creep behavior of the material needs to be investigated.

In this study, the creep behaviors of a LCER and a non-LCER prepared from the same epoxy monomer were studied using short-term creep experiments at various elevated temperature isotherms. The Burgers model was utilized to simulate the creep performance of both systems. Parameters extracted from the model were analyzed to explain the reinforcing effect of the LC phase. In addition, the long-term mechanical performance of the material was evaluated by constructing a master curve using the time-temperature-superposition principle. Differences in the creep behavior of the LCER and the non-LCER were discussed and possible reinforcing mechanisms were proposed.

4.3 Experimental

4.3.1 Materials

Benzyltrimethylammonium bromide, 4,4'-dihydroxybiphenyl with 97% purity, and sulfanilamide (SAA) were purchased from Sigma-Aldrich (Milwaukee, WI). Epichlorohydrin with 99% purity was obtained from Acros Organics (Belgium). Sodium hydroxide, isopropyl alcohol, chloroform, methanol, hydrochloric acid, and acetone were supplied by Fisher Scientific (Fair Lawn, NJ). All chemicals were used as received without further purification. The epoxy monomer, 4,4'-diglycidyloxybiphenyl (BP), was synthesized according to a procedure reported in an earlier work by Su and coworkers [16]. The chemical structures of the epoxy monomer and the curing agent are illustrated in Figure 4.1.

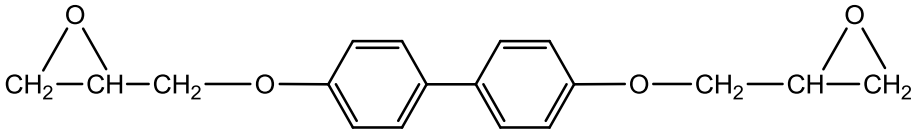

4,4'-diglycidyloxybiphenyl (BP)

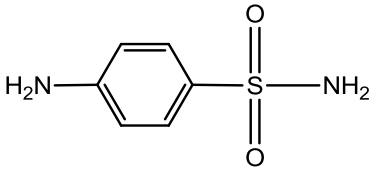

Sulfanilamide (SAA)

Figure 4.1 Chemical structures of the epoxy monomer and the curing agent.

4.3.2 Sample Preparation

The epoxy monomer was placed in a beaker and heated in an oil bath. Once the monomer was completely melted, the curing agent was added in a stoichiometric ratio, followed by vigorous stirring for approx. 1 min. The mixture was then placed in a pre-heated convection oven at a selected temperature. Because the formation of the LC phase is sensitive to the curing temperature, different curing schedules were used to produce resins with and without LC phases. The LCERs were prepared by curing the mixture at 170 ºC, 180 ºC, and 190 ºC for 12 h; while the non-LCER was prepared by curing the mixture at 200 ºC for 12 h. After the initial curing process, all samples were post-cured at 230 ºC for 2 h. The solid bulk samples were machined into small pieces with appropriate size for dynamic mechanical analysis using a diamond blade saw.

4.3.3 Creep Measurements

Creep tests were carried out using a TA Instruments (New Castle, DE) dynamic mechanical analyzer (DMA) Q800 with liquid nitrogen gas cooling accessory in three-point bending mode. Creep and creep recovery tests were performed at isotherms from 200 ºC to 295 ºC in intervals of 5 ºC. An equilibrium time of 5 min was used for each interval before the load was applied. A constant stress of 0.35 MPa was applied for 20 min, followed by a 20 min recovery period [26]. The creep data were fitted using the four-parameter Burgers model. The fitting process was performed using the nonlinear curve fit function in OriginPro 9.0 (OriginLab Corporation).

4.4 Results and discussion

4.4.1 Creep Strain

The time-dependent creep strain values for all resin systems at different temperature intervals are shown in Figure 4.2. As can be seen, the creep strain values increased with increasing temperature independent of the type of resin, illustrating the response of the resin networks to applied thermal energy. At temperatures below the glass transition temperature (T_g), the movement of the polymer networks was greatly restricted by the crosslinking sites; therefore, all systems exhibited limited strain behavior. At high temperatures, on the other hand, the networks were thermally activated and became soft, allowing larger deformation. It was also seen that the creep behaviors of the LCER and the non-LCER were not identical, especially at higher creep temperatures, indicating the influence of the LC phase on the viscoelastic properties of the resins, which will be discussed in detail in a later section.

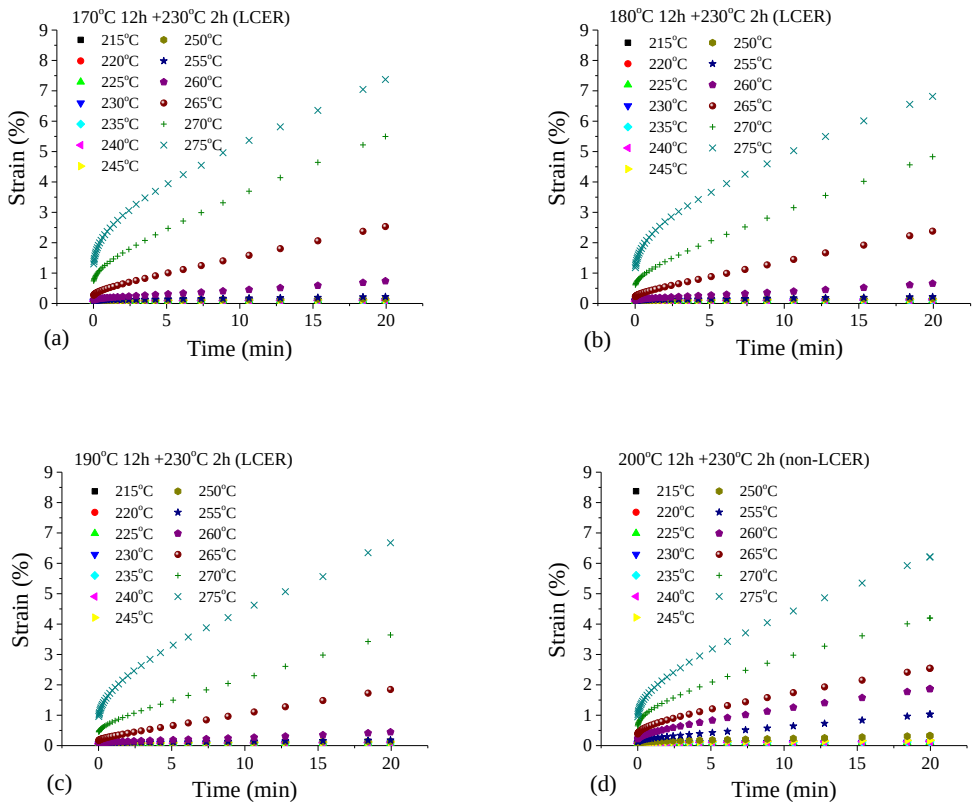

Figure 4.2 Time-dependent creep strain of the resins at different temperature intervals. (a) LCER cured at 170 ºC; (b) LCER cured at 180 ºC; (c) LCER cured at 190 ºC; (d) non-LCER cured at 200 ºC.

4.4.2 Creep Strain Rate

In addition to creep strain, the creep strain rate is another important factor that determines the dimensional stability of a material. In general, the creep behavior of polymers can be divided into four stages: instantaneous response, primary creep, secondary creep, and tertiary creep [2]. The instantaneous response is a result of the elastic deformation of a material. Primary creep is caused by the slippage and orientation of the polymer chains. Secondary creep is characterized by a steady-state creep evolution, where a balance between thermal softening and work hardening is established. Tertiary creep

involves the rupture or necking of a material, and is accompanied by large deformation. Characterized by a relative linear strain-time relationship, the secondary creep stage is often used to determine the creep strain rate of a material.

In order to relate the different responses of the LCER and non-LCER systems to the applied load, the secondary creep stage in the original creep curves was fitted with a linear line to determine the creep strain rate of each system. The fitting region was carefully selected to ensure that the creep behavior reached a steady state (Supplementary Material, Figure S1). The fitting results were then plotted as a function of temperature ranging from 215 ºC to 275 ºC. Four different temperature regions were identified based on T_g of the resins as shown in Figure 4.3. In general, an increase of creep strain rate with temperature was observed, suggesting the increased mobility of the resin networks at elevated temperatures. However, the LCER systems exhibited lower creep strain rate values than the non-LCER system for temperatures lower than 265 ºC as shown in Figure 4.3a, 4.3b, and 4.3c, indicating improved creep resistance of the LCER systems.

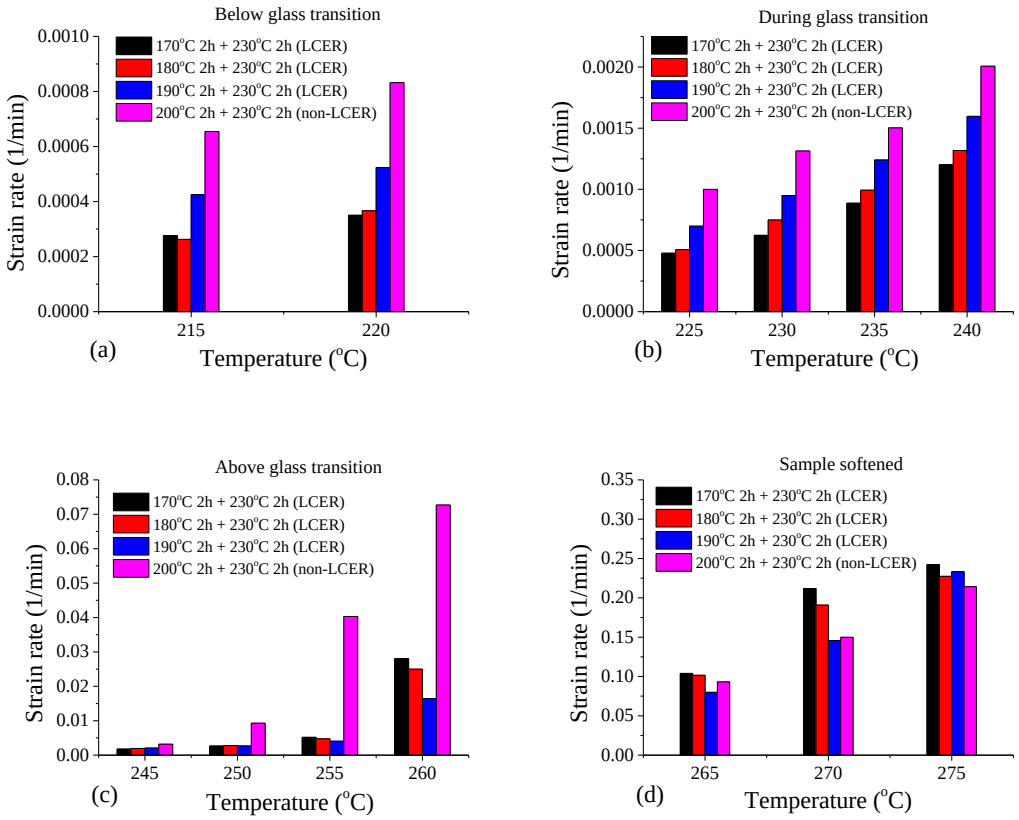

Figure 4.3 Temperature dependence of creep strain rate.
(a) Below glass transition; (b) During glass transition;
(c) Above glass transition; (d) Sample softened.

Furthermore, this difference in creep strain rate between two systems exhibited a temperature dependence as shown in Table 4.1, suggesting that the reinforcing mechanism of the LC phase might be different at different temperature regions. For instance, below glass transition (from 215 ºC to 220 ºC), the ratio of average creep strain rate value of LCER to non-LCER was 0.503, while during glass transition (from 225 ºC to 240 ºC), the ratio increased to 0.652, indicating that the creep-resistant effect of the LC phase became less effective. However, above glass transition (from 245 ºC to 260 ºC), the ratio decreased to 0.273, suggesting that the reinforcing effect of the LC phase was particularly strong after

T_g. At temperatures higher than 265 ºC, the two systems exhibited similar creep strain rates, because the resins softened at these temperatures. The presence of the LC phase was no longer able to restrict the motion of the resin networks, and thus lost its reinforcing effect.

Table 4.1 Average creep strain rate values of LCER and non-LCER systems at different temperature regions.

Temperature regions	Average creep strain rate value of LCER (1/min)	Average creep strain rate value of non-LCER (1/min)	Ratio of creep strain rate value of LCER to non-LCER
Below glass transition	0.000349	0.000695	0.503
During glass transition	0.000900	0.001380	0.652
Above glass transition	0.008291	0.030415	0.273
Sample softened	0.162933	0.142167	1.146

4.4.3 Creep Modeling

The Burgers model, also known as the four-parameter model, is widely used to simulate the creep behavior of polymers [2]. It consists of a consecutively connected Maxwell and a Kelvin unit, as illustrated in Figure 4.4.

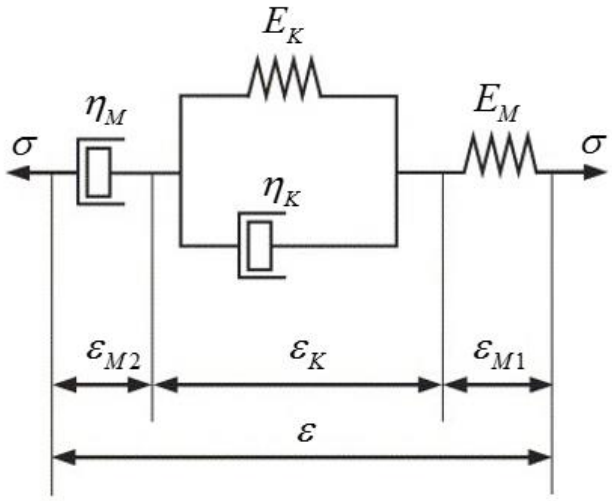

Figure 4.4 Schematic representation of the Burgers model [2].

Under a constant applied stress, the total strain of the system is the sum of the strains resulting from the Maxwell spring, the Maxwell dashpot, and the Kelvin unit shown in the figure:

$$\varepsilon = \varepsilon_{M1} + \varepsilon_{M2} + \varepsilon_K \tag{1}$$

where ε_{M1}, ε_{M2}, and ε_K are the strains of the Maxwell spring, Maxwell dashpot, and the Kelvin unit, respectively. The strain-time relationship can be expressed by the four parameters in Burgers model:

$$\varepsilon = \frac{\sigma_0}{E_M} + \frac{\sigma_0}{E_K}(1 - \mathrm{e}^{-t/\tau}) + \frac{\sigma_0}{\eta_M} t \tag{2}$$

where, $\tau = \eta_K / E_K$ is the retardation time of the Kelvin unit; E_M and η_M are the modulus and viscosity of the Maxwell spring and dashpot; E_K and η_K are the modulus and viscosity of the Kelvin spring and dashpot. The three terms in the equation represent the instantaneous deformation, delayed deformation, and viscous flow of a material, respectively.

The four parameters in Eq. 2 can be extracted through direct modeling of the experimental creep data, which provide valuable insight into the viscoelastic properties and related deformation mechanisms of a material. The fitting process was accomplished using the nonlinear curve fit function provided by Origin software and the results are shown in Figure 4.5. The creep behavior of the resins was well simulated by the Burgers model at all temperatures examined with a correlation coefficient, R, greater than 0.99. Similar to the results of the creep strain rate, a decrease in creep strain value was observed for all LCER systems at temperatures lower than 265 ºC. The reinforcing effect of the LC phase was dependent on temperature, as discussed in the previous section; therefore the four parameters extracted from the Burgers model are plotted as functions of temperature for all resin systems, and the results are shown in Figure 4.6.

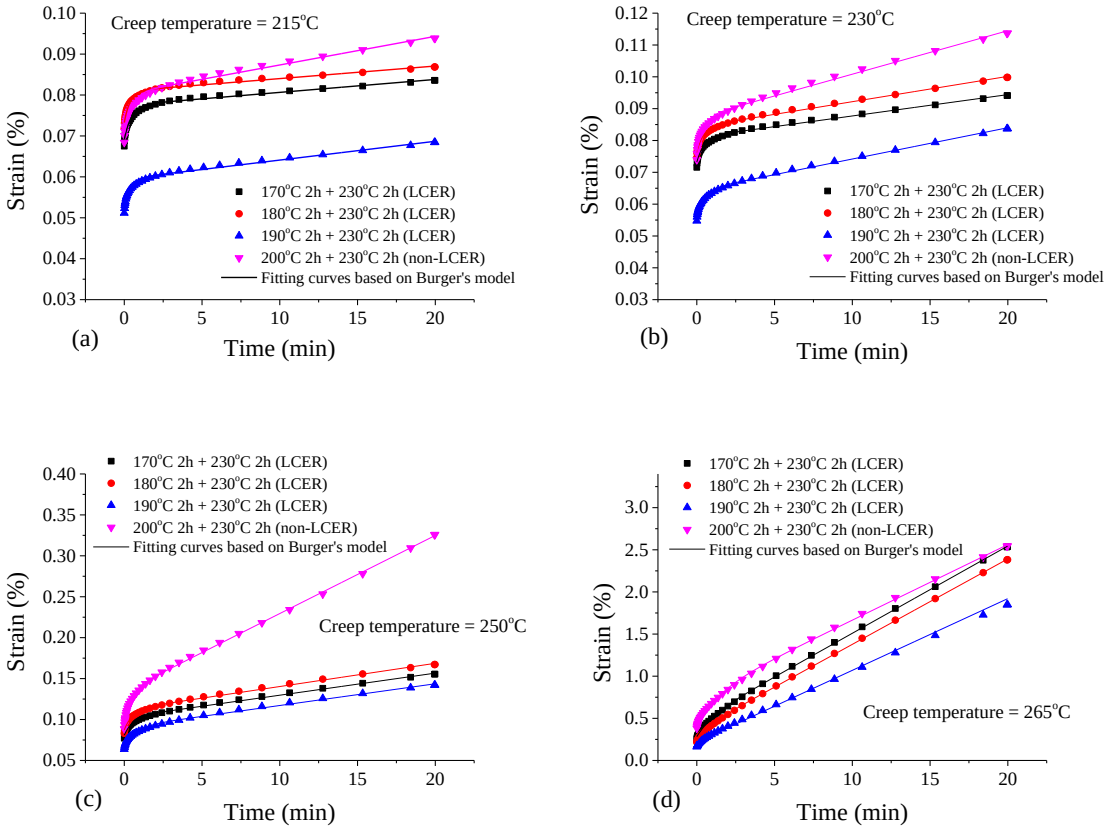

Figure 4.5 Modeling results of creep behavior at different creep temperatures. (a) T_{creep}=215 ºC (below glass transition); (b) T_{creep}=230 ºC (during glass transition); (c) T_{creep}=250 ºC (above glass transition); (d) T_{creep}=265 ºC (sample softened).

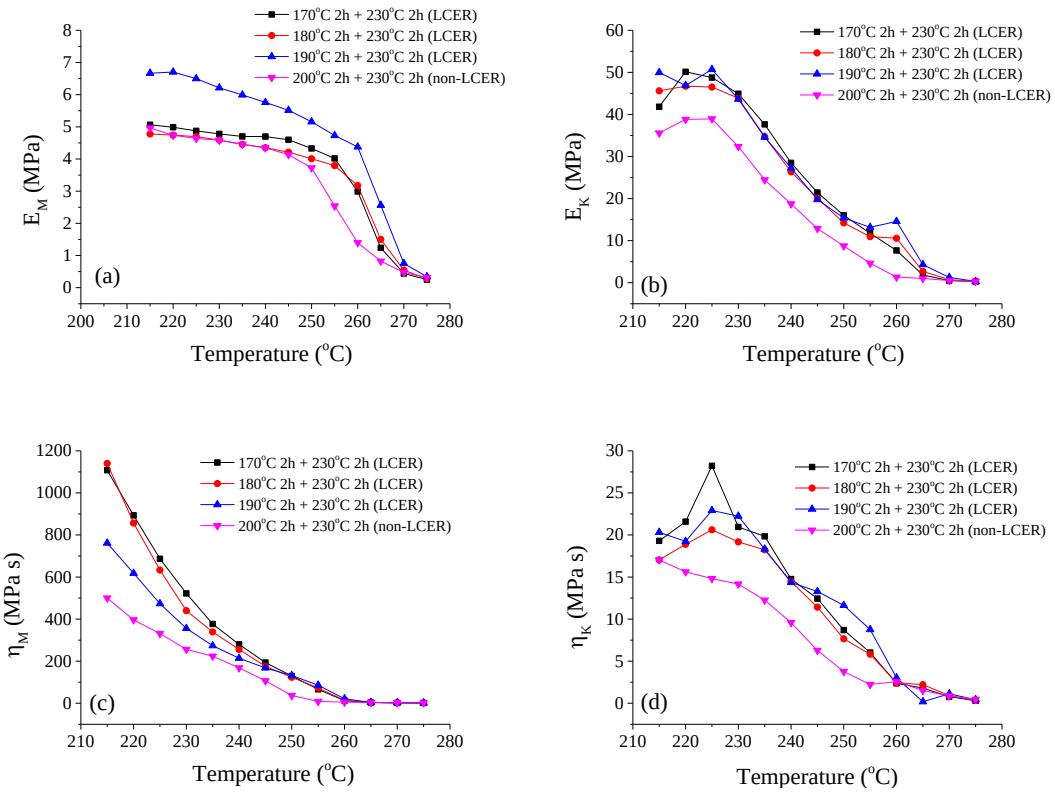

Figure 4.6 Temperature dependence of the four parameters in the Burgers model. (a) Instantaneous elasticity E_M; (b) Retardant elasticity E_K; (c) Permanent flow viscosity η_M; (d) Retardant viscosity η_K.

The parameter E_M represents the modulus of the Maxwell spring and reflects the instantaneous elasticity of the material. As shown in Fig. 6a, E_M values decreased with increasing temperature for all resin systems, which again illustrated the thermal softening process of the resin networks at elevated temperatures. It was also seen that the LCER systems generally exhibited higher E_M values than the non-LCER system, indicating the reinforcing effect of the LC phase on the instantaneous elasticity of the resins. Our previous investigation showed that the LCER system had a polydomain structure with individual smectic LC domains randomly distributed in the amorphous networks [25]. These smectic

LC domains were composed of rigid LC mesogens that were closely packed in a layered manner. It is believed that the modulus of the LC domains was higher than that of the amorphous regions, and thus behaved as rigid fillers in the resin matrix. In addition, the simulation results were in good agreement with our earlier findings from dynamic mechanical analysis (DMA), in which higher storage moduli (E') were observed for the LCER systems in the glassy region, an indication of increased elastic modulus of the LCER (Supplementary Material, Figure S2). However, it should be noted that at temperatures higher than 265 ºC, the LC phase lost their reinforcing effect because at these temperatures the networks were extremely softened. Another interesting observation is that although E_M curve and E' curve shared similarities, they showed different transition temperatures, which was considered to be related with the underlying properties they are representing. In DMA, storage modulus is a measure of the energy stored and recovered in cyclic loadings. In addition to the contribution of liquid crystalline phases to the stored elastic energy, regions with highly crosslinked networks will also have in-phase response under cyclic loadings. While in Burgers model, E_M represents the elastic modulus of the Maxwell spring, which is mainly associated with the liquid crystalline regions. Therefore, E' curve exhibits a sharp drop at 230ºC-250ºC, whereas E_M curve shows a sharp drop at 260ºC-270ºC. However, both parameters (E' and E_M) are closely related with the time-independent elastic response of the resin to external forces, and thus exhibited similar temperature responses.

The parameters E_K and η_K represent the modulus and viscosity of the Kelvin spring and dashpot, respectively. In the Kelvin unit, the two elements are connected in parallel and instantaneous deformation is restricted because the presence of the dashpot. Therefore, E_K and η_K are associated with the mechanical properties of the amorphous regions in the

resin. They cannot exhibit effective instantaneous response to an applied load, but provide time-delayed support to the network through slow reorientation. Figures 6b and 6d show that LCERs generally exhibited increased values of both E_K and η_K. A possible reason for this improvement is the increased crosslink density of the LCER system. In a previous work, it was found that the LCER system had higher total enthalpy of curing reaction compared to that of the non-LCER system and the formation of a LC phase led to a decrease in activation energy of the reacting system, which was considered to facilitate the curing reaction and result in higher degree of reaction. Additionally, the curve of η_K is similar to the loss modulus (E'') curve determined by DMA, (Supplementary Material, Figure S3). Both parameters are related with the time-dependent viscous response of the resin to external forces. The parameter η_K represents regions with slow deformation. E'' represents the energy dissipated in cyclic loading. Since both slow deformation (related with η_K) and permanent deformation (related with η_M) are considered to be out-of-plane responses, they result in energy dissipation. However, in highly crosslinked thermosets, permanent deformation is restricted and slow deformation is the main cause for energy dissipation. Therefore, the curve of η_K and the curve of E'' exhibited similar shapes.

Among the four Burgers model parameters, η_M is probably most important because it represents the irrecoverable deformation of the material. Figure 6c compares this parameter for the LCER and the non-LCER. It can be seen that LCER systems exhibited increased values of η_M, indicating the resistance to viscous flow, which was attributed to the crosslinking effect of the LC phase. Unlike in nanoparticle reinforced polymer matrix composites, which often have insufficient particle-matrix bonding, the LC domains in this

system had covalently bonded with the amorphous matrix, because the rigid mesogens were physically involved in the crosslinking reaction and became an inseparable part of the resin system. Under an applied load, the LC domains can act as crosslinks, tying the amorphous regions together, and greatly restricting the mobility of the network. This reinforcing effect is more effective at temperatures above T_g because the LC domains do not relax or become soft at elevated temperatures. Therefore, the LCER systems were more resistant to permanent creep deformation compared to the non-LCER system.

Additionally, in the LCER systems, the curing temperature seemed to influence the reinforcing effect of the LC phase. This influence may be associated with the difference in LC content and morphology created at different curing temperatures (Supplementary Material, Figure S4).

4.4.4 Predication of Creep Behavior

Long-term performance and durability are of particular importance for structural materials; however, it is impractical to perform creep experiment covering the entire service life time. The prediction of long-term properties based on relatively short-term experimental data is necessary and favorable [26, 27]. The time-temperature superposition (TTSP) principle is commonly used to study the time-dependent mechanical properties of polymers. It is worth mentioning that TTSP exhibits limitations when multi-phase systems are studied, especially in inhomogeneous systems. However, TTSP can be applied to multi-component systems which are homogeneous and isotropic. Our previous studies on this LCER system showed that there was no observable phase separation. Although local orientation was present in individual LC domains, the whole system is isotropic. Therefore,

the TTSP can be applied to the current LCER system. According to the TTSP principle, a creep experiment conducted at an elevated temperature is equivalent to one performed for an extended period of time. Therefore, the short-term creep test data collected at different temperature isotherms can be used to construct a master curve that provides a prediction for long-term performance of a polymeric material.

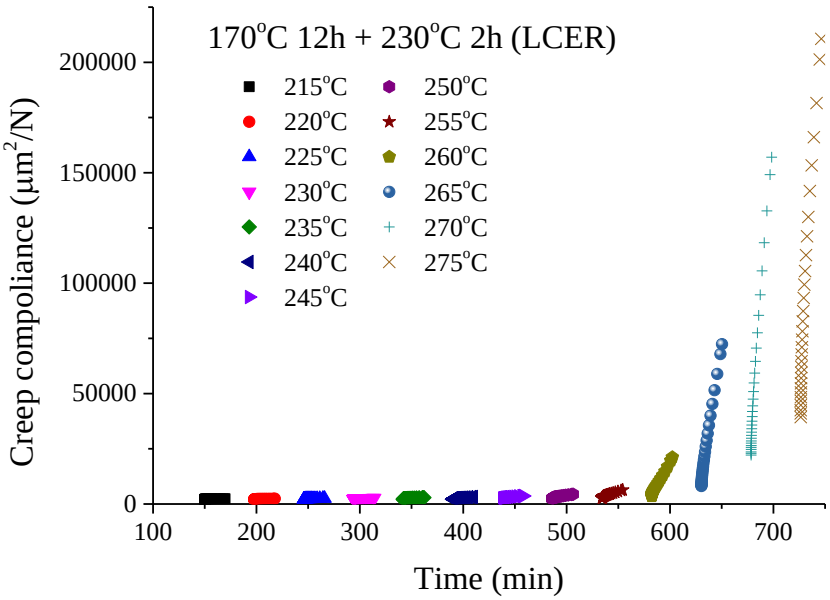

Figure 4.7 Dependence of creep compliance on creep time at different temperature intervals for LCER cured at 170 ºC.

The dependence of creep compliance on actual experiment duration for a LCER cured at 170 ºC is shown in Figure 4.7. The time intervals between two creep temperatures represent the recovery process and the equilibrium time used to reach the desired temperature [26]. The creep compliance data were then manually shifted to construct a master curve at a reference temperature of 215 ºC on a log-time scale, as shown in Figure 4.8. For the creep experiments carried out at the temperatures higher than 215 ºC, the data

were shifted to the right, representing the creep behavior for an extended period of time.

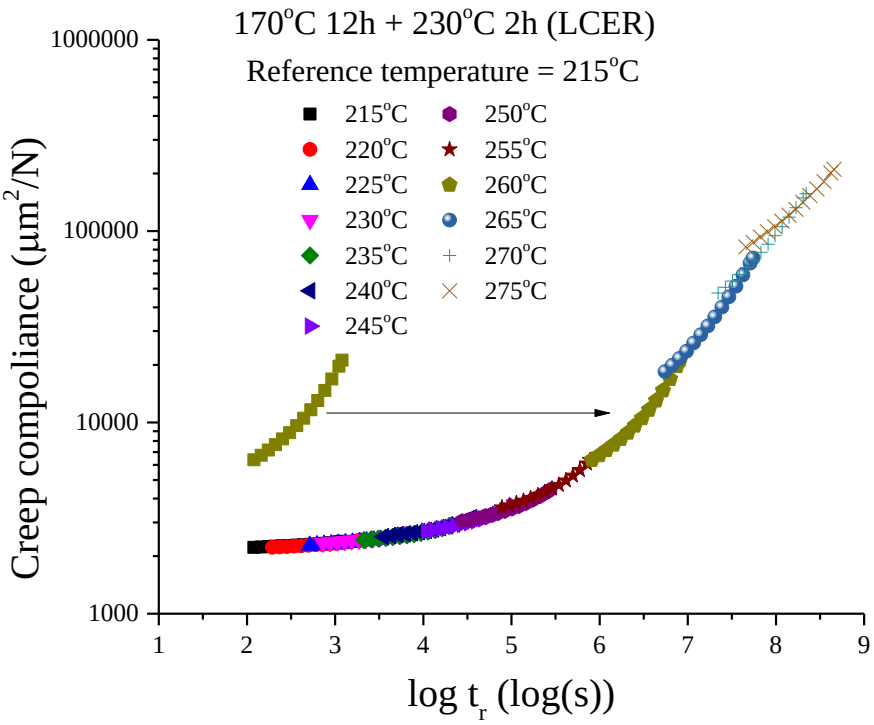

Figure 4.8 Manually shifted creep compliance data for the LCER cured at 170 ºC at a reference temperature of 215 ºC.

In order to determine the long-term performance of the resins, the master curves generated for all systems at a reference temperature of 215 ºC are shown in Figure 4.9 with lines representing times of 1 month, 1 year, and 10 years, respectively. As can be seen, the LCER systems exhibited a lower values of predicted creep compliance, illustrating the reinforcing effect of the LC phase on the creep resistance of the material.

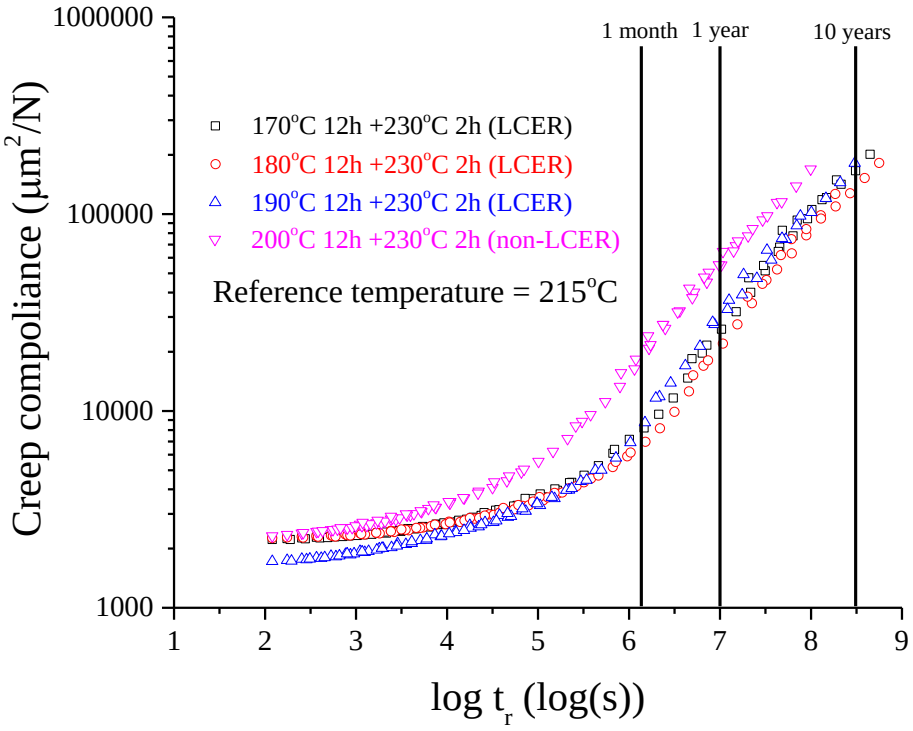

Figure 4.9 Master curves generated from manually shifted creep compliance data for the LCER and non-LCER systems.

4.5 Conclusions

In this work, the creep behavior of a LCER and a non-LCER prepared from the same epoxy monomer was investigated at different temperature isotherms. The Burger model was used to simulate the creep performance of both systems. The long-term creep compliance was evaluated using the time-temperature superposition principle. The study revealed that the presence of a LC phase can improve creep resistance of the resins. The experimental results showed that, compared to the non-LCER, the LCER systems exhibited a decrease in both creep strain and creep rate at the same temperature. The modeling revealed that the introduction of the LC phase into the resin network is an effective

approach to reinforce the viscoelastic properties of the resin, including instantaneous elasticity, retardant elasticity, and permanent deformation resistance. The rigid filler effect and the crosslinking effect of the LC phase are considered to be two important self-reinforcing mechanisms. In addition, the resins cured in LC phase showed improved long-term performance and durability.

4.6 Acknowledgements

Support from the Air Force Office of Scientific Research (AFOSR) Award No. FA9550-12-1-0108 is gratefully acknowledged.

4.7 References

[1] Yang J-L, Zhang Z, Schlarb AK, and Friedrich K. Polymer 2006;47(8):2791-2801.

[2] Yang J-L, Zhang Z, Schlarb AK, and Friedrich K. Polymer 2006;47(19):6745-6758.

[3] Dai Z, Gao Y, Liu L, Pötschke P, Yang J, and Zhang Z. Polymer 2013;54(14):3723-3729.

[4] Carfagna C, Amendola E, and Giamberini M. Progress in Polymer Science 1997;22(8):1607-1647.

[5] Ortiz C, Kim R, Rodighiero E, Ober CK, and Kramer EJ. Macromolecules 1998;31(13):4074-4088.

[6] Ortiz C, Belenky L, Ober CK, and Kramer EJ. Journal of Materials Science 2000;35(8):2079-2086.

[7] Harada M, Okamoto N, and Ochi M. Journal of Polymer Science Part B: Polymer Physics 2010;48(22):2337-2345.

[8] Liu Y-L, Cai Z-Q, Wang W-C, Wen X, Pi P, Zheng D, Cheng J, and Yang Z. Macromolecular Materials and Engineering 2011;296(1):83-91.

[9] Carfagna C, Acierno D, Di Palma V, Amendola E, and Giamberini M. Macromolecular Chemistry and Physics 2000;201(18):2631-2638.

[10] Carfagna C, Meo G, Nicolais L, Giamberini M, Priola A, and Malucelli G. Macromolecular Chemistry and Physics 2000;201(18):2639-2645.

[11] Jang J and Bae J. Advanced Functional Materials 2005;15(11):1877-1882.

[12] Hsu S-H, Wu M-C, Chen S, Chuang C-M, Lin S-H, and Su W-F. Carbon 2012;50(3):896-905.

[13] Vincent L, Mija A, and Sbirrazzuoli N. Polymer Degradation and Stability 2007;92(11):2051-2057.

[14] Lin QH, Yee AF, Sue HJ, Earls JD, and Hefner RE. Journal of Polymer Science Part B-Polymer Physics 1997;35(14):2363-2378.

[15] Harada M, Ochi M, Tobita M, Kimura T, Ishigaki T, Shimoyama N, and Aoki H. Journal of Polymer Science Part B-Polymer Physics 2003;41(14):1739-1743.

[16] Su WFA, Chen KC, and Tseng SY. Journal of Applied Polymer Science 2000;78(2):446-451.

[17] Lee JY, Jang J, Hwang SS, Hong SM, and Kim KU. Polymer 1998;39(24):6121-6126.

[18] Lee JY and Jang J. Polymer 2006;47(9):3036-3042.

[19] Nie L, Burgess A, and Ryan A. Macromolecular Chemistry and Physics 2013;214(2):225-235.

[20] Benicewicz BC, Smith ME, Earls JD, Priester RD, Setz SM, Duran RS, and Douglas EP. Macromolecules 1998;31(15):4730-4738.

[21] Shiota A and Ober CK. Macromolecules 1997;30(15):4278-4287.

[22] Jahromi S, Kuipers WAG, Norder B, and Mijs WJ. Macromolecules 1995;28(7):2201-2211.

[23] Hikmet RAM and Broer DJ. Polymer 1991;32(9):1627-1632.

[24] Li Y and Kessler MR. Polymer 2013;54(21):5741-5746.

[25] Li Y, Badrinarayanan P, and Kessler MR. Polymer 2013;54(12):3017-3025.

[26] Sheng X, Akinc M, and Kessler MR. Materials Science and Engineering: A 2010;527(21–22):5892-5899.

[27] Goertzen WK and Kessler MR. Materials Science and Engineering: A 2006;421(1–2):217-225.

CHAPTER 5. LIQUID CRYSTALLINE EPOXY RESIN BASED ON BIPHENYL MESOGEN: EFFECT OF MAGNETIC FIELD ORIENTATION DURING CURE

A paper published in *Polymer*[1]

Yuzhan Li[2], Michael R. Kessler[3,4]

5.1 Abstract

A biphenyl based epoxy monomer, 4,4'-diglycidyloxybiphenyl (BP), was synthesized and cured with a tetra-functional amine, sulfanilamide (SAA), to obtain a liquid crystalline epoxy network. The curing behavior of BP with SAA was studied using differential scanning calorimetry, polarized optical microscopy, and parallel plate rheology. Macroscopic orientation of the liquid crystalline epoxy resins (LCERs) was achieved by curing in a high strength magnetic field, and quantified by an orientation parameter determined with wide angle X-ray diffraction. The effects of orientation on the glass transition temperature, coefficient of thermal expansion, and dynamic mechanical properties of the LCERs were investigated. The results reveal that the formation of the liquid crystalline phase has a dramatic influence on the curing reaction, leading to a decrease in viscosity of the reacting system. Oriented LCERs exhibit anisotropic thermal expansion behavior and significant improvements of thermomechanical properties.

---

[1] Reprinted with permission of *Polymer*, 2013, 54(21), 5741-5746.
[2] Graduate student, Department of Materials Science and Engineering, Iowa State University
[3] Professor and Director, School of Mechanical and Materials Engineering, Washington State University
[4] Author for correspondence

5.2 Introduction

Orientation is a phenomenon of great theoretical and technical importance in polymer science. Oriented polymers are usually highly anisotropic and possess excellent physical properties. However, polymers tend to lose their orientation when subjected to elevated temperature or through relaxation with time. The development of liquid crystalline thermosets (LCTs) has the potential to solve the problem described above. LCTs are a unique class of thermosetting materials formed upon curing of low molecular weight, rigid rod, multifunctional monomers resulting in the retention of a liquid crystalline (LC) phase, as well as retention of orientation of that LC phase, by the three dimensional crosslinking network [1, 2].

Among all the LCTs synthesized from monomers with different functional groups, liquid crystalline epoxy resins (LCERs) have receive the most attention because of their excellent thermal and mechanical properties [3-11]. Of particular interest to our work is the ability to tailor the coefficient of thermal expansion (CTE) of LCERs by processing them under an external field. Such design flexibility in the CTE of the resins makes them attractive candidates for polymer matrices in high performance composites, where significant mismatches can occur between the polymer matrix and glass or carbon fiber reinforcement. The LCERs with low thermal expansion can ensure minimal mismatch in CTE with the fiber reinforcements, thereby reducing the magnitude of residual stresses; facilitating the development of high performance polymer matrix composites.

Various techniques have been utilized to produce an oriented LC phase, including surface field orientation, electric field orientation, and magnetic field orientation [12-24]. Compared to surface field and electric field orientation, the use of magnetic field to orient

LCTs has several advantages. The effective field strength remains relatively constant when bulk samples are cured. In addition, the high strength magnetic field will not have an adverse effect on the properties of the resins[25].

Several research groups have prepared and studied the orientation of LCERs. Barclay and coworkers synthesized a methylstilbene based LCER. The networks were oriented under the influence of both a mechanical and a magnetic field [26]. Orientation parameters of 0.13 to 0.57 were achieved. Benicewicz and workers investigated the magnetic field orientation of the same LCER, and found that high levels of orientation and substantial improvements of physical properties were achieved under a magnetic field strength of approximately 12 T [25]. However, the rheological behavior of the LC system needs to be further studied to understand the effect of LC phase formation on the curing reaction. Systematic study of thermomechanical properties of macroscopically oriented LCERs is necessary to explore the potential application of this unique material.

In the present work, a biphenyl mesogen based LCER is synthesized, and the rheological behavior of the resins during the curing reaction is studied. In addition, the influence of magnetic field on the structure and thermomechanical properties of the resins is investigated. The degree of orientation, glass transition temperature, dynamic mechanical properties, thermal expansivity, and thermal stability of the resins cured with and without magnetic field are examined systematically.

5.3 Experimental

5.3.1 Materials

4,4’-dihydroxybiphenyl with 97% purity, benzyltrimethylammonium bromide, and

sulfanilamide (SAA) were purchased from Sigma-Aldrich (Milwaukee, WI). Epichlorohydrin with 99% purity was obtained from Acros Organics (Belgium). Sodium hydroxide, isopropyl alcohol, chloroform, methanol, hydrochloric acid, and acetone were supplied by Fisher Scientific (Fair Lawn, NJ). All chemicals were used as received without further purification. 4,4'-diglycidyloxybiphenyl (BP) was synthesized according to a procedure reported in an earlier work by Su and coworkers [27]. The chemical structures of the epoxy monomer and the curing agent are illustrated in Figure 5.1.

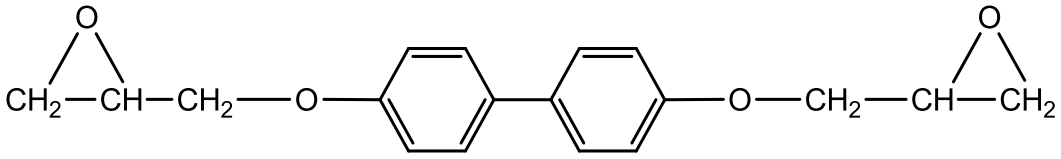

4,4'-diglycidyloxybiphenyl (BP)

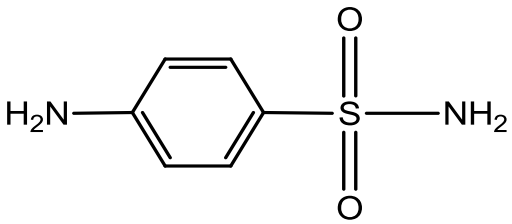

Sulfanilamide (SAA)

Figure 5.1 Chemical structures of the epoxy monomer and the curing agent.

5.3.2 Sample preparation and magnetic field processing

Uncured resin samples were prepared by dissolving BP and SAA in tetrahydrofuran (THF) in a stoichiometric ratio. Then the solvent was removed at room temperature and the mixture was dried under vacuum for 24 hours to prevent further reaction. Oriented LCERs were prepared by premelting the powder mixture in a 5mm NMR tube. The curing

and orientation were carried out at 150 ºC for 4 hours using a 400 MHz (9.4T) high temperature NMR spectrometer (Bruker DRX-400). The NMR bore was preheated to 150 ºC before the tube was inserted. Unoriented LCERs samples were prepared in the same manner, but were cured in an oil bath for comparison purpose.

5.3.3 Characterization methods

The rheological measurements of the curing reaction were conducted using an AR2000ex stress-controlled rheometer (TA Instruments, Inc.) with parallel plate geometry and an aluminum plate fixture with a diameter of 25 mm. The aluminum plates were preheated to the curing temperature. Approximately 0.5 g of the powder mixture was placed on the bottom plate, and then the top plate was lowered to a gap of ca. 1mm. Oscillatory experiments were carried out at an isotherm of 150 ºC with an amplitude of 1000 Pa and at a frequency of 1 Hz.

The LC Morphologies of the LCERs were investigated using a polarized optical microscope (POM) from Olympus (model BX51-TRF equipped with a Linkam LTS-350 hot stage and TMS-94 temperature controller). The isothermal curing of BP with SAA was monitored using POM to examine the formation and development of the LC phase.

The X-ray diffraction (XRD) patterns of the LCERs were collected using a Bruker D8 Advance Diffractometer in transmission mode. The system was equipped with a HI-STAR area detector and controlled via Bruker software (GADDS version 4.1.44). The X-ray source used in the experiments consisted of a chromium X-ray tube energized via a Kristalloflex 760 generator and maintained at 30 kV and 50 mA. A graphite monochromator was used to tune the source to CrKα radiation. In the experiment,

a 0.8 mm collimator was used to control the divergence of the primary X-ray beam. A 6 mm×4 mm specimen was mounted in the transmission fixture 40 mm from the collimator assembly. A beam stop (2.5 mm diameter) was placed 25 mm behind the test specimen. The detector was positioned 15 cm from the specimen. Data was collected by moving the detector in three individual increments (0º, 17º and 34º) in the positive 2-theta direction. A counting time of 300 seconds was used for each step. Data was corrected for spatial and flood field aberrations using the GADDS software.

The curing behavior and the thermal properties of the LCERs were studied using a Q2000 DSC (TA Instruments, Inc.). The DSC cell was purged with helium gas at a flow rate of 25 mL/min. For the glass transition temperature measurements, the first heating scan was used to erase the thermal history. While the second heating scan was recorded to evaluate Tg.

The dynamic mechanical properties of the LCERs cured with and without magnetic field were studied using a model Q800 dynamic mechanical analyzer (DMA, TA Instruments, Inc.). All the samples were heated from room temperature to 280 ºC at 3 ºC/min, at a frequency of 1 Hz and an amplitude of 25 μm in three-point bending mode.

The CTE of the LCERs was measured with a model Q400 thermomechanical analyzer (TMA, TA Instruments, Inc.) in expansion mode with a heat-cool-heat cycle at a rate of 5 ºC/min- 3 ºC/min- 3 ºC/min. The second heating scan was recorded to calculate the value of CTE.

The thermal stability of the LCERs was investigated using a thermogravimetric analyzer (TGA) on a model Q50 TGA (TA Instruments, Inc.). About 10 mg of resins was placed in an alumina pan and heated from 25 ºC to 800 ºC at a rate of 20 ºC/min under an

air purge of 60 mL/min.

5.4 Results and discussion

5.4.1 Curing behavior

An isothermal DSC scan was performed to study the curing behavior of BP with SAA. Unlike the curing reaction of conventional epoxy resins which is characterized by a single exothermic peak, two peaks were observed as shown in Figure 5.2. The first exothermic peak results from the reaction between an epoxy group of BP and the aromatic amine group of SAA. While the second peak is related to the formation of the LC phase that develops with increasing molecular weight, which has been confirmed in our previous investigation. In our previous work, a series of isothermal curing experiments were performed at different temperatures [28]. It was found that the curing temperature had a great influence on the LC phase formation, and the resins cured in LC phase exhibited two exothermic peaks in the DSC thermogram. Similar results were also reported by other researchers for different LCER systems [29, 30]. However, the influence of LC phase formation on the curing reaction is not fully understood.

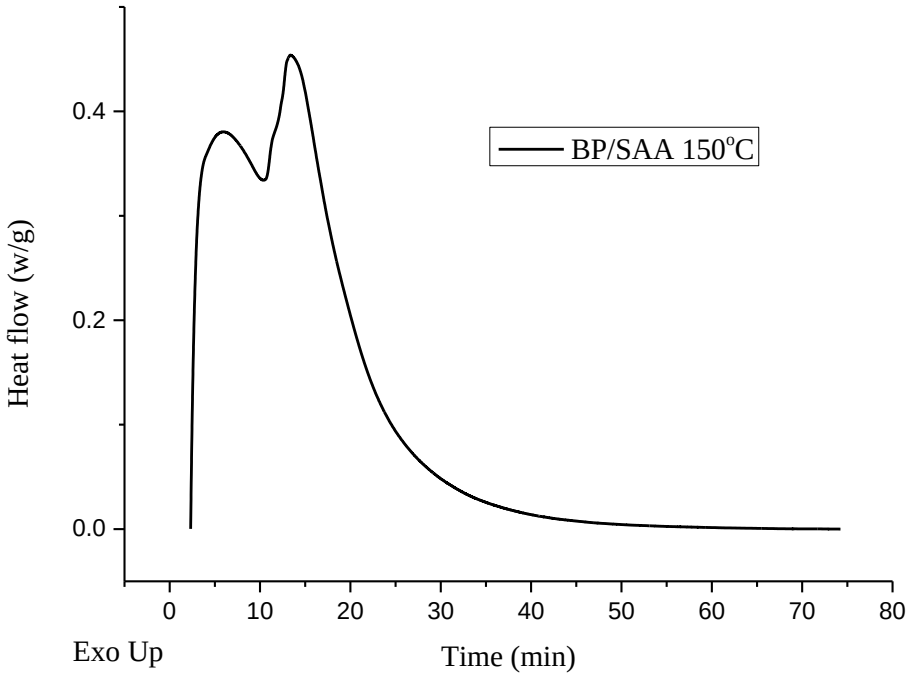

Figure 5.2 Isothermal DSC curve showing the exothermic cure of BP with SAA at 150 ºC.

In order to study the effect of LC formation on the curing reaction, a parallel plate rheology experiment was carried out to examine the phase transition of the curing system. The evolution of complex viscosity, storage modulus (G'), and loss modulus (G'') during cure is shown in Figure 5.3.

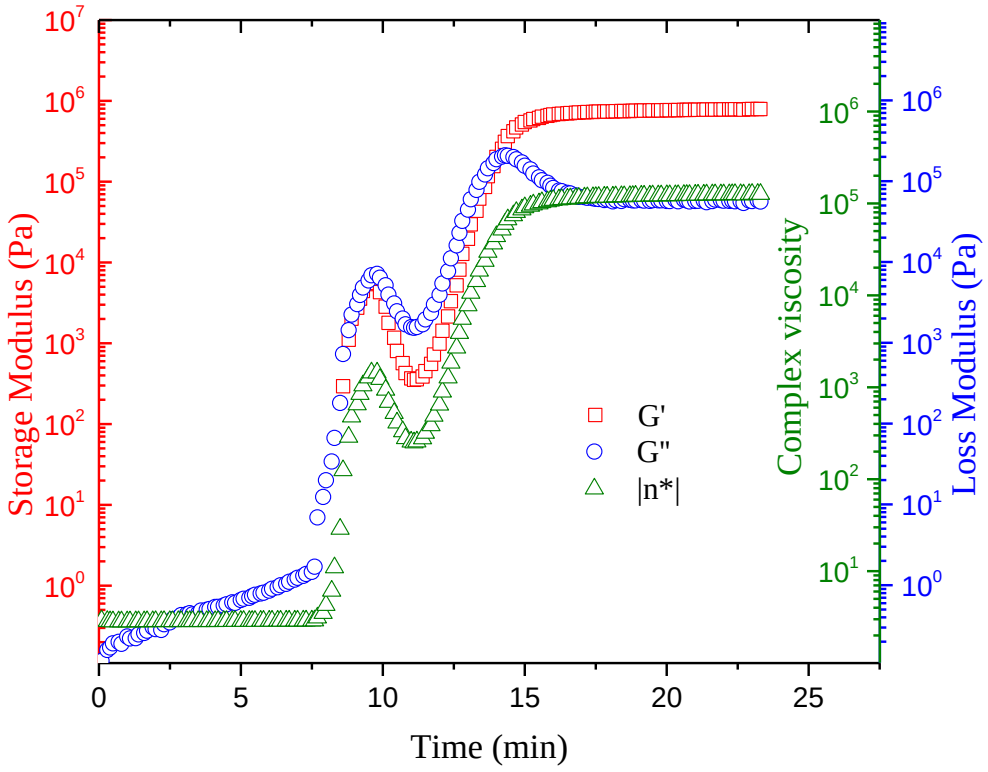

Figure 5.3 Evolution of the complex viscosity, storage (G'), and loss (G'') moduli as a function of the reaction time at 150 ºC (frequency = 1 Hz).

The curing reaction starts immediately after the melting of the two components and the system is initially isotropic. Reaction in the early stage of cure (0-8 min) involves the growth and branching of the polymer chains. In this study, the chain branching is substantially reduced by using SAA as the curing agent, because the two amine groups have unequal reactivity. At this time in the cure, the reacting system behaves like a viscoelastic liquid, therefore only the loss modulus representing the liquid-like part of the system can be observed. As the reaction proceeds (8-10 min), the molecular weight of the polymer chains increases rapidly, leading to a dramatic increase in viscosity of the system as shown in Figure 5.3. However, unlike the curing reaction in traditional epoxy resins,

which exhibits a continuous increase in viscosity with time, a decrease of viscosity was observed in the curing process of BP with SAA from ca. 10 min to 12 min. Of particular note is that in the isothermal DSC curing study, the second exothermic peak starts forming after about 10 min of the curing reaction. Concomitant evidence from temperature controlled polarized optical microscopy confirm these findings and were reported in our previous work [28]. Therefore, the decrease of viscosity is readily related to the LC formation. The complex viscosity, storage modulus, and loss modulus of the curing system continue to increase after the formation of LC phase. Further curing leads to gelation, where the reacting system transforms from a viscous liquid to an elastic gel. The gel time can be determined from the crossover point of the storage and loss moduli. For the present system, the gel time was determined to be 15 min. Additionally, the vitrification time of the system is determined from the time when the loss modulus curve reaches its maximum, indicating the transformation of LCERs from a rubbery state to a glassy state, due to the increase of T_g with time during the curing reaction. After 20 min of cure, both G' and G'' level off, indicating that no significant additional reaction takes place at this isothermal cure temperature. Based on the DSC and rheology experiments, we could conclude that the formation of the LC phase leads to a decrease in viscosity of the reacting system, thereby facilitating the curing reaction, and resulting in an additional cure exotherm.

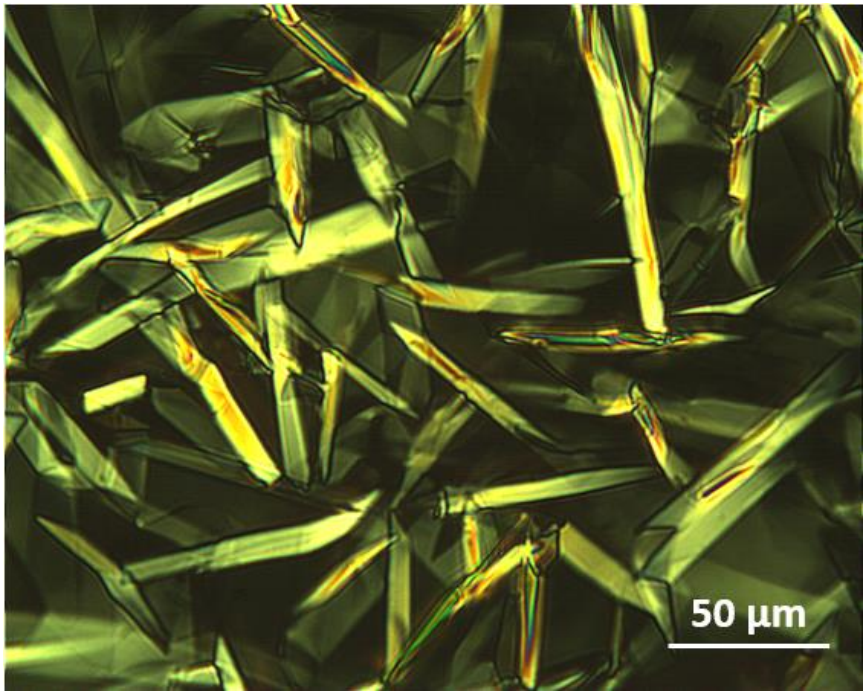

Figure 5.4 POM image after 1 h of isothermal curing of BP with SAA at 150 ºC.

The isothermal curing of BP with SAA was also observed with a microscope under polarized light to examine the morphology of the resins. The LCERs show a polycrystalline structure which consists of a large number of individual LC domains. Additionally, the diffraction peak at ca. 5º in the XRD experiment is indicative of the presence of layered smectic LC phase. In the absence of external fields, the molecular orientation of the LC domains is completely random.

5.4.2 Orientation

Orientation of LC domains in LCERs usually needs to be carried out before gelation when the mesogens are still able to response to the applied field. However, it is worth mentioning that Koerner and coworkers investigated the electric response of a LC cyanate ester system in a recent work and found that the reorientation of the LC phase is still

possible after gelation [24]. Although the gel time of curing reaction between BP with SAA is relatively short, the extremely low initial viscosity of the system is able to facilitate the alignment of the LC domains. The principle of LC orientation under magnetic field is extensively described in the literature [31, 32]. The anisotropy of the diamagnetic susceptibility of the LC molecules and the cooperative motion of the LC mesogens are the driving force for the orientation of LC domains. In this work, the curing and orientation of LCERs were performed at 150 ºC using a high temperature NMR which is able to create a magnetic field strength of 9.4 Tesla. Then various experimental techniques were utilized to characterize the oriented LCERs.

Photographic XRD is commonly used to determine the molecular orientation because the orientation distribution can be calculated directly from the quantified diffraction pattern. In liquid crystal science, the order parameter, S also known as the Hermann's orientation parameter is used to quantify the degree of LC order. The XRD patterns of the oriented and unoriented LCERs collected at different Bragg angles are shown in Figure 5.5. For both samples, the sharp diffraction rings at smaller Bragg angle correspond to the layered structure of the smectic LC domain. While the diffuse diffraction ring at higher Bragg angle is a result of the lateral spacing between the LC mesogens. Of particular interest is that the oriented LCERs have much higher diffraction intensity and second order diffraction, indicating that the networks have an exceptionally regular layered molecular organization. In addition, the concentrated diffraction ring confirms the successful orientation of the LCERs. On the other hand, the diffraction intensity of the unoriented LCERs is uniformly distributed along the ring, suggesting the absence of orientation.

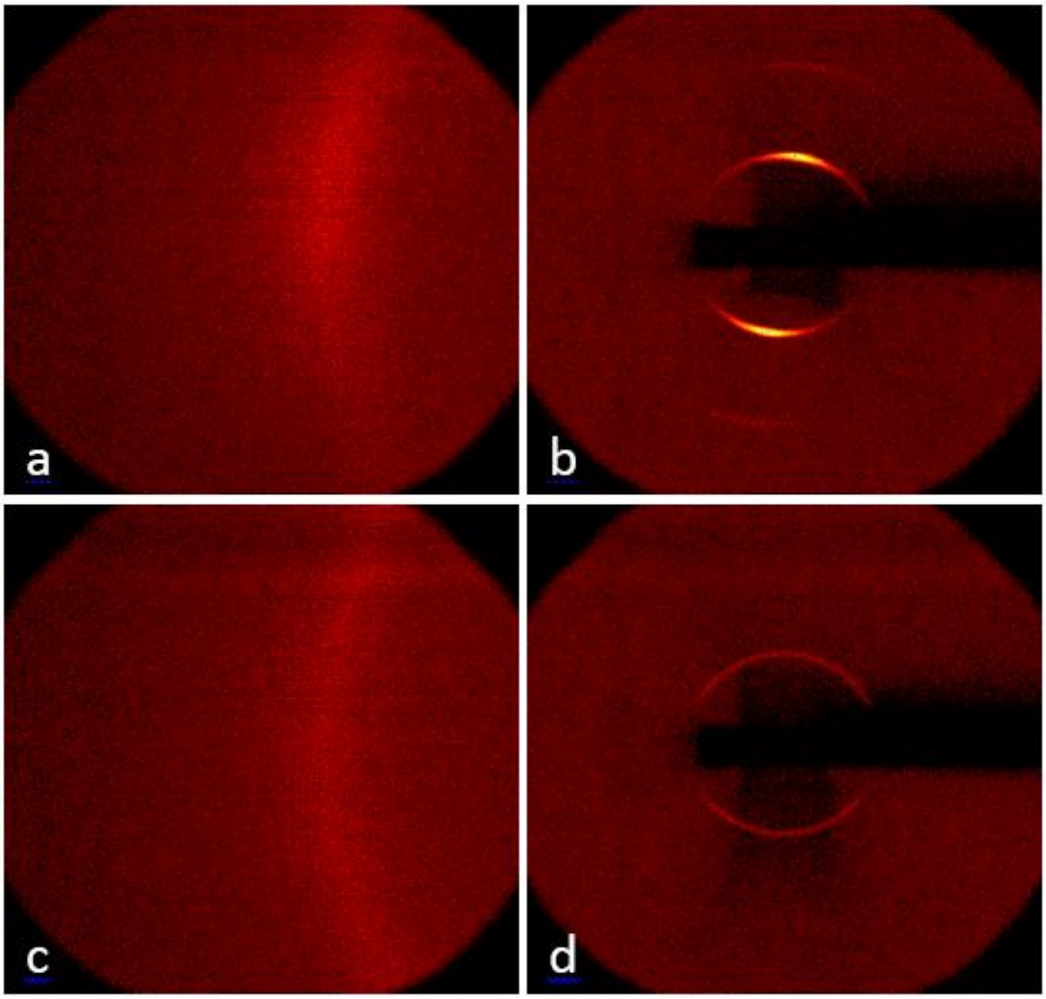

Figure 5.5 XRD patterns of oriented LCERs and unoriented LCERs.
(a), (b) Oriented LCERs at 2θ=34º, 0º
(c), (d) Unoriented LCERs at 2θ=34º, 0º

The diffraction patterns were quantified by integrating along the Bragg angle. Figure 5.6 shows the XRD spectra of the resins after the 2-theta integration. When the incident X-ray beam is perpendicular to the smectic layer normal, most of the oriented LC domains satisfy the diffraction condition, leading to a strong diffraction peak at ca. 5º in the spectra, which corresponds to the thickness of the smectic layer ca. 20 Å. However, if the incident beam is parallel to the layer normal, the intensity of the diffraction from smectic layer is

decreased substantially (18% of the perpendicular case) since the diffraction condition is no longer satisfied for most of the LC domains. It also can be seen that the diffraction intensity from the smectic layer of unoriented LCERs are in an intermediate state (21% of the perpendicular case), between the parallel and perpendicular incident beam measurements for the oriented samples.

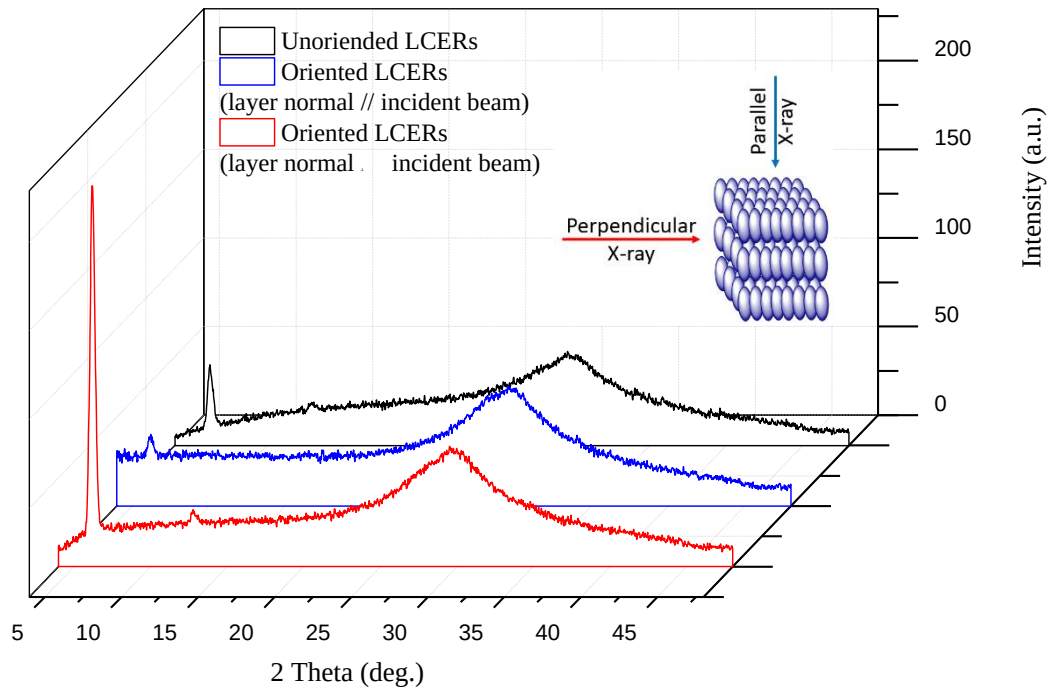

Figure 5.6 XRD spectra after integration along the Bragg angle.

In order to calculate the order parameter, the azimuthal intensity distribution I(χ) was evaluated by integrating along the inner diffraction ring of the oriented LCERs with a step size of 0.02 deg. In this study, only the inner diffraction caused by the smectic layer of the LC phase was used to calculate the order parameter because of its completeness and higher

intensity compared to the outer diffraction. The intensity distribution in the samples I(α) was then calculated from the azimuthal intensity distribution I(χ) by

$$\cos(\alpha) = \cos(\chi)\cos(\theta)$$

where θ is the Bragg angle and α is the angle between the smectic layer normal of the LC domain with respect to the magnetic field direction. However, this transformation results in no data being available for α from 0º, and therefore the data were fitted using the Pearson VII function shown in Figure 5.7 to acquire intensity values over the entire range [33]. The intensity maxima was set at an angle of α=0º.

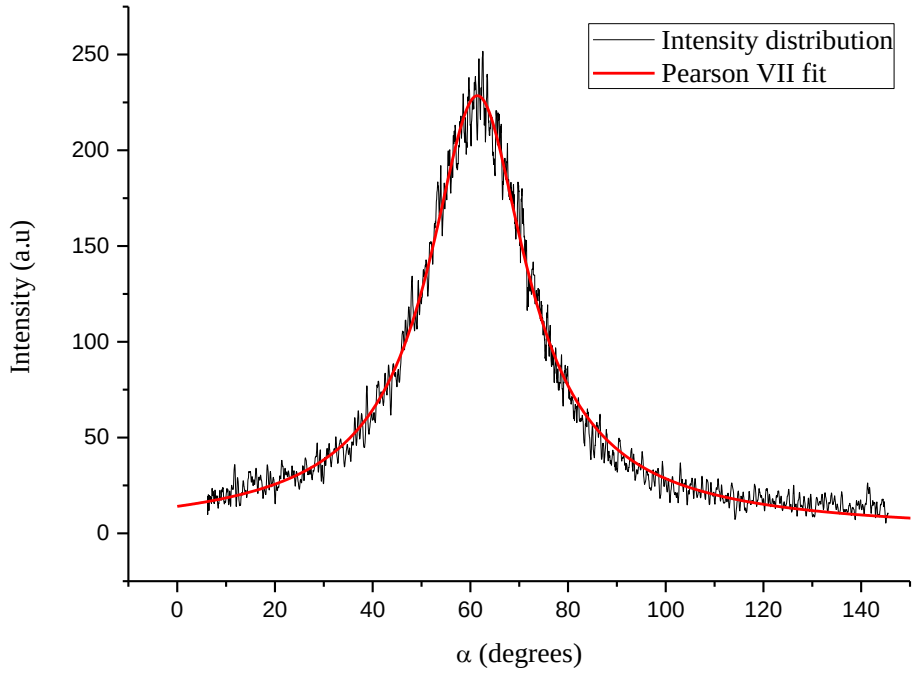

Figure 5.7 Intensity distribution evaluated by integration through the inner diffraction ring of LCERs with a step size of 0.02 deg. The red line is the Pearson VII fit of the experimental data.

From the intensity distribution I(α), the average cos2α over all of the orienting smectic LC domains is determined according to

$$<\cos^2\alpha>=\frac{\int_0^{\pi/2} I(\alpha)\sin\alpha\cos^2\alpha\, d\alpha}{\int_0^{\pi/2} I(\alpha)\sin\alpha\, d\alpha}$$

and then the orientation parameter S was calculated according to

$$S=\frac{1}{2}(3<\cos^2\alpha>-1)$$

Figure 5.8 shows the integrands used to calculate <cos2α> from the ratio of the areas under the black and the red lines. The orientation parameter of the smectic layer normals was determined to be 0.4.

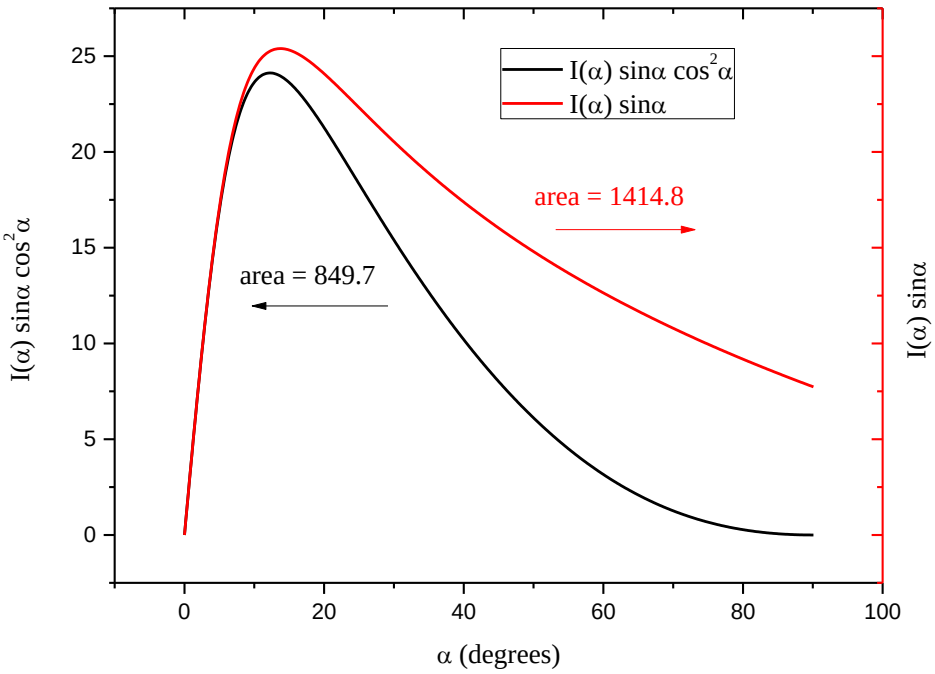

Figure 5.8 Graphical presentation of the two integrals in the ratio that determines $<\cos^2\alpha>$ for the oriented LCERs.

5.4.3 Thermomechanical properties

The dynamic mechanical properties of the LCERs cured with and without a magnetic field were investigated using DMA. The results are shown in Figure 5.9. Oriented LCERs exhibit higher values of glassy storage modulus, rubbery storage modulus, and glass transition temperature. For the oriented LCERs, in the direction parallel to the orientation, the applied force largely acts on the rigid LC domains, while in the direction perpendicular to the orientation the force is mostly applied to the relatively soft crosslinks between LC mesogens. Therefore, in the orientation direction, oriented LCERs show significantly higher values of storage modulus and loss modulus. In addition, compared to unoriented LCER, oriented LCER exhibits lower tanδ value, indicating the rigid characteristic in the direction of orientation. Moreover, the Tg was determined from the peak of the mechanical damping curve (tanδ). Oriented LCERs have a higher Tg, possibly due to the decrease in free volume during the magnetic field processing.

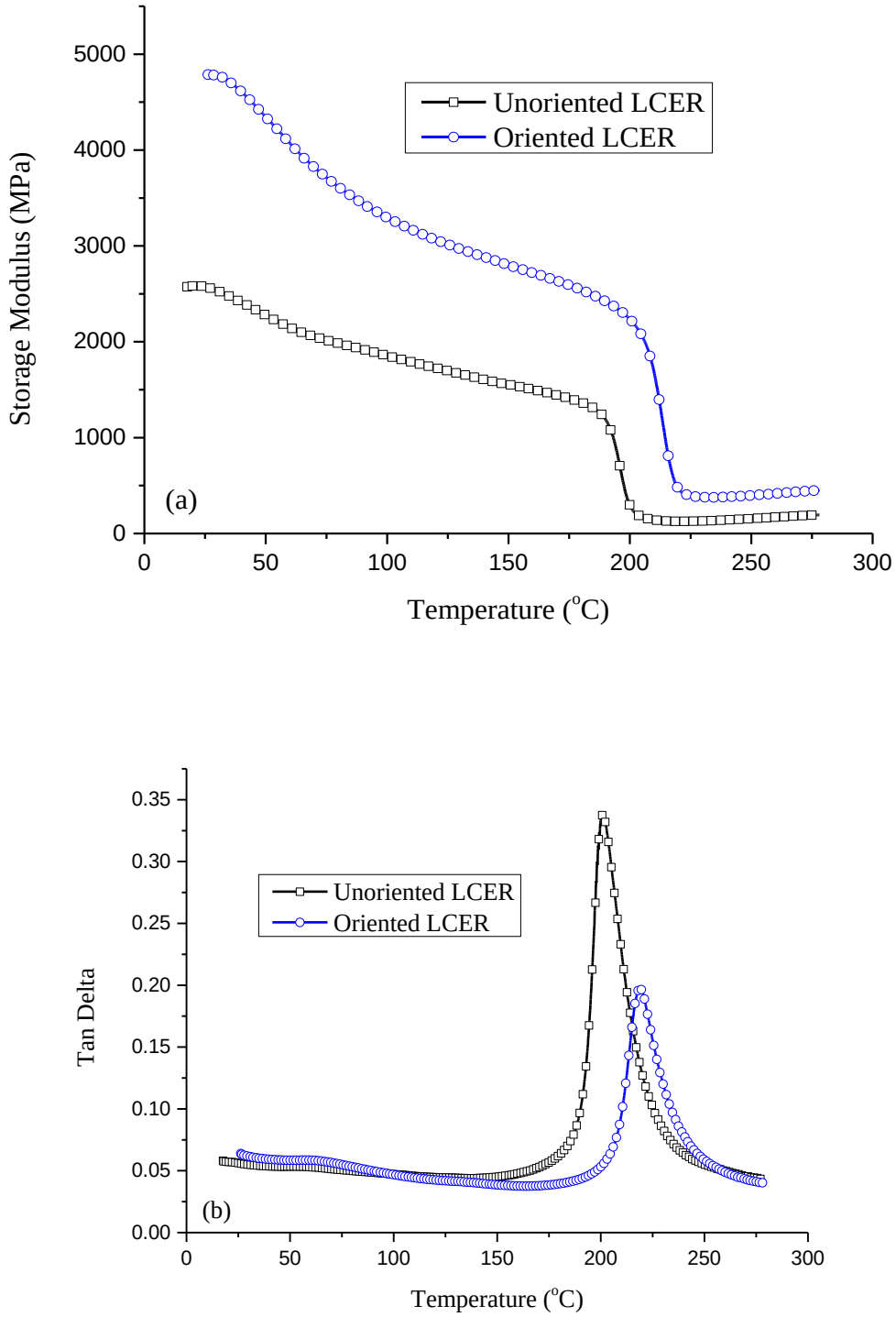

Figure 5.9 Dynamic mechanical properties of oriented and unoriented LCERs.
(a) Oriented LCER; (b) Unoriented LCER

The CTE values of the LCERs cured with and without magnetic field were determined using TMA and the results are shown in Figure 5.10. A substantial reduction of CTE was observed for the oriented LCERs. They possess anisotropic CTE values in the glassy region with 16 ppm/ºC in the direction parallel to the orientation and 72 ppm/ºC in the direction perpendicular to the orientation. It is thought that the thermal expansion of the resins is greatly restricted by the rigid and oriented LC domains in the orientation direction. In addition, a negative CTE value was observed for the oriented LCERs in the rubber regime, indicating that while the resins expand in the transverse direction, a simultaneous shrinkage takes place in the direction of orientation. However, for unoriented LCERs, the CTE values are almost the same in both directions, suggesting the random distribution of LC domains in the crosslinking networks. Additionally, it is thought that the CTE value of this LCERs can be further reduced if stronger magnetic field is utilized. Smith and coworker reported CTE values of 4.7 ppm/^{o}C and 4.3 ppm/^{o}C for a LCER cured under a magnetic field strength of 12T and 18T, respectively [34].

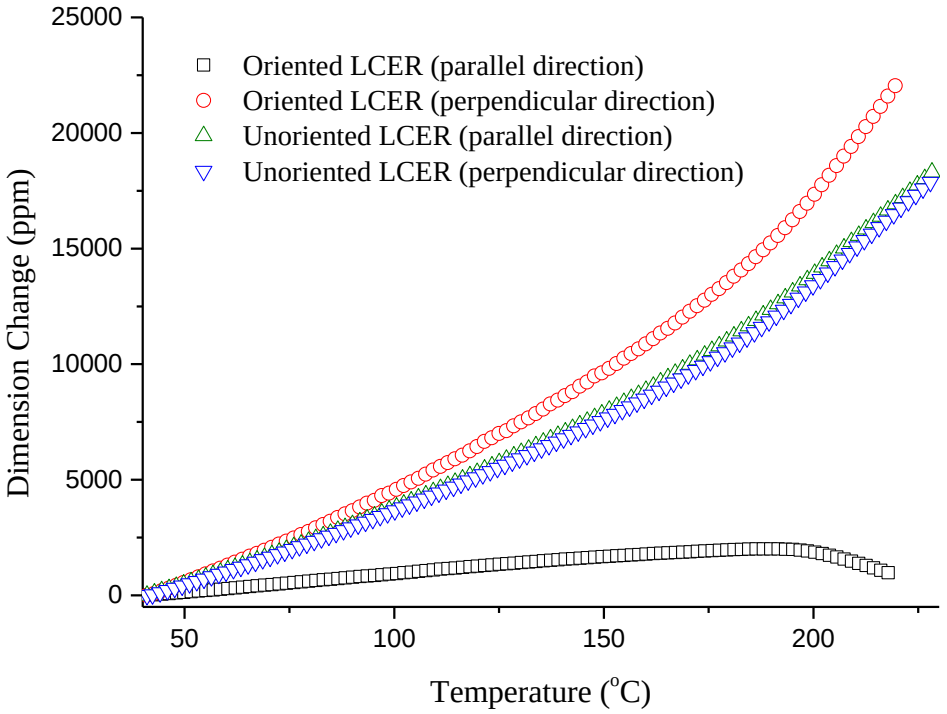

Figure 5.10 Dimension change of oriented and unoriented LCERs upon heating.

The thermal stability of the LCERs cured with and without a magnetic field was also examined. The thermal decomposition temperature was defined as the temperature when the samples lost 5% of their initial weight. The results show that the orientation of the LC domains does not have an influence on the thermal stability of the LCERs, which indicates that the major factor that affects thermal stability of the resins is chemical bonding rather than morphologies and orientation. All the thermomechanical properties of the oriented and unoriented LCERs are summarized in Table 5.1.

Table 5.1 Thermomechanical data obtained from DMA, TMA and TGA.

	Oriented LCERs	Unoriented LCERs
E' at 30°C (MPa)	4774.9	2532.1
E' at 280°C (MPa)	396.8	155.2
T_g DMA (°C)	219.0	201.0
Glassy CTE (ppm/°C) longitudinal direction	16.4	60.0
Rubbery CTE (ppm/°C) longitudinal direction	-57.6	155.5
Glassy CTE (ppm/°C) transverse direction	72.6	59.5
Rubbery CTE (ppm/°C) transverse direction	251.2	159.5
T_d (°C) at 95% weight	305.2	307.2

5.5 Conclusions

The curing behavior of the LCERs is studied using various experimental techniques. DSC and rheological results show that the formation of the LC phase leads to a decrease in viscosity of the system, resulting in a rate acceleration the curing reaction between BP with SAA. The synthesized LCERs were successfully oriented under a high strength magnetic field, and the effects of orientation on the thermomechanical properties of the LCERs were investigated. Macroscopically oriented LCERs possess highly anisotropic physical properties. In the direction of orientation, LCERs cured under a magnetic field

have a substantial reduction of CTE and significant improvements in dynamic mechanical properties.

5.6 Acknowledgements

The authors would like to thank Dr. Scott Schlorholtz in the Materials Analysis Research Laboratory at Iowa State University for his help in X-ray diffraction tests. Support from the Air Force Office of Scientific Research (AFOSR) Award No. FA9550-12-1-0108 is gratefully acknowledged.

5.7 References

[1] Barclay GG and Ober CK. Progress in Polymer Science 1993;18(5):899-945.

[2] Shiota A and Ober CK. Progress in Polymer Science 1997;22(5):975-1000.

[3] Carfagna C, Amendola E, and Giamberini M. Progress in Polymer Science 1997;22(8):1607-1647.

[4] Ortiz C, Kim R, Rodighiero E, Ober CK, and Kramer EJ. Macromolecules 1998;31(13):4074-4088.

[5] Mallon JJ and Adams PM. Journal of Polymer Science Part A-Polymer Chemistry 1993;31(9):2249-2260.

[6] Liu JP, Wang CC, Campbell GA, Earls JD, and Priester RD. Journal of Polymer Science Part a-Polymer Chemistry 1997;35(6):1105-1124.

[7] Punchaipetch P, Ambrogi V, Giamberini M, Brostow W, Carfagna C, and D'Souza A. Polymer 2002;43(3):839-848.

[8] Harada M, Okamoto N, and Ochi M. Journal of Polymer Science Part B-Polymer Physics 2010;48(22):2337-2345.

[9] Sue HJ, Earls JD, Hefner RE, Villarreal MI, Garcia-Meitin EI, Yang PC, Cheatham CM, and Plummer CJG. Polymer 1998;39(20):4707-4714.

[10] Barclay GG, Ober CK, Papathomas KI, and Wang DW. Journal of Polymer Science Part a-Polymer Chemistry 1992;30(9):1831-1843.

[11] Jahromi S and Mijs WJ. Molecular Crystals and Liquid Crystals Science and Technology Section a-Molecular Crystals and Liquid Crystals 1994;250:209-222.

[12] Jahromi S, Kuipers WAG, Norder B, and Mijs WJ. Macromolecules 1995;28(7):2201-2211.

[13] Hikmet RAM and Broer DJ. Polymer 1991;32(9):1627-1632.

[14] Hikmet RAM and Howard R. Physical Review E 1993;48(4):2752-2759.

[15] Andersson H, Sahlen F, Trollsas M, Gedde UW, and Hult A. Journal of Macromolecular Science-Pure and Applied Chemistry 1996;A33(10):1427-1436.

[16] Hoyle CE, Watanabe T, and Whitehead JB. Macromolecules 1994;27(22):6581-6588.

[17] Broer DJ, Lub J, and Mol GN. Macromolecules 1993;26(6):1244-1247.

[18] Shiota A and Ober CK. Macromolecules 1997;30(15):4278-4287.

[19] Korner H, Shiota A, Bunning TJ, and Ober CK. Science 1996;272(5259):252-255.

[20] Moore JS and Stupp SI. Macromolecules 1987;20(2):282-293.

[21] Lembicz F. Polymer 1991;32(16):2898-2901.

[22] Zhao Y and Lei HL. Macromolecules 1992;25(15):4043-4045.

[23] Kishi R, Sisido M, and Tazuke S. Macromolecules 1990;23(16):3868-3870.

[24] Koerner H, Ober CK, and Ku H. Polymer 2011;52(10):2206-2213.

[25] Benicewicz BC, Smith ME, Earls JD, Priester RD, Setz SM, Duran RS, and Douglas EP. Macromolecules 1998;31(15):4730-4738.

[26] Barclay GG, McNamee SG, Ober CK, Papathomas KI, and Wang DW. Journal of Polymer Science Part a-Polymer Chemistry 1992;30(9):1845-1853.

[27] Su WFA, Chen KC, and Tseng SY. Journal of Applied Polymer Science 2000;78(2):446-451.

[28] Li Y, Badrinarayanan P, and Kessler MR. Polymer 2013;54(12):3017-3025.

[29] Carfagna C, Amendola E, Giamberini M, Filippov AG, and Bauer RS. Liquid Crystals 1993;13(4):571-584.

[30] Shiota A and Ober CK. Polymer 1997;38(23):5857-5867.

[31] De Gennes P and Prost J. The Physics of Liquid Crystals. Oxford University Press, 1993.

[32] Alexander L. Journal of Materials Science 1971;6(1):93-93.

[33] Beekmans F and deBoer AP. Macromolecules 1996;29(27):8726-8733.

[34] Smith ME, Benicewicz BC, and Douglas EP. Abstracts of Papers of the American Chemical Society 1996;211:4-POLY.

CHAPTER 6. GENERAL CONCLUSIONS

6.1 General discussions

The first part of this research focused on synthesis and characterization of a biphenyl-based liquid crystalline epoxy resin (LCER). An epoxy monomer, 4,4'-diglycidyloxybiphenyl (BP), was synthesized and cured with a tetra-functional amine, sulfanilamide (SAA) to produce novel LCERs. It was observed that BP was not a liquid crystalline (LC). However, the use of SAA resulted in the formation of a smectic LC phase. Cure temperature showed a great influence on the formation and development of the LC phase and an isotropic network was obtained for cure temperatures greater than 200^{o}C. A rate acceleration of the curing reaction was observed for the resins cured in the LC phase and was further investigated in the second part of this research. Compared to the resins cured into an amorphous network, the LCERs exhibited a polydomain structure with individual LC domains distributed in the resin matrix, resulting in higher values of storage modulus in both glassy region and rubbery plateau region and higher glass transition temperature.

The second part of this research investigated the unusual cure behavior of the LCER observed in the first part. The effects of LC phase formation on the cure kinetics were studied using differential scanning calorimetry (DSC). Both a model-free isoconversional method and a model-fitting method were used to analyze the DSC data. Results from the isoconversional analysis were applied to develop tentative multi-step kinetic models describing the curing reaction. Kinetic analysis showed that compared to the resins cured in amorphous phase, LCERs exhibited higher values of reaction enthalpy and a complex dependence of activation energy on the degree of cure. The formation of the LC phase

resulted in a decrease in activation energy, leading to higher degree of reaction.

The third part of this research focused on understanding the self-reinforcing mechanism of the LCER. The creep behavior of the resins were studied and compared with that of a non-LCER prepared from the same epoxy monomer. The experimental data was evaluated using Burgers' model to explain the reinforcing effect of the LC phase. The long-term performance of the material was predicted using the time-temperature superposition principle. The results revealed that the introduction of an LC phase into the resin network can reduce creep strain and creep strain rate of the material, especially at elevated temperatures. Parameters extracted from the simulation indicated that instantaneous elasticity, retardant elasticity, and permanent flow resistance of the resins were enhanced by the presence of the LC phase. It was thought that the self-reinforcing mechanism was related to a rigid filler effect and a crosslinking effect of the liquid crystals, where the LC domains can not only behave as rigid fillers to strengthen the resins, but also act as crosslinks tying different amorphous regions together.

The fourth part of this research investigated magnetic field orientation of the LCER and its effects on thermal and mechanical properties of the resins. Macroscopic orientation of the LCER was achieved by curing in a high strength magnetic field, and quantified by an orientation parameter determined with two-dimensional X-ray diffraction. Oriented LCER exhibited highly anisotropic properties. In the direction of orientation, LCER showed a substantial reduction of coefficient of thermal expansion (CTE) and significant improvements in dynamic mechanical properties.

6.2 Recommendations for future research

The introduction of LC phase into amorphous epoxy networks has shown great

potential to improve thermal and mechanical properties of resins. The application of magnetic fields provides another parameter which can be used to further tailor the properties of the material. For example, the CTE of the reins can be significantly reduced after magnetic field processing. By using low CTE polymer matrices, it is expected that the residual stresses developed during the processing of carbon fiber reinforced polymer composites (CFRP) can be greatly reduced, facilitating the development of CFRP for advanced applications.

With regard to this objective, it is recommended that efforts be placed on understanding the alignment process of the LCER under magnetic fields since alignment quality is closely related to thermomechanical properties of the resin. Although there were reports on thermal and mechanical properties of aligned LCER systems, several fundamental aspects such as the alignment kinetics are still not fully understood. A systematic study on alignment kinetics can provide valuable insight into the effects of magnetic field processing on morphologies, orientation, and thermomechanical properties of the resin. The results can be used as a guide for the preparation of carbon fiber (CF) reinforced LCER composites.

During the preparation of CF/LCER composites, the anisotropic properties of the resin after magnetic field processing need to be considered. There are several types of architectures available. For example, when using unidirectional carbon fibers, the LCER can be aligned perpendicular to the fiber direction, resulting a ply with near-zero in-plane thermal expansion. When these plies are bonded together, it is expected that the residual stresses between different plies can be substantially reduced. Alternatively, woven carbon fabrics can be used since they provide balanced in-plane properties. The LCER can be

aligned in the out-of-plane direction to strengthen the composite laminates.

APPENDIX A: SUPPLEMENTARY INFORMATION FOR CHAPTER 2

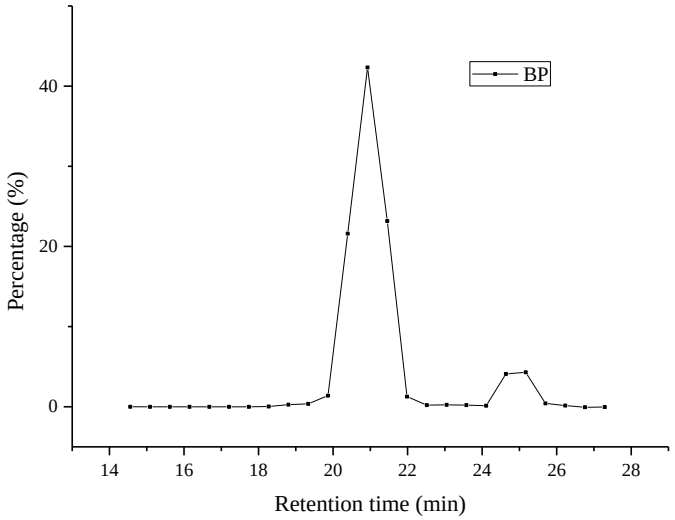

Figure A1. Gel permeation chromatography analysis of BP, indicating the presence of low molecular weight fraction of BP.

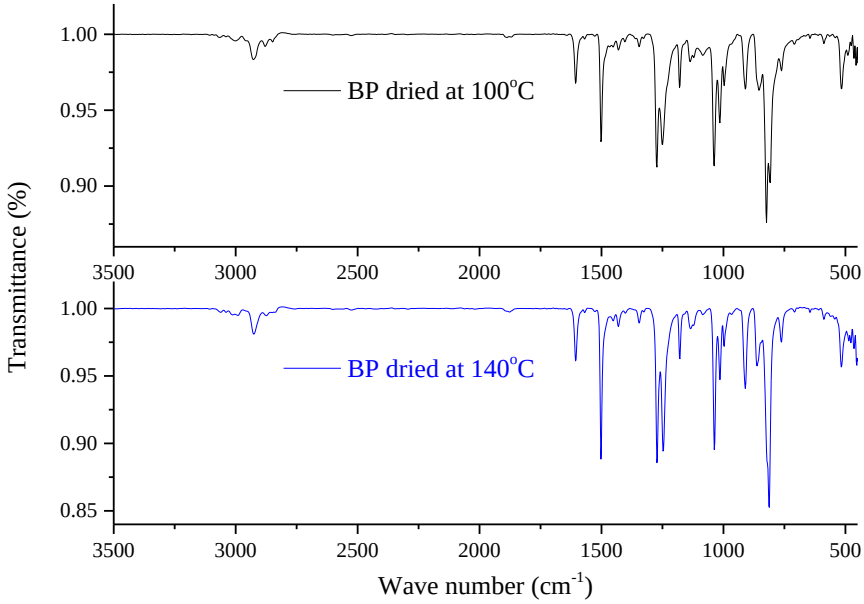

Figure A2. FTIR spectra of BP after drying at 100ºC and 140ºC respectively.

Table A1. Assignment of major peaks in the FTIR spectrum of BP.

Wavenumber (cm^{-1})	Associated chemical groups
2927	Stretching of (CH_2)
1606	Stretching of (C=C) on aromatic rings
1500	Bending of (C=C) on aromatic rings
1244	Stretching of (C-O) on aromatic rings
1037	Stretching of (C-O) on aliphatic chain
910	Epoxy group
814	Bending of (C-H) on aromatic rings

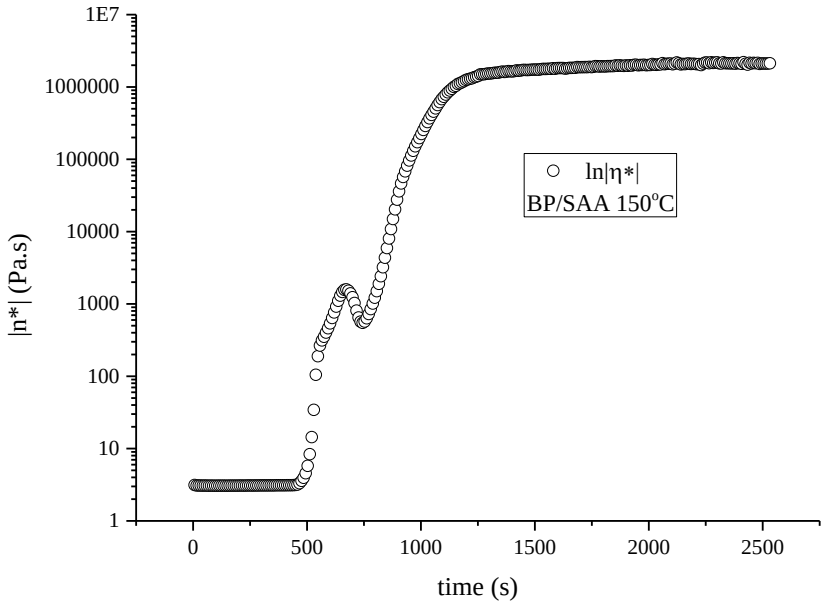

Figure A3. The evolution of complex viscosity of BP/SAA cured at 150°C, indicating the decrease of viscosity when the reacting medium undergoes a transition from amorphous phase to liquid crystalline phase.

APPENDIX B: SUPPLEMENTARY INFORMATION FOR CHAPTER 4

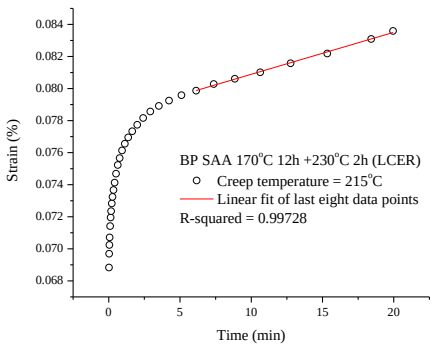

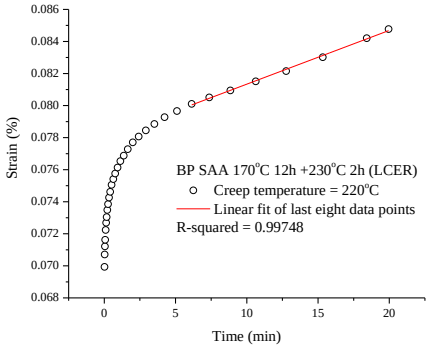

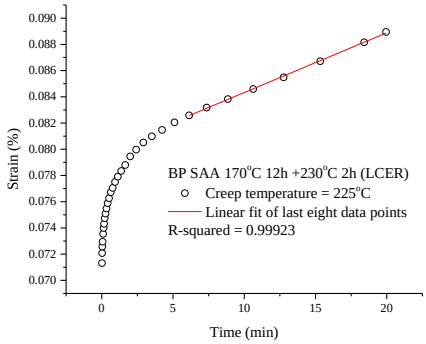

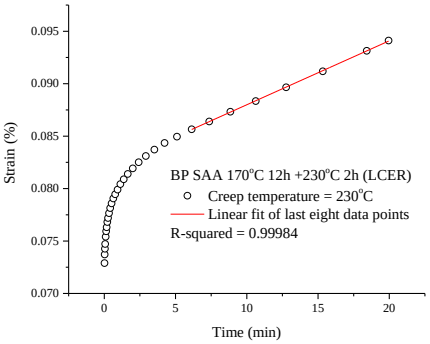

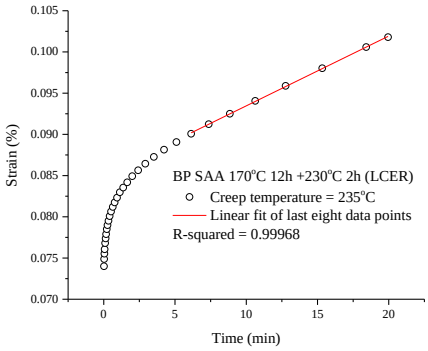
BP SAA 170°C 12h +230°C 2h (LCER)
Creep temperature = 235°C
Linear fit of last eight data points
R-squared = 0.99968
Strain (%)
Time (min)

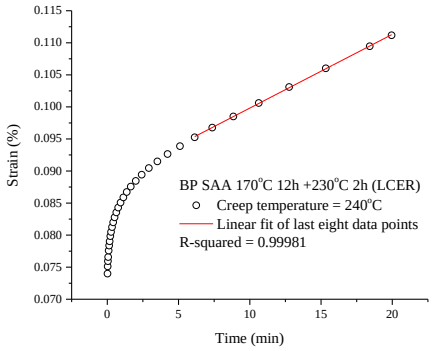
BP SAA 170°C 12h +230°C 2h (LCER)
Creep temperature = 240°C
Linear fit of last eight data points
R-squared = 0.99981
Strain (%)
Time (min)

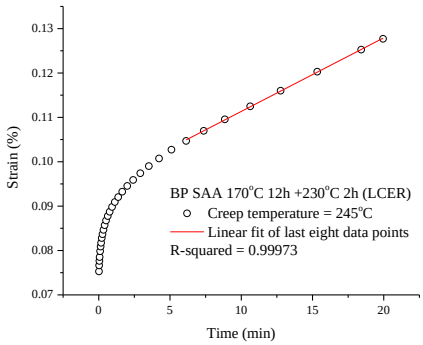
BP SAA 170°C 12h +230°C 2h (LCER)
Creep temperature = 245°C
Linear fit of last eight data points
R-squared = 0.99973
Strain (%)
Time (min)

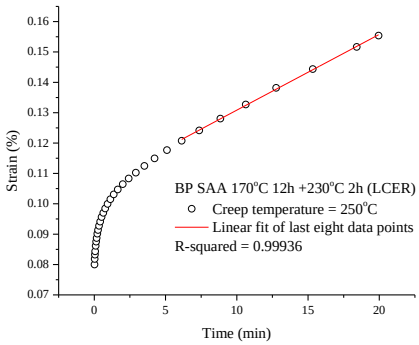
BP SAA 170°C 12h +230°C 2h (LCER)
Creep temperature = 250°C
Linear fit of last eight data points
R-squared = 0.99936
Strain (%)
Time (min)

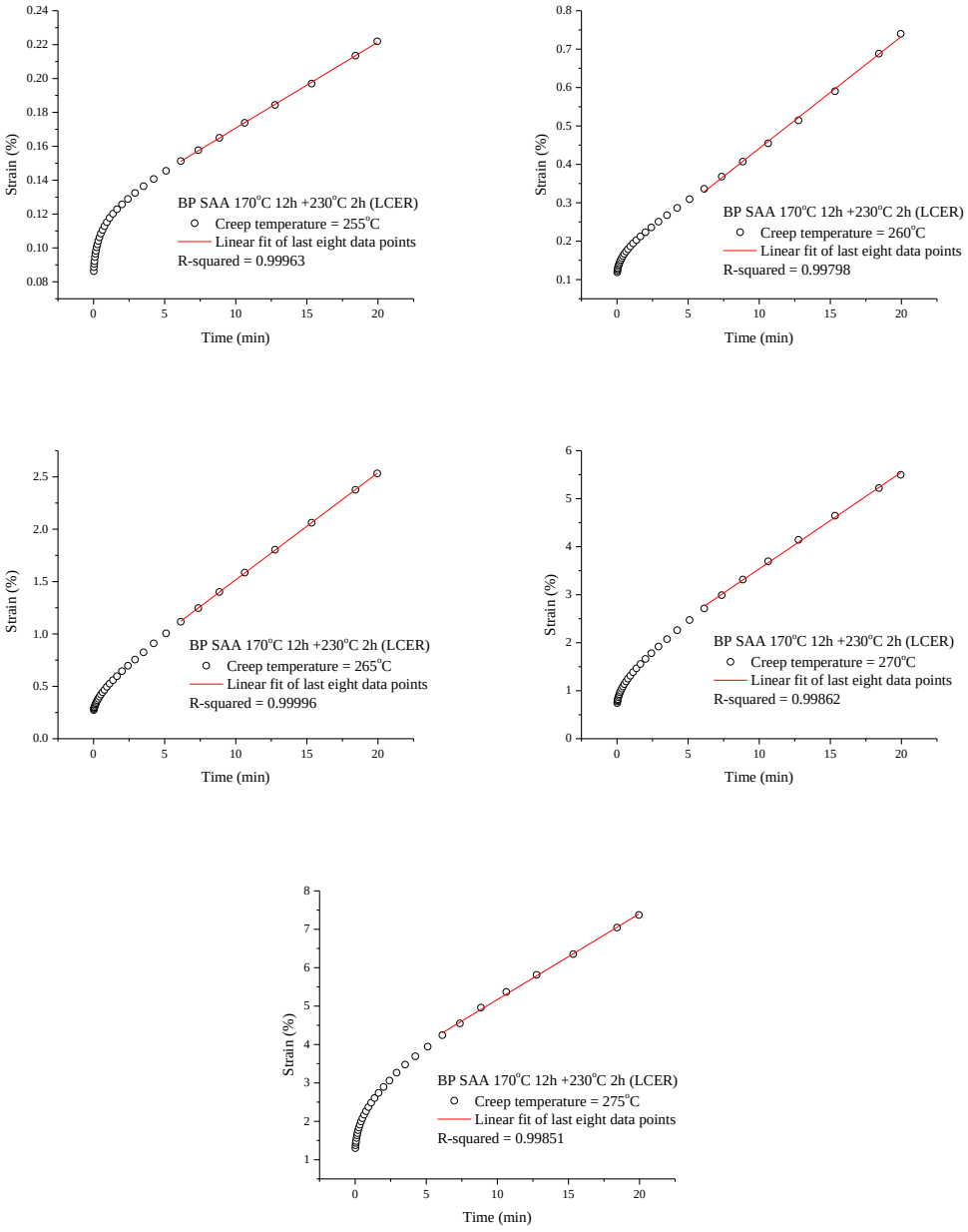

Figure B1. Original creep curves of the LCER cured at 170 ºC under different creep temperatures. Red lines represent a linear fitting applied on the last eight data point to determine creep strain rate.

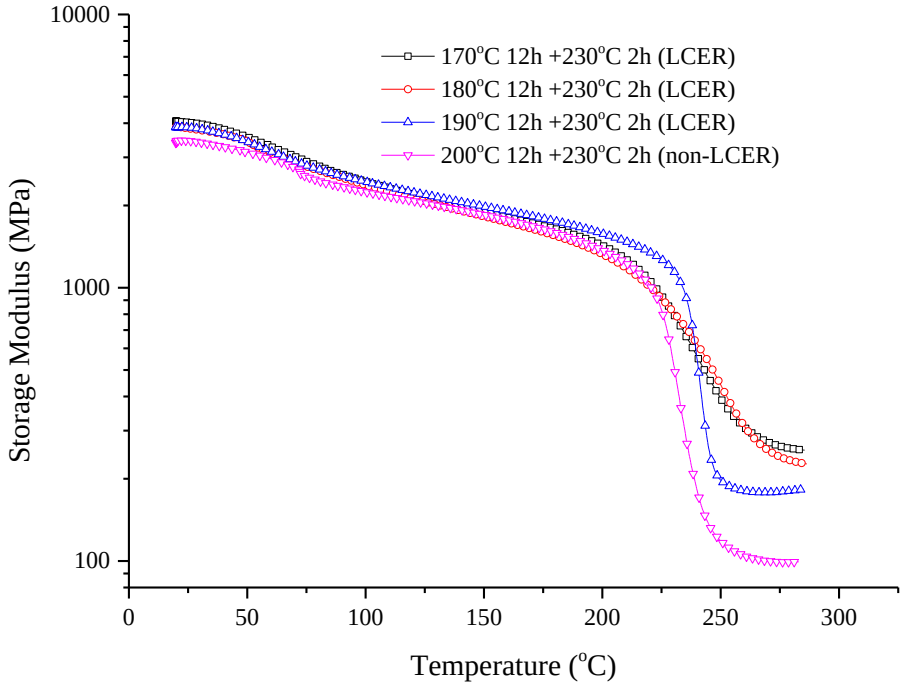

Figure B2. Temperature dependence of storage modulus of the resins cured at different temperatures. LCERs exhibit increased storage modulus in both glassy and rubbery region, indicating a reinforcing effect.

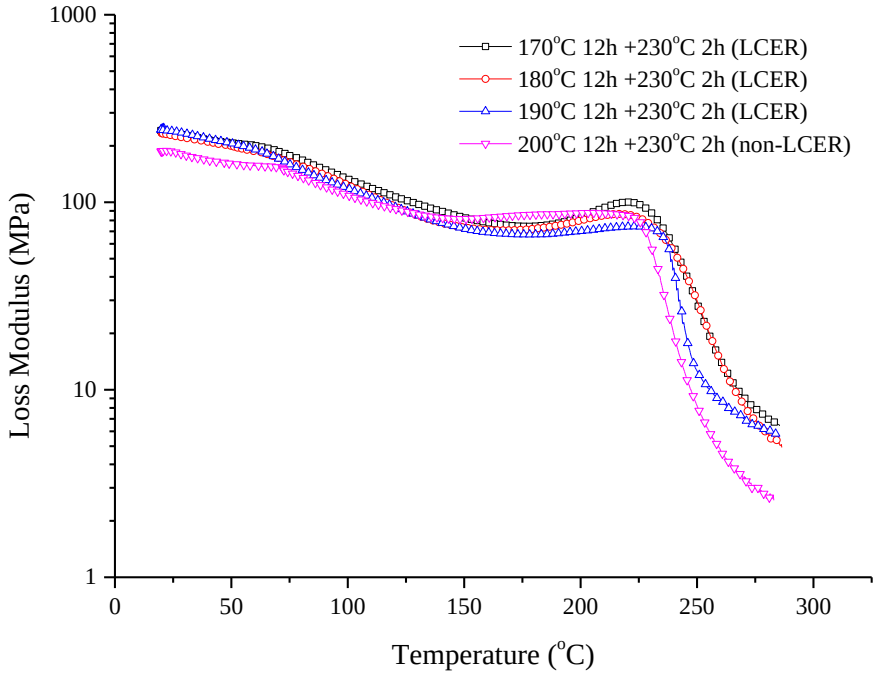

Figure B3. Temperature dependence of loss modulus of the resins cured at different temperatures. The shape of these curves is similar to that in Fig. 6b because both of them represent the viscous part of the resin.

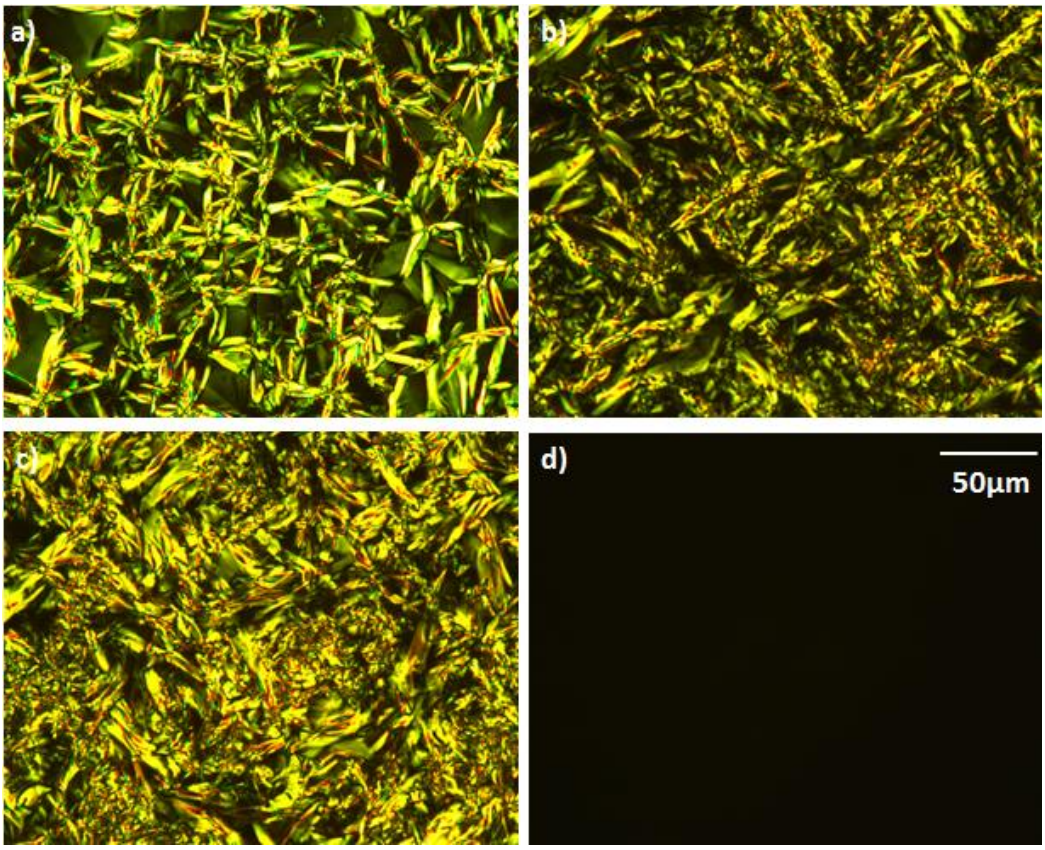

Figure B4. POM images after 2h of isothermal cure of BP with SAA at different temperatures. (a) 170°C; (b) 180°C; (c) 190°C; (d) 200°C. For the LCERs, the morphology of the LC phase depends on curing temperatures, which might be the reason for the difference in their creep behaviors.